Technische Universität München
Fakultät für Maschinenwesen
Institut für Energietechnik
Professur für Thermofluiddynamik

Warning system for thermoacoustic instability in annular combustion systems

Driek Rouwenhorst

Vollständiger Abdruck der von der Fakultät für Maschinenwesen der Technischen Universität München zur Erlangung des akademischen Grades eines

DOKTOR – INGENIEURS

genehmigten Dissertation.

Vorsitzender:
Prof. dr.ir. Daniel J. Rixen
Prüfer der Dissertation:
1. Prof. Wolfgang Polifke, Ph.D.
2. Prof. Dr.-Ing. Steffen Marburg

Die Dissertation wurde am 16.04.2020 bei der Technischen Universität München eingereicht und durch die Fakultät für Maschinenwesen am 20.10.2020 angenommen.

Acknowledgment

Many people have contributed to this dissertation, directly and indirectly.

First of all, I would like to thank my supervisors in this project. In his position as CEO of IfTA Dr. Jakob Hermann knows very well the demands and conditions in industry with regard to thermoacoustics and related topics in the monitoring of heavy machinery. This guidance enabled the research to be steered towards relevant topics and has resulted in a technological advancement that quickly found an application in the field. Discussions with Professor Dr. Wolfgang Polifke, my other supervisor, were always fruitful and have helped me to publish relevant results in an academic setting, helping appropriate conference and journal selection in the field. It has been an honor to be part of his department, the Thermo-Fluid Dynamics group at the Technical University of Munich.

Additionally, I would like to thank everyone in the TANGO group. A great deal of personal and professional development during my doctorate period can be attributed to being part of the TANGO Network. It was a great pleasure to meet and interact with fellow students and supervising scientists at workshops, training events and conferences around the globe. A special thanks to Maria Heckl for coordinating this fantastic group.

I would also like to acknowledge the support by many colleagues at IfTA, assisting me in the laboratory and supporting me using the in-house hardware and software. Being part of this SME resulted in a valuable and broad experience in the industry, complementing the academic side of the Ph.D.

Finally, on a personal level I would like to thank family and friends for supporting me during this adventure. Without the kind stimulus from several sides, this work would neven have been finished.

Abstract

Thermoacoustics deals with interactions between thermodynamics and acoustics. One of the environments where such interactions occur is inside combustion systems. Feedback loops, in which acoustics and heat release fluctuations amplify each other, can quickly lead to unacceptably high amplitudes of pressure oscillations, potentially interfering with the combustion process and challenging the structural integrity of combustor components.
It has proven hard to predict and avoid all possible thermoacoustic interactions in the design stage of combustion systems. Design changes, for example to accommodate emission reduction technologies, can unexpectedly introduce new thermoacoustic instabilities, also referred to as combustion dynamics. Even though it is possible to attenuate the high-amplitude oscillations effectively using active control, it is preferred to avoid instabilities and apply passive stabilization measures if required.
The stationary gas turbine industry is prognosticated to play an important role in the energy transition, flexibly filling the supply shortage when renewable production falls short of the electricity demand. Increased flexible operation of gas turbines comes with extended operational windows in which thermoacoustic instability may occur.

Stability margin measures, or precursors, are a tool to detect oncoming thermoacoustic instabilities based on real-time measurements in order to avoid high amplitude pressure oscillations. A precursor should provide a quantitative measure of the distance to instability, leaving time to take action and prevent high amplitude limit cycle oscillations. Depending on the type of thermoacoustic interactions and the geometry of the combustion chamber, precursors can be defined using appropriate measurements.
This work focuses on azimuthal thermoacoustic modes in gas turbines. Azimuthal modes are special due to the dynamical freedom these modes possess, posing challenges that have not yet been addressed with regard to the real-time identification of stability margins.
A stability margin is proposed on the basis of a linear decay rate, obtained by the identification of a state space representation that describes the azimuthal thermoacoustic dynamics. The low order model description is explored in detail to understand the preference of spinning and standing modes. The thermoacoustic system is shown to be defective (i.e. feature a pair of identical eigenvectors) under specific conditions, resulting in nonnormal growth and a significant influence on the amplitude distribution anywhere near this defective point.
The precursor is demonstrated on surrogate and experimental data from a laboratory scale combustor in which it is shown that splitting of the degenerate azimuthal modes is identified well. Ultimately, the method was successfully implemented on a pair of industrial gas turbines, protecting them from an azimuthal thermoacoustic instability during extended part-load operation.

Contents

1 Introduction **1**
1.1 Thermoacoustic interaction . . . 1
1.2 Instabilities in combustion systems . . . 1
1.3 Mitigation of combustion dynamics . . . 2
1.4 Scope of the work . . . 3

2 Thermoacoustics **5**
2.1 Governing equations . . . 6
2.2 Acoustics . . . 6
2.2.1 Example: eigenmodes in a combustor can . . . 7
2.3 Heat release: an acoustic source . . . 8
2.4 Heat release description . . . 8
2.5 Thermoacoustic stability . . . 9
2.5.1 Alternative synchronized feedback loops . . . 10
2.6 Nonlinearities . . . 10
2.6.1 Bifurcation . . . 11
2.7 Eigenvalue solution . . . 12
2.8 Nonnormal growth . . . 12
2.9 Stability margin approaches . . . 13
2.9.1 Linear decay rate . . . 14
2.9.2 Nonlinear data analysis . . . 15

3 Combustion stability monitoring and control **17**
3.1 Monitoring in the field . . . 17
3.1.1 Instrumentation . . . 18
3.1.2 Real-time capability . . . 18
3.2 Instability control . . . 19
3.2.1 Passive control . . . 19
3.2.2 Active control . . . 19
3.3 Existing stability margins . . . 19
3.3.1 Linear system fitting . . . 20
3.3.1.1 Autocorrelation fitting . . . 20
3.3.1.2 Spectral fitting . . . 20
3.3.1.3 Other . . . 20
3.3.2 Nonlinear stability margins . . . 20
3.3.2.1 Phase space methods . . . 21

3.3.2.2 Entropy (information theory) methods 21
3.4 Annular combustion systems 22
3.4.1 Rotational symmetry 22
3.4.2 Degeneracy 23
3.4.3 Symmetry breaking 24
3.4.4 Consequences for stability margins 24

4 Summary and Discussion of Achievements 27
4.1 On the Performance of Stability Margin Measures for Thermoacoustic Instabilities in Turbulent Combustion Systems 29
4.2 Online Monitoring of Thermoacoustic Eigenmodes in Annular Combustion Systems Based on a State-Space Model 30
4.3 Bifurcation Study of Azimuthal Bulk Flow in Annular Combustion Systems with Cylindrical Symmetry Breaking 32
4.4 Part-Load Limit Reduction of a Frame 9E Using a Precursor for Combustion Dynamics 34
4.5 In Situ Identification Strategy of Thermoacoustic Stability in Annular Combustors 35

Reprints of Original Publications 41
.1 ICSV21 2014 42
.2 Journal of Engineering for Gas Turbines and Power 2017 50
.3 International Journal of Spray and Combustion Dynamics 2017 58
.4 ASME Turbo Expo 2018 72
.5 International Journal of Spray and Combustion Dynamics 2018 82

List of Figures

2.1 supercritical bifurcation $\dot{A} = A(\lambda - A^2 - 0.1A^4)$ 11
2.2 subcritical bifurcation $\dot{A} = A(\lambda + A^2 - 0.1A^4)$ 11
2.3 Two non-orthogonal eigenvectors, with cancelling initial conditions 13
2.4 Evolution of the system, showing how the decay along $\mathbf{v}_2$ causes an increase in amplitude. 13
2.5 Lorenz attractor, original variables in 3d phase space 16
2.6 Lorenz attractor, embedded phase space of L_z 16

3.1 Three-dimensional example of the acoustic field in an annulus, reproduced from [39] 23
3.2 Propagation of the azimuthal waves F and G, reproduced from [40] 23
3.3 Decay of synchronized damped harmonic oscillators with $\zeta = 0.002$ 25
3.4 Decay of beating damped harmonic oscillators with $\zeta = 0.002$ and $M = 0.01$ . . 25

Nomenclature

Latin Symbols

A	$[\mathrm{N/m^2}]$	Absolute acoustic amplitude
c	$[\mathrm{m/s}]$	Speed of sound
e	$[\mathrm{J/kg}]$	Specific energy
f	$[\mathrm{N/m^2}]$	Acoustic plane pressure wave in positive direction
g	$[\mathrm{N/m^2}]$	Acoustic plane pressure wave in negative direction
i	$[-]$	imaginary unit $\sqrt{-1}$
k	$[\mathrm{1/m}]$	Wave number
L	$[-]$	Lorenz attractor variable
m	$[-]$	Azimuthal mode order
M	$[-]$	Mach number
n	$[\mathrm{J/m}]$	Interaction index for heat release
$\mathbf{n}$	$[-]$	Outward unit vector
p	$[\mathrm{N/m^2}]$	Pressure
$\dot{Q}$	$[\mathrm{W/m^3}]$	Volumetric heat release
r	$[\mathrm{m}]$	Radial coordinate
R	$[\mathrm{m}]$	Autocorrelation function
S	$[\mathrm{J/K}]$	Entropy
$S(V)$	$[\mathrm{m^2}]$	Surface of a volume
t	$[\mathrm{s}]$	Time
u_x	$[\mathrm{m/s}]$	Axial velocity
$\mathbf{u}$	$[\mathrm{m/s}]$	Velocity vector
v	$[\mathrm{m^3/kg}]$	Specific volume $1/\rho$
V	$[\mathrm{m^3}]$	Volume
$\mathbf{u}$	$[\mathrm{m/s}]$	Velocity vector
x	$[\mathrm{m}]$	Axial carthesian coordinate
$\mathbf{x}$	$[\mathrm{m}]$	Coordinate vector (x, y, z) or (x, r, θ)
z	$[-]$	Coordinate in the complex plane

Greek Symbols

α	[1/s]	Acoustic attenuation/damping
β	[1/s]	Growth rate through thermoacoustic interaction
ε	[−]	Perturbation strength
λ	[1/s]	Eigenvalue
ρ	[kg/m^3]	Density
ω	[rad/s]	Angular frequency
τ	[s]	Time delay
θ	[−]	Azimuthal coordinate
γ	[−]	Heat capacity ratio
ζ	[−]	Damping ratio
Ψ	[−]	Wave field along radial and axial coordinates
Φ	[−]	Wave field along azimuthal coordinate

Super- and subscripts

$\square'$	[−]	Fluctuating quantity
$\square_0$	[−]	Average quantity
$\square_r$	[−]	At the reference location
$\square_h$	[−]	At the heat release location

Chapter 1

Introduction

1.1 Thermoacoustic interaction

Thermoacoustics was first observed by the generation of sound in systems with an acoustic resonator and heat gradients. This phenomenon is believed to be observed in ancient history, but Rijke and Rayleigh are among the first authors describing thermoacoustics in modern history. In a note dated 1859, Rijke describes the sound production of a heated wire mesh in an open pipe [37], a setup which is now referred to as the Rijke tube. In the publication it was reasoned that the sound must be produced by the subsequent expansion and rarefaction of the air that passes the wire mesh through natural convection. In 1878 Lord Rayleigh described the coupling between acoustics and heat release more precisely [35]:

"*If heat be given to the air at the moment of greatest condensation, or taken from it at the moment of greatest rarefaction, the vibration is encouraged. On the other hand, if heat be given at the moment of greatest rarefaction, the vibration is discouraged.*"

This explanation, expressed in the form of a thermodynamic equation, now goes under the name Rayleigh criterion. When the vibration is encouraged enough to overcome damping mechanisms, a state of thermoacoustic instability is obtained. In this state, a limit cycle oscillation develops with a certain frequency and amplitude.

1.2 Instabilities in combustion systems

Understanding and predicting thermoacoustic coupling mechanisms has become increasingly important, particularly regarding industrial applications where heat is released in compact enclosures. Research was originally driven in particular by instabilities in propulsion systems [7, 8], due to the high power density in such systems. The transfer of a small fraction of the released thermal power into the acoustic field of the enclosure can readily cause catastrophic

failure of components. As land-based gas turbines were scaled up in power output and efficiency, thermoacoustic interaction and instability became an increasingly important issue, because of the high economical impact of gas turbine down-time in these power plants.

Increasingly strict regulations on air pollution emissions have aggravated the problem of thermoacoustic instability. Lean premixed combustion systems form a crucial technology to minimize the formation of NOx, but the premixed flames are more sensitive to acoustic perturbations and the combustion chambers tend to have less acoustic absorption through the reduction of dilution holes. Another factor of the modern power generation market is the demand for flexibility in order to complement and stabilize the electricity supply, of which a growing contribution is provided by renewable sources. Flexible, unsteady operation means that a broad range of operating conditions are in use, yielding constantly changing thermoacoustic interactions and thus increased likelihood to encounter thermoacoustic instabilities.

The two elements that predominantly define the thermoacoustics in a gas turbine are the combustion chamber geometry and the burner design. The geometry determines the acoustic boundary conditions that influence the thermoacoustic coupling. Whether a gas turbine makes use of multiple cans around the main shaft or uses a single annular combustion chamber, affects the possibilities for thermoacoustic interaction. The burner design determines the flame characteristics and the heat release response to acoustic perturbations.

1.3 Mitigation of combustion dynamics

With the help of dedicated design tools and experiments, major problems with thermoacoustic instabilities have been mitigated in the design stage of combustion systems. Nevertheless, problems with thermoacoustic stability are encountered in the field on a regular basis. Thermoacoustic interactions have proven to be very sensitive to the state of the system, the operating conditions, boundary conditions and the environment it is operated in and therefore hard to eliminate in general.

Active control of the oscillations is an effective solution, in which the acoustic fluctuations are counteracted by modulation of the fuel flow in a real-time feedback loop. However, if possible passive control is preferred. Examples include increasing the attenuation of acoustics through dampers and modification of the flame response through burner modifications.

In the case that the problems due to thermoacoustic oscillations are not that severe because they occur in a limited, uncritical operating range, operation in said range may simply be avoided. When the limit cycle oscillation amplitudes are moderate, a short term encounter of instability can be allowed. In this case amplitude monitoring is adequate; In a matter of seconds the operating parameters can be changed to a stable operating regime. However, in the case the limit cycle amplitudes are unacceptably high, either the combustion system must be operated far from the potential thermoacoustic hazard, or the margin to the instability needs to be identified on basis

of real-time measurements.

1.4 Scope of the work

This dissertation originated as a part of the Marie Curie Initial Training Network TANGO: **T**hermo and **A**eroacoustic **N**onlinearities in **G**reen Combustors with **O**rifice Structures. The scope of this project (funded by the European Commission) is to gain combustion-related aero- and thermoacoustic knowledge in order to develop tools and methods to abate acoustic problems in combustion systems.

The task within the TANGO project addressed in this dissertation is the development of an instability warning system. A quantitative evaluation of the thermoacoustic stability is sought, based on real-time measurements. The host beneficiary of the task is IfTA GmbH, an established SME in the field of monitoring and control of thermoacoustics in combustion systems. Based on the competence of the host and input from industry, heavy duty land-based gas turbines with annular geometry are addressed in particular.

Chapter 2

Thermoacoustics

This chapter gives a brief physical basis of established theory in thermoacoustics.

In order to understand and predict thermoacoustics, model descriptions are required that match observations in controlled thermoacoustic experiments. A system that includes interaction between acoustics and fluctuating heat release can be modeled at different levels of complexity.

Studying the complex multiphysics problem taking place in a combustion system as a whole involves extensive experiments on the combustor of interest and/or detailed numerical simulations that solve the full Navier-Stokes equations. This allows all coupling mechanisms between acoustics, heat release, the unsteady flow field and other potential dynamics at play, such as structural interaction, to be obtained. The drawback of such a global approach is that the obtained dynamics is very specific to the combustion setup under investigation and the knowledge gained that can be transferred to a different setup is limited.

In a more fundamental approach, the multiphysics problem is divided into its components and analytical descriptions are found for them independently. Coupling these building blocks together to resemble a certain setup can then yield an approximation of the expected behavior of the full system.

The following three examples list the possibilities to model a thermoacoustic system. From top to bottom, model descriptions range from detailed and expensive (millions of degrees of freedom) to low-order and analytic (few degrees of freedom).

- Full numeric solver (DNS or LES), including chemistry for combustion
- Euler solver coupled with a reduced order model for the flame (e.g. FTF or FDF)
- Network/analytic acoustic model coupled with low-order heat release model (e.g. n-τ)

The focus in this work is on the last category, describing low-order behavior of generic systems. Building blocks in this case are plane acoustic propagation (with or without mean

flow) and fundamental heat release response characteristics. Low-order models are widely applicable to different combustion setups and the limited degrees of freedom vastly increase the feasibility to develop real-time model-based monitoring implementations. To ensure that the low-order description of the thermoacoustic system contains the desired key features of the physical solution, a cross-validation with experiments and/or more complex models is essential.

Not all topics in the field of thermoacoustics are covered in the scope of this work. For example, the interaction of thermoacoustics with unsteady flow fields and entropy waves is not considered.

2.1 Governing equations

Disregarding viscous effects and heat conduction, the Navier-Stokes equations can be reduced to the Euler equations. The PDE (partial differential equation) in non-conservation form [36] can be condidered as a good starting point:

$$\frac{\mathrm{D}\rho}{\mathrm{D}t} + \rho\nabla\cdot\mathbf{u} = 0 \tag{2.1}$$

$$\rho\frac{\mathrm{D}\mathbf{u}}{\mathrm{D}t} = -\nabla p \tag{2.2}$$

$$\frac{\mathrm{D}e}{\mathrm{D}t} + p\frac{\mathrm{D}v}{\mathrm{D}t} = v\dot{Q} \tag{2.3}$$

Note that the volumetric heat release is contained, whereas heat conduction is neglected. This is justifiable in a combustion system in which the vast majority of the released heat leaves the combustion chamber through convection.

2.2 Acoustics

Acoustics describes wave propagation in a medium. The waves consist of small disturbances of the thermodynamic state variables with respect to their undisturbed magnitude, allowing linearization of the Euler equations.
Besides the flame region, all fluid domains within a combustion system are isentropic and therefore unaffected by the energy equation (Eq. 2.3). Writing the variables in the mass (Eq. 2.1) and momentum (Eq. 2.2) conservation equations in terms of mean and fluctuating quantities and neglecting contributions of squared fluctuations, yields:

$$\frac{\mathrm{D}\rho'}{\mathrm{D}t} + \rho_0\nabla\cdot\mathbf{u}' = 0 \tag{2.4}$$

$$\rho_0\frac{\mathrm{D}\mathbf{u}'}{\mathrm{D}t} = -\nabla p' \tag{2.5}$$

Assuming a quiescent state of the gas, a combination of the time derivative of 2.4 and the divergence of 2.5 eliminates $\mathbf{u}'$.

$$\frac{\partial^2 \rho'}{\partial t^2} - \nabla^2 p' = 0 \tag{2.6}$$

A convenient equation of state for isentropic flow quantifies the change of pressure with respect to the density at constant entropy.

$$\left(\frac{\partial p}{\partial \rho}\right)_S = c^2 \tag{2.7}$$

Insertion in equation 2.6 yields the wave equation.

$$\frac{\partial^2 p'}{\partial t^2} = c^2 \nabla^2 p' \tag{2.8}$$

As it turns out, the constant c is the propagation speed of acoustic fluctuations, i.e. the speed of sound.

In a first approximation, a combustion chamber can be described by a volume filled with a quiescent perfect gas at a prescribed temperature. The geometry and inlet/outlet impedances of the combustion chamber define the boundary conditions that are imposed on the wave equation, such that solutions of the acoustic field can be found.

2.2.1 Example: eigenmodes in a combustor can

A low order model for a combustor can would only consider axial fluctuations and neglect the convection velocity with respect to the speed of sound (i.e. a low Mach number). The general solution consists of two arbitrary functions f and g that travel upstream and downstream respectively and meet the boundary conditions at the end of the domain.

$$p' = f(x - ct) + g(x + ct) \tag{2.9}$$

$$u'_x = \frac{1}{\rho_0 c}\big(f(x - ct) - g(x + ct)\big) \tag{2.10}$$

An infinite set of complex harmonic functions is used to describe f and g and enforce the posed boundary conditions. For example, closed ends ($u'_x = 0$) at the boundaries at $x = 0$ and $x = L$ yields

$$p'(x,t) = \frac{1}{2}e^{i\omega t - ikx} + \frac{1}{2}e^{i\omega t + ikx} = \cos(kx)e^{i\omega t} \tag{2.11}$$

$$u'_x(x,t) = \frac{k}{2\rho_0\omega}\left(e^{i\omega t - ikx} - e^{i\omega t + ikx}\right) = \frac{-ik}{\rho_0\omega}\sin(kx)e^{i\omega t}. \tag{2.12}$$

With wave numbers $k = \pi j/L$, where $j = 1, 2, 3, ...$ assuring that the boundary conditions are fulfilled.

2.3 Heat release: an acoustic source

To establish the coupling between heat release and the acoustic field through the energy equation 2.3, the considered gas is assumed to behave as a calorically perfect gas around the mean thermodynamic state,

$$c^2 \frac{\partial \rho'}{\partial t} = \frac{\partial p'}{\partial t} - (\gamma - 1)\dot{Q}'. \tag{2.13}$$

This yields the inhomogeneous wave equation with a heat release term on the right-hand side.

$$\frac{\partial^2 p'}{\partial t^2} - c^2 \nabla^2 p' = (\gamma - 1)\frac{\partial \dot{Q}'}{\partial t} \tag{2.14}$$

It must be noted that the ratio of specific heats γ and in particular the speed of sound c need not be constant, as a large increase in temperature is present over the flame surface.
Integrating equation 2.14 over time yields

$$\frac{\partial p'}{\partial t} + \rho_0 c^2 \nabla \mathbf{u}' = (\gamma - 1)\dot{Q}'. \tag{2.15}$$

Multiplying with $p'/\rho_0 c^2$ and rewriting the with help of the momentum equation, the balance equation for the acoustic energy is obtained.

$$\frac{\partial}{\partial t}\left(\frac{1}{2\rho_0 c^2} p'^2 + \frac{\rho_0}{2}\mathbf{u}'^2\right) + \nabla \cdot (p'\mathbf{u}') = \frac{\gamma - 1}{\rho_0 c^2} p'\dot{Q}' \tag{2.16}$$

The rate of change of compression and kinetic energy in an infinitesimal volume plus the energy leaving the boundaries is equal to the acoustic energy gained through the volumetric heat release. The acoustic energy is indeed increasing if the heat release fluctuations $\dot{Q}'$ are released when the acoustic pressure p' is positive as Lord Rayleigh described [35].

2.4 Heat release description

In general, heat release fluctuations are present in combustors with turbulent flow. For example, heat is released both as a function of time and location as eddies interact with the flame front, giving rise to acoustic perturbations. Another heat release mechanism involves fluctuations in the equivalence ratio of the fuel mixture caused by turbulence in the premixing process. Turbulence causes a broadband noise spectrum that is typically uncorrelated to acoustic eigenmodes. As $E[p'\dot{Q}'] = 0$, the acoustic energy will not grow without bounds. Higher acoustic energy can be found at the eigenfrequencies because the energy decays relatively slowly at these resonance points.

The thermoacoustics becomes particularly interesting when the heat release is simultaneously modulated by the acoustic field. This results in a correlation between heat release and acoustics and constructs a closed feedback loop. Acoustic particle velocity can modulate the heat release via several mechanisms, such as vortex shedding at the burner or periodically changing of the

fuel equivalence ratio.

A low-order model describing this effect relates the heat release to the particle velocity at a certain location with a response strength and a time lag. This could be a velocity modulation of the fuel at the injection point, causing unsteady heat release after the fuel has been convectively transported from the injector point to the flame front[6]. This model structure has also been used to model the Rijke Tube [18].

$$\iiint_{V_h} \dot{Q}'(\mathbf{x}, t)\,\mathrm{d}V = n\mathbf{u}'(\mathbf{x}_r, t-\tau)\cdot\mathbf{v}_r \tag{2.17}$$

Here, the heat release concentrated in the volume V_h is sensitive to velocity fluctuations at reference location $\mathbf{x}_r$ in the unit direction $\mathbf{v}_r$. More sophisticated models describe a frequency dependent transfer function between acoustic perturbations at a sensitive location and the heat release. This so-called Flame Transfer Function (FTF) can be described by a model or obtained through experiments.

$$\iiint_{V_h} \dot{Q}'(\mathbf{x}, \omega, t)\,\mathrm{d}V = FTF(\omega)\mathbf{u}'(\mathbf{x}_r, \omega, t)\cdot\mathbf{v}_r \tag{2.18}$$

When the heat release is also a function of the acoustic amplitude A, the method is referred to as a Flame Describing Function (FDF). This allows to find limit cycle behavior through amplitude saturation.

$$\iiint_{V_h} \dot{Q}'(\mathbf{x}, \omega, t)\,\mathrm{d}V = FDF(\omega, A)\mathbf{u}'(\mathbf{x}_r, \omega, t)\cdot\mathbf{v}_r \tag{2.19}$$

2.5 Thermoacoustic stability

Integrating the acoustic energy balance equation 2.16 over the volume of the system and using the divergence theorem leads to the balance of total acoustic energy W_a in the system.

$$\overbrace{\frac{\mathrm{d}W_a}{\mathrm{d}t}}^{\text{Rate of change}} + \overbrace{\oiint_{S(V)} p'\mathbf{u}'\cdot\mathbf{n}\,\mathrm{d}S}^{\text{Outward flux}} = \overbrace{\iiint_V \frac{\gamma-1}{\rho_0 c^2} p'\dot{Q}'\,\mathrm{d}V_h}^{\text{Rayleigh source term}} \tag{2.20}$$

Where $W_a = \iiint_V \left(\frac{1}{2\rho_0 c^2} p'^2 + \frac{\rho_0}{2}\mathbf{u}'^2\right)\mathrm{d}V$ is the total acoustic energy within the system bounds.

With the heat release being (among other things) a function of acoustic perturbations in the same domain, a feedback loop is obtained. For a linear heat release description, it can be quantitatively stated that a thermoacoustic eigenmode averaged over an acoustic cycle behaves as follows:

$$\frac{\mathrm{d}A}{\mathrm{d}t} = (\beta - \alpha)A \tag{2.21}$$

Where α reflects the natural decay of the eigenmode (mainly) due to the flux of acoustic energy leaving the acoustic domain and β is the growth rate resulting from the Rayleigh source term

(see equation 2.20).

$$A(t) = A(0)e^{(\beta-\alpha)t} \tag{2.22}$$

The complex proportionality constant β depends on the acoustic field, the reference and heat release location(s) and the (phase) delay between the reference velocity and heat release. With $\Re(\beta) > 0$ the heat release adds energy to the thermoacoustic field. Conversely for $\Re(\beta) < 0$ the heat release dampens out the eigenmode. The imaginary part of β is the oscillatory part of the solution, yielding the eigenfrequency of the thermoacoustic system: $e^{i\Im(\beta)t} = e^{i\omega t}$.

Typically the type of thermoacoustic instability studied is dominated by a standing wave acoustic field. In such case the outward flux is very small, i.e. the waves dominantly reflect at or outside of the volume boundary. This results in an acoustic sub-domain with $\alpha \ll \omega$, in which a relatively small positive feedback of the heat release is sufficient to cause exponential thermoacoustic growth. The focus in this work is on this type of instabilities, where the combined thermoacoustic system is a perturbation from the acoustic solution. It must be noted that this need not be the case, briefly discussed in the next subsection.

2.5.1 Alternative synchronized feedback loops

Significant thermoacoustic feedback may take place under purely active acoustics (no reflections), where all generated acoustic energy leaving the control volume (enclosing $\mathbf{x}_r$ and $\mathbf{x}_h$) is lost. Such intrinsic thermoacoustic feedback can be strong enough to become unstable [10, 20].

In an alternative scenario, the acoustic fluctuations $u'(\mathbf{x}_r, t)$ are not caused by the heat release itself, but are an indirect feature of the heat release: convected vorticity and/or entropy waves [45] interact with (non-quiescent) flow regions, such as the strong contraction towards the first stage of a turbine [13, 22]. If one wants to focus on such effects, these interactions can be described/modeled additionally by relaxing the presented assumptions.

In this dissertation, intrinsic feedback and indirect sound sources are not considered, because thermoacoustic instabilities in industrial gas turbines are typically caused by an acoustic eigenmode with direct feedback from the heat release of the perturbed flame(s).

2.6 Nonlinearities

When $\Re(\beta) > \alpha$ the thermoacoustic eigenmode would exponentially grow in the linearized case stipulated above. This would then quickly violate one of the instances where small fluctuations were assumed, invalidating the solution. The acoustic propagation remains valid for quite high amplitude (as long as $p' \ll p_0$, $\rho' \ll \rho_0$ and $|\mathbf{u}'| \ll c$). The heat release response on the other hand might be prone to nonlinearities as soon as $|\mathbf{u}'| \approx u_0$, where u_0 is some local mean flow velocity near the reference location[19]. Alternatively, the heat release fluctuations are limited

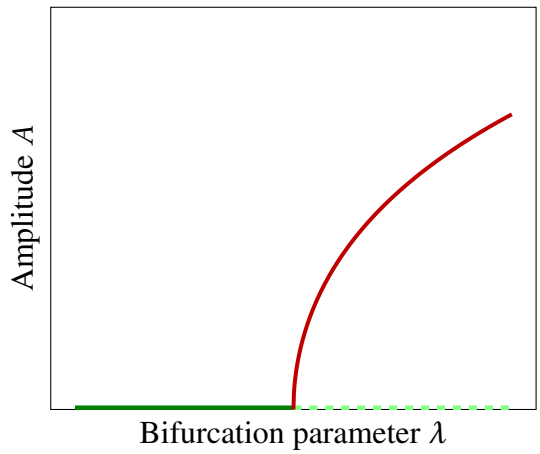

Figure 2.1: supercritical bifurcation $\dot{A} = A(\lambda - A^2 - 0.1A^4)$

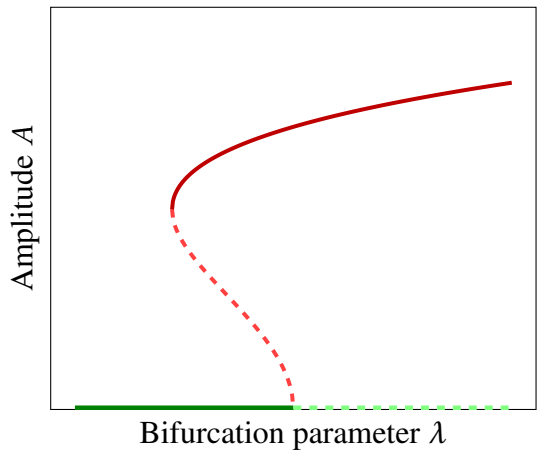

Figure 2.2: subcritical bifurcation $\dot{A} = A(\lambda + A^2 - 0.1A^4)$

by the total available heat power $\dot{Q}' \leq \dot{Q}_0$ entering the system. Furthermore, acoustic impedances of perforated structures may change, affecting α. Sooner or later, the losses will balance the growth rate, resulting in a finite limit cycle amplitude.

2.6.1 Bifurcation

When the solution of a thermoacoustic system crosses the imaginary axis (from the negative real to positive real) and nonlinear balancing terms force the amplitude to a limit cycle solution, this is known as a Hopf bifurcation. Starting with the ODE for the pressure 2.21, nonlinear restoring forces can be introduced by any even function of the amplitude A.

$$\dot{A} = A\left(\lambda + a_1 A^2 + a_2 A^4\right), \tag{2.23}$$

where $\lambda = (\beta - \alpha)$.

Two examples with solutions of $\dot{A} = 0$ are shown in figure 2.1 and 2.2. The fourth order coefficient is used to limit the amplitude by setting $a_2 = -0.1$. The quadratic order term a_1 is set positive and negative unity, respectively, to demonstrate a subcritical and a supercritical bifurcation as main transitions classes between the fixed point solution and the limit cycle. The amplitude is counteracted by the quadratic term in the supercritical case, yielding a continuous relationship between the bifurcation parameter and the amplitude. In case of a subcritical bifurcation the driving source is (initially) increasing with amplitude. This causes both a discontinuity of the amplitude and hysteresis, as multiple solutions for the amplitude are present for certain values of the bifurcation parameter.

2.7 Eigenvalue solution

Solutions of linear dynamic systems with arbitrary degree of freedom are obtained by solving the eigenvalue problem. Let the change of the state vector $\mathbf{q}$ be described by the matrix $\mathbf{A}$.

$$\frac{\mathrm{d}\mathbf{q}}{\mathrm{d}t} = \mathbf{A}\mathbf{q} \tag{2.24}$$

The evolution of the system released with initial state $\mathbf{q}(0)$ is given by

$$\mathbf{q}(t) = \mathbf{q}(0)e^{t\mathbf{A}}. \tag{2.25}$$

which can be readily evaluated for particular initial conditions $\mathbf{q}(0)$, but does not reveal any general information about the behavior of the system. For example, it may be hard to deduce whether the system is bounded (i.e. stable) by inspection of the transient dynamic evolution from some arbitrarily chosen initial condition.

Solutions of the form $\mathbf{A}\mathbf{v} = \lambda\mathbf{v}$ with scalar λ are of interest, because the rate of change is collinear with the current state and the relative rate of change will remain constant. In other words, these are invariant solutions of the system.

$$(\mathbf{A} - \lambda\mathbf{I})\mathbf{v} = 0 \tag{2.26}$$

The scalar values λ are eigenvalues and the corresponding bases $\mathbf{v}$ are the eigenvectors of the eigenvalue solution. For nonzero eigenvector $\mathbf{v}$, solutions for λ are found by solving the characteristic polynomial given by $\det(\mathbf{A} - \lambda\mathbf{I}) = 0$.

For complex λ, the real and imaginary part represent the growth rate and oscillatory frequency of the eigensolution, equivalent to $(\beta - \alpha)$ in section 2.5. Any initial state of the dynamic system might be written with the eigenvectors as basis. The solution is readily obtained by the sum of all analytic eigensolutions.

2.8 Nonnormal growth

A linearized dynamic system with all complex eigenvalues located in the left-half plane is stable. It is often assumed that the energy in the system decays with the least negative eigenvalue or faster, for all possible initial conditions. This is, however, only true for systems that commute with themselves, i.e. in which all eigenvectors are orthogonal to each other. Figures 2.3 and 2.4 show a textbook example of transient growth of a linear system. Two eigenvectors in 2d space have a relative angle of 150°, i.e. are strongly nonnormal. Consider the evolution of the system with both vectors initially unity and eigenvalues of $\lambda_1 = 1s^{-1}$ and $\lambda_2 = 10s^{-1}$. The effective amplitude of $\mathbf{v}_1 + \mathbf{v}_2$ is smaller than either of the contributions as the nonorthogonality allows amplitudes to cancel. When one of the two solutions quickly decays

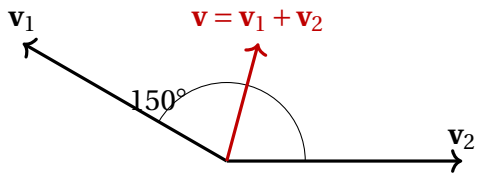

Figure 2.3: Two non-orthogonal eigenvectors, with cancelling initial conditions

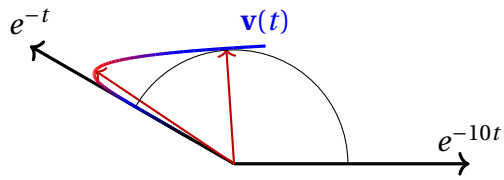

Figure 2.4: Evolution of the system, showing how the decay along $\mathbf{v}_2$ causes an increase in amplitude.

the canceling is reduced and the solution climbs up the slower decaying vector, yielding a transient growth in energy.

Linearized systems of equations describing thermoacoustics are usually not normal. Considering the acoustic energy, it is not surprising that transient growth can occur, as the flame acts as an acoustic source. Initial acoustic conditions can be chosen to have energy localized at the reference location to which the flame response is sensitive, activating the acoustic source and amplifying the acoustic energy. The strength of transient growth is strongly related to the energy norm chosen. The transient growth can be strongly reduced or eliminated by including sources of acoustic energy in the energy norm of the system [4].

Nonnormal transient growth was brought to attention in relation to nonlinear effects described in 2.6. It was postulated that transient growth from certain low energy initial conditions can trigger a subcritical thermoacoustic bifurcation, causing an amplitude jump from the fixed point stable solution to the limit cycle solution. Using low order modeling and experiments, it has been asserted that this can indeed occur[1, 27]. Triggering in thermoacoustics is analogous to bypass transition to turbulence[21] but carries less significance as the transition to a thermoacoustic limit cycle is typically assisted by linear instability.

2.9 Stability margin approaches

Current research on thermoacoustic monitoring focuses on real-time prediction of instability, rather than quantifying whether the current level of oscillations is permissible. When high oscillation levels can be avoided, reduction of component life does not have to be accounted for. In case of a subcritical bifurcation (refer to figure 2.2) the increase of amplitude can be very sudden and the hysteresis may make it hard to stabilize the dynamics again. Conversely, predictive tools can allow operators to approach the stability limit more closely, extending the operating window of the combustion system.

In industrial applications it is unusual to have an option to excite the thermoacoustic system. As a result, stability margins are based on output-only quantification, relying on the reading of installed dynamic sensors. Output-only identification of stability margin measures can be

categorized in two main branches; fitting the data to a linear model and nonlinear data analysis.

2.9.1 Linear decay rate

In the stability analysis of linear systems, it is common practice to solve the eigenvalue problem of the dynamic system. The real part of the eigenvalues $\Re(\lambda)$ constitutes the growth rates of the eigensolutions. As the name suggests a positive growth rate gives rise to exponentially growing solution, which is referred to as an unstable solution.

$$A(t) = A(0)e^{\lambda t} \tag{2.27}$$

A negative growth rate implies that any perturbation of the modal vector will exponentially decay back to zero. The special case of $\Re(\lambda) = 0$ is marginally stable; There is neither amplification nor decay and a perturbation will be conserved. Where the eigenvalue contains an imaginary part, it describes the additional oscillating frequency of the solution. In the absence of energy sources, a dynamic system is characterized by dissipation and growth rates that are never positive. This encourages the usage of the equivalent terms damping rate and/or decay rate $-\Re(\lambda)$.

The decay rate is a natural measure for stability. It is readily obtained from linear models and yields a qualitative measure for the stability of the system. The point at which the system changes from stable to unstable is well defined: at the marginally stable point $Re(\lambda) = 0$. An estimate of the linear decay rate from measurements can be obtained with several different approaches [24, 28, 32, 44]. Estimating the decay rate without perturbation input (output only) and calculating the estimate in real-time reduces the number of available methods.

Output only identification methods of the linear decay rate rely on the condition that the eigenmode of interest is excited by a broadband process. In case of turbulent combustion such excitation is provided. In general the frequency spectrum of the excitation is smooth enough to locally consider it to be white noise.

In a further step, the decay rate can be projected on the governing operating parameters. For example, the distance to instability could be expressed in terms of MW load increase, holding all other parameters equal. To achieve this, an online sensitivity analysis would be required, in which the change in stability is monitored while perturbing the operating parameter of interest.

Modeling the dynamics in more detail introduces additional uncertainties due to the model assumptions. It also requires a significantly longer identification time for output-only identification due to the increasing number of system parameters to be estimated. For industrial combustion systems, it is currently considered infeasible to identify how each change to the system affects the stability estimation.

2.9.2 Nonlinear data analysis

An argument against stability margins derived from linear theory is that combustion processes inherently contain nonlinear dynamics. For one, the combustion is continuously perturbed by upstream turbulence, a deterministic nonlinear phenomenon. Furthermore, when the amplitude rises, effects emerge that cause saturation as discussed in section 2.6. In fact, there may be many other nonlinear processes that influence the observed dynamics and might deteriorate attempts to fit a linear model to the data, depending on the application at hand.

In nonlinear data analysis, a measured signal is considered to come from a multidimensional nonlinear dynamic system. The states that such a system may assume can be represented geometrically by an attractor in a phase space that possesses at least as many dimensions as the system variables. Following Takens theorem [46], a single signal from a nonlinear system can be used to build a phase space by considering delayed versions of the signal as independent signals. Subsequently, properties of the obtained multidimensional attractor can be used to define stability measures.

A simplified nonlinear system representing cellular (Rayleigh-Bénard) convection, formed the basis of the Lorenz attractor [26]. This three-dimensional system of equations is used to demonstrate the chaotic behavior of a strange attractor. The attractor in 3d phase space is shown in its physical variables in Figure 2.5. All points on the attractor correspond to a unique state of the system, i.e. there are no crossing trajectories in 3d space. However, the evolution of two arbitrarily close points will eventually diverge and follow very different trajectories; popularly referred to as the butterfly effect.

Imagine the Lorenz system is describing some dynamic system and the only parameter we can measure is the third variable L_z. This chaotic signal becomes structured again in a 3d phase space after two other variables are defined as time delayed versions of the measured variable, see Figure 2.6. When the time delay is chosen well, it is observed that there are indeed no trajectory crossings.

The stability margin methods that use nonlinear data analysis quantify the predictability or conversely the unpredictability (chaos) of the data. Turbulence and noise show high-dimensional behavior which is related to a stable system, whereas the self-organized dynamics of a limit cycle can be embedded in a low-dimensional phase space. Several stability margins have been proposed based on nonlinear data analysis. Most methods focus on close neighbors (points that are close to each other in phase space) using recurrence quantification analysis. A very chaotic system would show merging and diverging of trajectories on a short time scale. The divergence of trajectories in phase space is directly related to the Lyapunov exponents, i.e. the linear rate of separation of nonlinear trajectories that are near to each other.

Measures also exist that do not rely on phase space embedding, but use the multifractal or chaotic property of turbulence in conjunction with the nonfractal, orderly behavior of limit

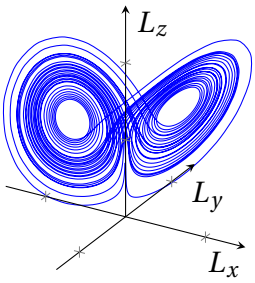

Figure 2.5: Lorenz attractor, original variables in 3d phase space

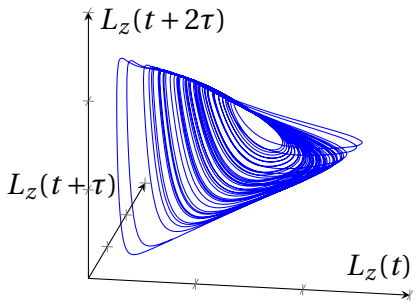

Figure 2.6: Lorenz attractor, embedded phase space of L_z

cycle oscillations. A list of existing stability margin methods is included in section 3.3 where the individual methods are discussed in more detail.

Chapter 3

Combustion stability monitoring and control

During development of combustion systems it is possible to analyze the dynamic behavior in detail and relate it to expectations from experience and/or modeling of thermoacoustics. Flame transfer functions (FTFs) or flame describing functions (FDFs) are determined, dynamic pressure fluctuations are measured and heat release indicators are obtained optically.

Once a gas turbine is commissioned and running within its operability window, it is no longer subject to detailed tests and instrumentation is kept to a bare minimum for monitoring purposes.

3.1 Monitoring in the field

Historically, combustion systems have a specified operating range where they can be safely operated for a certain amount of running hours and/or starts. The operating range can be restricted as necessary such that high amplitude combustion dynamics that could limit the operability are excluded.

In recent years, pollution emissions (NO_x in particular) have been reduced significantly with the introduction of lean premixed combustion in gas-fired power plants. At the same time, this approach has increased the susceptibility of the system to combustion dynamics, negatively affecting gas turbine reliability and availability [25]. As a result, monitoring combustion dynamics online on heavy duty land-based gas turbines has become common practice.

The standard method for monitoring is to acquire the acoustic amplitude in the combustor for a discrete set of frequency bands. Operating conditions with high amplitude can be mapped and avoided or reduced in future instances. This can be sufficient when the limit cycle amplitude can be sustained for longer periods without damage. Such a strategy could be included in an automatic tuning system [25] where the operating parameters are automatically optimized on a constant basis. In cases where thermoacoustic instability issues affect the operability range or

maintenance interval significantly, other measures need to be considered. This includes passive control, active instability control and online stability margin measures.

3.1.1 Instrumentation

Typically, the instrumentation on gas turbines is limited to the sensors required to ensure specified fluctuation levels are not exceeded. Of the fluctuating quantities in thermoacoustic oscillations, the dynamic pressure is overall the most viable choice for monitoring; the sensors are relatively robust, inexpensive and easy to install and the pressure fluctuations are of direct relevance for fatigue of combustor components. Depending on gas turbine geometry and sensor specifications, the sensors are usually installed in a location that represents the acoustic fluctuations in the combustion chamber. A mount slightly upstream of the burners yields good proximity under the limitations of thermal management.
Installing more instrumentation to monitor combustion dynamics on an entire fleet of a gas turbine type is currently not considered economically viable. Taking in consideration that the instrumentation needs to be highly robust and long-lived, many sensors used in a test environment are not suitable for industrial application. For instance optical access to the hot gas path (e.g. flow visualization, surface temperature measurements or heat release determination) would require major hardware modifications and periodic cleaning of optical elements.

3.1.2 Real-time capability

Besides the sparse instrumentation on industrial combustion systems, the need for real-time processing of the data is a constraint for more advanced monitoring algorithms. With real-time, it is meant that the average calculation time per incoming data point does not exceed the sampling period, in order to ensure that the processing can keep up with the data acquisition. When the output of an algorithm returns a parameter estimate of the system with a constant delay (for example because averaging is required), this is still regarded to be real-time.

Dynamic measurements of thermoacoustics involves a data rate of roughly 10 kHz per sensor. It is important to extract the relevant information from the data stream quickly and efficiently in order to perform the intended processing without overloading the digital signal processor (DSP) of the data acquisition hardware. With the current clock speed of DSP's, many types of analysis can be performed in real-time. More problematic are iterative methods, such as root-finding algorithms of high-dimensional dynamic systems, as the number of required arithmetic operations is not fixed/known.

Typical averaging and filtering methods for real-time applications include recursive methods, such as exponential moving average (EMA) and infinite impulse response (IIR) filters respectively. These recursive methods require significantly less data points in memory and less arithmetic operations to achieve a similar outcome to the more conventional counterparts simple moving average (SMA) and finite impulse response (FIR) filters.

3.2 Instability control

Severe instability issues due to thermoacoustic oscillations require a better solution than to stay well clear of the hazardous operating range and monitor the amplitude as a back-up net. With an appropriate understanding of the physical system it is possible to solve the instability problem through passive or active control without a total redesign of the combustion system.

3.2.1 Passive control

Passive control aims to control the instability issues by making targeted hardware or process adaptations. The aim is to stabilize a specific instability without the need to redesign the system. A typical solution is the installation of acoustic dampers that attenuate acoustic energy at the frequency of the instability [5]. The damper results in an additional outward flux of acoustic energy in equation 2.20 that negates the Rayleigh source term and therewith stabilizes the system. Alternative approaches change the dynamics of the flame, for example by modification of the burner outlets [3]. Another possibility is open loop control, in which the flame dynamics changes through continuous excitation of the air upstream of the burner [15]. Passive control stabilizes a specific mode by purposely changing the dynamics of the system. It is possible that these changes inadvertently affect other modes as well.

3.2.2 Active control

A more drastic approach makes use of active instability control (AIC) [43]. An actuator and control loop is required to actively dampen the oscillations, such that stable operation is possible under otherwise unstable operating conditions. For favorable control authority, the heat release fluctuations are controlled at the frequency of the impending instability by modulation of the fuel injection. The phase delay between the acoustics and the heat release modulation is critical, as it determines whether the added contribution to the Rayleigh source term (equation 2.20) is positive or negative. An AIC system can stabilize instabilities at different frequencies, making it a flexible and robust solution. Nevertheless the use of active control is avoided in industrial power plants partly due to the complexity and additional moving parts.

3.3 Existing stability margins

A stability margin for online monitoring of thermoacoustics in industrial applications is limited by the following considerations:

- Availability of only a few pressure transducer sensors, typically one per can or a few around the circumference of an annular combustor.
- No means to perturb or control the combustion process, i.e. output-only determination of the stability margin.

- Computational complexity to be kept low to allow continuous real-time evaluation.
- Robustness: repeatable results required on time scales from 1 second to multiple years.

3.3.1 Linear system fitting

Fitting measured dynamic data to a low order linear model of the physical system is an established method. System identification is applied to obtain an estimate of the parameters of the low order model, which allows calculation of the system damping rate(s).

3.3.1.1 Autocorrelation fitting

Lieuwen proposed to fit the autocorrelation function of a time series to estimate the decay rate [24]. For a single underdamped harmonic oscillator excited by stochastic forcing of the turbulence in the system, this approach stands out by its simplicity. Nevertheless, filtering other dynamic content out of the time series and choosing the autocorrelation interval used for fitting are not trivial. There have been attempts to optimize the fitting process of the exponential decay by replacing the least square fitting by a more sophisticated approach [44]. Fitting the autocorrelation causes some bias towards a stable estimate as the system gets closer to marginal stability, since the autocorrelation always decays; when the time series is separated into multiple smaller segments to update the stability prediction, segments with a net growth will erroneously be interpreted as a decay and contribute accordingly.

3.3.1.2 Spectral fitting

The Q-factor and power spectrum fitting [28] are alternatives to the autocorrelation fitting. The results have a dependency on the specific Fourier transform settings, such as window size and window function. As the autocorrelation is the inverse Fourier transform of the power spectrum, these methods are essentially equivalent to Lieuwen's method.

3.3.1.3 Other

The thermoacoustic decay rate may also be deduced from the dynamics of the envelope of the oscillating signal. Noiray has employed the conditional probability of the envelope evolution to fit the parameters of the Focker-Planck equations [32], where the linear contribution of the convection coefficient is an estimate of the growth rate.

3.3.2 Nonlinear stability margins

As introduced in section 2.9.2 stability margins have been proposed that do not use the assumption of linear behavior of the thermoacoustic system. These methods use the geometry of

the attractors in a phase space embedding, or a measure of the chaos or predictability of the measured time series.

3.3.2.1 Phase space methods

An example of a phase space method is the translation error proposed by Gotoda et al.[16], describing the divergence rate of close neighbors after a certain evolution time. When the neighbors quickly separate from each other the dynamics is rather chaotic, indicating dominant turbulent forcing. An impeding instability on the other hand results in more predictable path through the phase space with neighbors staying close together.

The recurrence plot is a tool that builds upon the near neighbors in a state space, showing whether every pair of two measurements are close neighbors in a 2d plot. The shapes in such a plot reveal whether the dynamics is chaotic, is in a limit cycle or shows signs of intermittency. Multiple measures can be constructed from the recurrence plot to serve as a stability margin, as proposed by Nair et al.[31].

Choosing the embedding dimension for the phase space methods is not a trivial task. Following a vast amount of neighbors through a high-dimensional phase space is a rather costly computational task which is not feasible in real-time. When the dimensionality of the phase space is reduced, false neighbors may be selected as they are near only because of the projection on a too low dimension.

3.3.2.2 Entropy (information theory) methods

Measures also exist that assume a nonlinear underlying dynamical system, but do not rely on phase space embedding. These methods use the multifractal or chaotic property of turbulence and the nonfractal property of limit cycle oscillations. Bypassing the computationally costly phase space reconstruction makes real-time application of nonlinear data analysis methods more feasible.

Nair et al. proposed to use a test developed by Gottwald and Melbourne to distinguish between regular (periodic / quasi-periodic) and chaotic dynamics [17, 30] in time-domain. Even though it was designed as a binary test, the region between stable and unstable thermoacoustics is characterized by a smooth transition.

A similar method introduced by the same research group uses the Hurst exponent as a stability margin [29]. This method also differentiates between chaotic dynamics and regular dynamics, by quantifying the multifractality. The Hurst exponent is a scaling factor for the variability of the time signal as a function of the time scale. When the time signal becomes periodic, the Hurst exponent approaches zero.

3.4 Annular combustion systems

Gas turbine combustion chambers are located around the main shaft between the axial compressor and turbine. In most cases, a discrete number of combustion chambers (cans or silos) is utilized, where acoustic interaction between the combustion chambers is impossible. Annular combustion systems on the other hand only utilize a single combustion chamber; an annulus around the shaft. From a thermoacoustic perspective, these gas turbines are fundamentally different, because acoustic waves can propagate azimuthally. Can-annular designs and can-type gas turbines with cross-firing tubes find themselves in between annular and can-type gas turbines, with constrained azimuthal propagation of acoustics.

None of the stability margin methods mentioned before specifically address azimuthal thermoacoustic modes. In fact, the majority of existing stability margin measures (implicitly or explicitly) assume that a measurement is performed statically with respect to the thermoacoustic mode shape. In annular combustion systems, however, azimuthal modes are not spatially fixed due to the circular (or rotational) symmetry of the annulus. The low frequency azimuthal thermoacoustic eigenmodes in annular systems are therefore particularly prone to instability [23]. For a perfectly symmetric system, a certain standing wave solution rotated around the circumference by any angle would be a valid solution too. A combination of such rotated solutions is also a possible solution by itself, rendering the mode shapes indeterminate: it can form standing waves with the nodes at any circumferential location, but also traveling (spinning) waves in clockwise and anticlockwise direction and any combination thereof.

Annular gas turbines are designed to be (very close to) rotationally symmetric, therefore the azimuthal mode shapes are not fixed [12, 48]. This poses a challenge in defining an appropriate stability margin for annular gas turbines that has not been addressed before.

3.4.1 Rotational symmetry

Annular combustion chambers typically have a discrete set of burners distributed equidistant around the circumference. Therefore, the geometry of an annulus with N burners corresponds to an N-fold rotational symmetry. Nevertheless, circular symmetry can usually be assumed without affecting the modeling results for low azimuthal mode order m (the amount of wavelengths around the circumference of the annulus). For $N \geq 2m$ a discrete set of identical burners does not cause any eigenvalue splitting for the modal solution with mode order m, provided the system is linear. Consequently, the heat release can be considered to take place on a continuous line through the annular combustion chamber. Replacing the burner-based network model description by a continuous analytic description of the physics is therefore justifiable [11]. For non-linear limit-cycle behavior, the eigenvalues do split for $N \geq 2m$ through an amplitude dependent heat release response, allowing solutions of either the standing or the traveling kind [14].

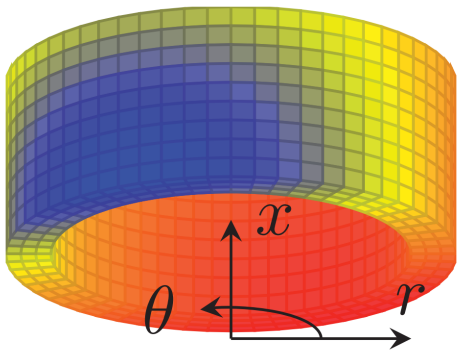

Figure 3.1: Three-dimensional example of the acoustic field in an annulus, reproduced from [39]

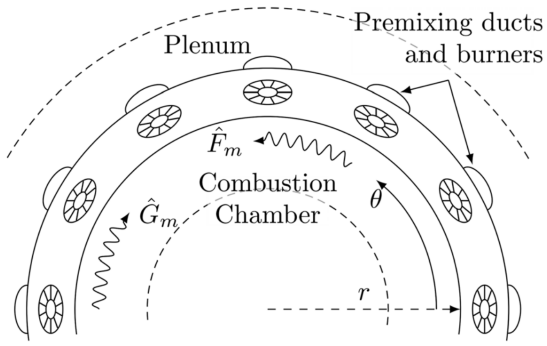

Figure 3.2: Propagation of the azimuthal waves F and G, reproduced from [40]

3.4.2 Degeneracy

Adopting the low-order modeling strategy outlined in chapter 2, the acoustic solution in an annular geometry is described by clockwise and anticlockwise waves. A generic full 3-dimensional acoustic solution of the Helmholtz equation (i.e. the wave equation 2.8 in frequency domain) can be written as follows:

$$p'(\mathbf{x}, t) = \Psi(x, r)\Phi(\theta)e^{i\omega t} \tag{3.1}$$

In which $\Psi(x, r)$ describes the axial and radial dependency of the acoustic field, fully defined by their respective boundary conditions for the frequency ω. An example of a three-dimensional acoustic solution in an annular geometry is shown in figure 3.1. The azimuthal dependency contains the two waves traveling around the circumference which can take any complex value as initial conditions.

$$\Phi(\theta) = Fe^{-im\theta} + Ge^{im\theta} \tag{3.2}$$

Propagation of these azimuthal components of the acoustic field in the annular combustor is sketched in figure 3.2. As these acoustic waves pass the burners, they affect the heat release and close the feedback loop. If the combustion system possesses mirror symmetry in addition to the rotational symmetry the heat release response to F and G must be identical. This can be violated by burners with co-rotating swirlers. It is established that the dominant coupling is caused by an induced axial flow at the burner at the moment a transverse rarefaction wave has passed [42]. This implies that the heat release response to both waves is identical at the first approximation, even in case of co-rotating swirlers.
When the acoustic amplitudes F and G in equation 3.2 decay with the same rate and generate an identical heat release response, the thermoacoustic system is 2-fold degenerate [47]. Eigensolutions of the azimuthal modes result in repeated eigenvalue pairs.

3.4.3 Symmetry breaking

Even though gas turbines are predominantly designed symmetrically, there are several processes that can cause this symmetry to break. Some possible causes are given in the following non-extensive list.

- Assembly margins, causing a θ-dependency for acoustic propagation
- Struts, baffles or heat sinks around the circumference
- Co-rotating swirlers in the burners
- Azimuthal bulk flow
- Varying flame response for the burners
- Azimuthal varying distribution of wear and fouling

In general these effects do not split the eigenvalues enough to observe two distinct peaks in the power spectrum of a measurement of the system. However, a very small split in the growth rate may well be significant since the (thermo)acoustic oscillations of interest are typically strongly underdamped: $\zeta \ll 1$, i.e. $\alpha - \Re(\beta) \ll \omega$.

3.4.4 Consequences for stability margins

Fitting a double-oscillator system for azimuthal modes with a model for a single oscillator will inevitably introduce errors in the damping estimate when eigenvalue splitting occurs. Consider a stochastically forced degenerate orthogonal pair of azimuthal waves of mode order $m = 1$ and an azimuthal bulk flow motion that gently rotates the acoustic field. When measuring the acoustic field at a fixed azimuthal position, a frequency split will be observed as a result of the Doppler effect: $\omega = (1 \pm M)\omega_0$. Determination of the damping α by fitting a single oscillator model will fail for $\zeta \approx M$ as the time scale of the frequency split is equal to the time scale of the exponential decay. With $M = \mathcal{O}(10^{-2})$ [48], this will be the case for very under-damped oscillations, where the need for an accurate stability margin measure is critical. Estimating the damping from the Q-factor will yield an overestimation of the damping as the two superimposed resonance peaks are wider than a single resonance peak. Fitting the envelope of the autocorrelation function will fail as a result of the beating phenomena.
Without eigenvalue splitting we have

$$R(\tau) = \cos(\omega t) e^{-2\alpha t} \tag{3.3}$$

which can be fitted to obtain α by application of the Hilbert transform [24], see figure 3.3. With frequency splitting through azimuthal bulk flow the autocorrelation takes a different form.

$$R(\tau) = \cos(\omega t)\cos(M\omega t) e^{-2\alpha t} \tag{3.4}$$

The beating adds a slow modulation to the autocorrelation such that the decay of the envelope cannot be fitted by a decaying exponential. Refer to figure 3.4 to see the beating phenomenon

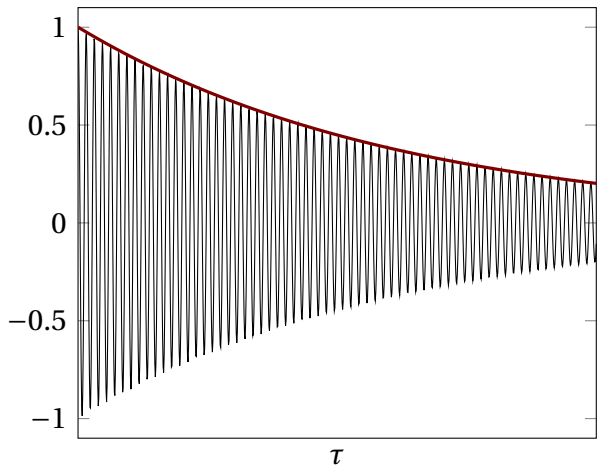

Figure 3.3: Decay of synchronized damped harmonic oscillators with $\zeta = 0.002$

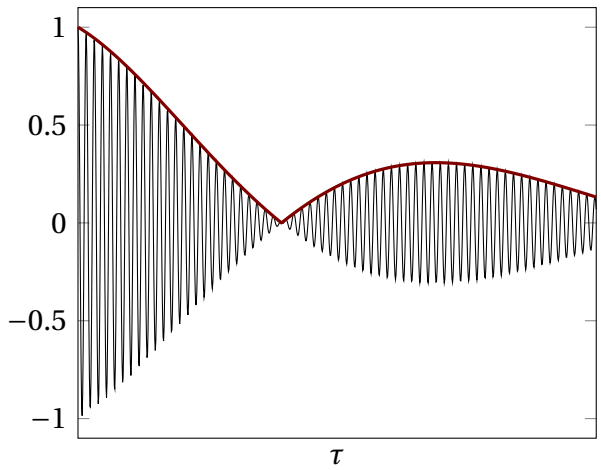

Figure 3.4: Decay of beating damped harmonic oscillators with $\zeta = 0.002$ and $M = 0.01$

in the autocorrelation, caused by a frequency split as a result of an azimuthal bulk flow of $M = 0.01$. A split in the decay rates affects the autocorrelation too, rendering autocorrelation fitting unsuitable for decay rate estimations of azimuthal modes.

Similarly, methods based on nonlinear data analysis are prone to a bias towards higher damping as soon as the symmetry of the system is broken. The superposition of two similar but distinct oscillators reduces the predictability of a time series, when compared to a single oscillator or degenerate pair of oscillators. Moreover, note that many wave number combinations (including mode order m) coexist in combustion systems. The more modes coexist, the higher the stability margin will be. For linear methods, these modes can generally be separated in frequency domain and fitted independently. Applying a linear filter in nonlinear analysis on the other hand may strongly affect the stability margin measure as the geometry of the manifold is deformed.

Chapter 4

Summary and Discussion of Achievements

In this chapter, the relevant publications for this dissertation are successively summarized. The author contributions are specified and the publication details are included.

The publications have contributed to subjects centered around the research objective: Development of a thermoacoustic stability margin measure for annular combustion systems. They cover stability margins in general, modeling of azimuthal thermoacoustics and output-only stability identification. The developed methodology was used to demonstrate eigenvalue splitting in a laboratory setup and was successfully implemented in an industrial application.

The first publication contains an exploration of existing stability margin methods that are proposed for thermoacoustic stability. These methods have been validated on separate data sets and test rigs, which do not allow for a comparison based on a literature review. A central question the work addresses is whether techniques from nonlinear data analysis (see section 2.9.2) can provide a significant contribution in early recognition of thermoacoustic instability. It is concluded that the capability of these methods to provide a stability margin is not primarily related to nonlinear behavior in the dynamics. The absence of a rigorous linear approach for azimuthal thermoacoustic modes steered this research in the direction of linear decay rate estimation in annular gas turbines.

The second publication proposes a method to identify the linear decay rate of an azimuthal thermoacoustic mode, based on multiple pressure sensors around the circumference of the combustion system. The method follows from low-order modeling of azimuthal modes, similar to previous publications including Noiray et al. [33] and Bauerheim et al. [2]. The resulting generalized state space representation of the dynamics is suitable for system identification and determination of the decay rate using available techniques. The low dimensional description allows for real-time application and is shown capable to follow slowly changing system parameters through recursive averaging techniques. The method is capable of identifying the decay rate of an azimuthal mode when symmetry breaking occurs, without prior knowledge of the resulting modal type (ie. standing and traveling) and orientation (angle and direction). Other available stability margin methods can not handle such modes, as the state of the system is not observable with a single time series.

The underlying dynamics of the low-order model of the proposed stability margin is further investigated in the third publication. In particular the work focuses on the interaction between an azimuthal mean flow and a non uniform burner response. A bifurcation point in the dynamic system, which was previously addressed in Bauerheim et al. [2], marks the boundary between standing and traveling solutions. It is found that the bifurcation point is characterized by collinear eigenvectors. As a result, the system shows strong nonnormal behavior (section 2.8) near this bifurcation point. When close to marginal stability, this can lead to nonnormal growth and have a significant affect on the magnitude and amplitude distribution of the acoustic fluctuations. These insights are essential to understand different behavior of stability margins that are based on decay rate and nonlinear data analysis.

The fourth publication reports about the successful industrial application of the stability margin in a pair of heavy duty stationary gas turbines. At extended part-load operation, a first order azimuthal mode comes close to the point of linear instability. The stability margin protects the machines for instability through a set of stability thresholds. Additionally, the method identifies the standing wave orientation, from which the locations of highest oscillation energy can be deduced.

In the last publication, the developed stability margin method is tested on a laboratory scale annular combustor. The experimental data of Dawson and Worth has previously been studied in detail in several publications [49, 50], mainly with regard to the limit cycle behavior. The stability margin yields a clear trend of decreasing stability while approaching the unstable operating conditions. Pronounced eigenvalue splitting is observed in the symmetric laboratory setup when the co-rotating swirl flames interact. This is a clear indication that eigenvalue splitting (symmetry breaking) is likely to occur in industrial applications.

A summary of the publications and a discussion in relation to relevant existing literature is listed in the following sections.

4.1 On the Performance of Stability Margin Measures for Thermoacoustic Instabilities in Turbulent Combustion Systems

D. Rouwenhorst, J. Hermann, R. Müller and W. Polifke, *21st International Congress on Sound and Vibration (ICSV21)*, Beijing, China, 13-17 July 2014. ISBN 978-616-551-682-2. Not peer reviewed, Scopus-Listed.
Reproduced on page 42.

Summary

This introductory work compares a selection of different existing stability margin measures on experimental data. Acoustic pressure time series of an axial instability (standing wave) were considered from an in-house laboratory burner. All methods were able to distinguish stable and unstable thermoacoustic state and added damping had a discernible effect in all cases. A test was performed to establish whether nearest neighbor methods provide particular benefits in defining stability margin measures that justify their increased computational cost.

Discussion

One of main the findings is that the hypothesis that the combustion data comes from a linear process is not easily rejected. This means that nonlinear data analysis, for the instability in the specific burner considered, will not significantly benefit from the nonlinear processes involved in the dynamic system. Although it must be acknowledged that nonlinear interactions are likely to occur between acoustics and hydrodynamics, it cannot be uniquely incorporated in a quantitative stability measure without a description that relates the nonlinearity with the stability of the system. This explains the variety of proposed precursors based on the nonlinear framework [16, 29, 31]. Nonlinearities related to saturation of the limit cycle amplitude after the bifurcation 2.6 are disregarded as the stability is already linearly unstable in this regime.

Contribution

The acquisition of experimental data for this work and the section in the manuscript regarding the experimental setup was performed in collaboration with Roel Müller. I implemented the presented analysis methods, lead the process of writing the manuscript and presented the work at the conference. Jakob Hermann and Wolfgang Polifke assisted by guiding the direction of the research and proofreading the manuscript. This publication was not subject to a peer review process.

4.2 Online Monitoring of Thermoacoustic Eigenmodes in Annular Combustion Systems Based on a State-Space Model

D. Rouwenhorst, J. Hermann and W. Polifke, *Journal of Engineering for Gas Turbines and Power*, vol. 139(2): pp. 021502, Febr. 2017. DOI:10.1115/1.4034260. Peer reviewed, Scopus-Listed.
Reproduced on page 50.

Summary

The thermoacoustic dynamics in annular combustors is modeled compactly in the form of a complex two-dimensional state-space system. When the state-space system is observable and stochastically perturbed, output-only identification can be carried out in order to obtain the pair of decay rates of the thermoacoustic eigenmodes. Different methods have been tested on artificially generated time series with dynamically changing system parameters. It is found that least square fitting of the system matrix and stochastic subspace identification yield a good trade-off between an accurate decay rate prediction while still showing a quick response to a change of the system parameters. To the knowledge of the authors, this is the first stability identification proposed for azimuthal modes in annular combustion systems.

Discussion

Inspired by the work of Noiray et al.[33], this work investigates the stability of azimuthal modes using a low-order model. Without loss of generality, traveling waves were taken as the basis of the pressure fluctuations instead of standing waves. The model was validated against the work of Bauerheim et al. [2], which used a network model[34] considering a discrete number of burners, yielding the same results as the mode order is small compared to the number of burners as explained in section 3.4.1. It is recognized that the state space representation of the dynamic model is suitable for identification of the linear stability, provided the system is observable, i.e. multiple sensors are installed around the circumference of the annulus. Although the (near-)degenerate nature of annular systems has been acknowledged by several previous authors[2, 33, 50], it hasn't been previously accounted for to identify the stability of such systems.

Contribution

As lead author, I developed the thermoacoustic state-space model and performed the validation and the system identification tests. Jakob Hermann was mainly involved in the formulation of the work and Wolfgang Polifke contributed significantly through discussion of the content and assistance during the review process.

Comment

A first (peer reviewed, Scopus-Listed) version of the manuscript was published in the *Proceedings of the ASME Turbo Expo 2016*[38].

4.3 Bifurcation Study of Azimuthal Bulk Flow in Annular Combustion Systems with Cylindrical Symmetry Breaking

D. Rouwenhorst, J. Hermann and W. Polifke, *International Journal of Spray and Combustion Dynamics*, vol. 9(4): pp. 438-451. DOI: 10.1177/1756827717715858. Peer reviewed, Scopus-Listed.
Reproduced on page 58.

Summary

This work focuses on a bifurcation in the solution of the dynamic system that was introduced in the previous publication[40]. The bifurcation lies on the transition of solutions governed by a broken cylindrical symmetry and solutions governed by a mean azimuthal flow field. Near the bifurcation point, the eigenvectors of the system are far from orthogonal, giving rise to transient growth for specific initial conditions, even though all eigenvalues are fixed point stable. It is found that the acoustic field is strongly influenced by the non-normality of the system when stochastic forcing is applied. The eigenvalues are more sensitive to the system parameters. The work shows a very insightful case of the transient growth, in which a mean flow rotates the acoustic field temporarily into an unstable orientation.

Discussion

Nonnormality has been a topic of interest with regard to nonlinear tripping of an instability in case of a subcritical bifurcation[1]. However, the probability for the initial perturbation for maximum amplification to occur is typically low and the maximum amplification is rather dependent on the chosen energy norm[4]. Yet, for azimuthal modes and in the light of stability margins, nonnormality is shown to have a relatively large potential impact. At the bifurcation point of an azimuthal mode, the *average amplitude* can be several times higher compared to the normal counterpart with equal eigenvalues. The stochastic distribution of the amplitude of the process moves from a χ_4 towards χ_2 for strong non-normality close to instability. This corresponds to increased predictability and thus typically a reduced stability margin for nonlinear data analysis methods, see section 2.9.2.

Contribution

The outline of this work was conceived after studying the properties of the state-space representation of the annular thermoacoustic system. I performed the analysis and led the writing and review process. Wolfgang Polifke and Jakob Hermann helped shaping the work through substantive discussions and proofreading. A considerable contribution to the work was provided by M. Meindl, numerically solving the Euler equations that showed how a radial flow gradient can rotate the acoustic field as if a mean azimuthal flow were present.

Comment

A first version of the manuscript was published in the proceedings of the *International Symposium: Thermoacoustic Instabilities in Gas Turbines and Rocket Engines*[39].

4.4 Part-Load Limit Reduction of a Frame 9E Using a Precursor for Combustion Dynamics

D. Rouwenhorst, R. Widhopf-Fenk, J. Hermann, M. Häringer, J. Becker, J. Gerhard and J. Niedermeier, *Proceedings of the ASME Turbo Expo 2018*, Lillestrøm, Norway, 11 – 15 June 2018. Peer reviewed, Scopus-Listed.
Reproduced on page 72.

Summary

This conference publication describes the first industrial application of the developed stability margin measure for azimuthal modes in gas turbines.The field case focuses on the first azimuthal mode that becomes unstable at low load. Even though the gas turbine comprises separate individual combustor cans, cross-firing tubes enable communication around the circumference. Online monitoring of thermoacoustic stability and CO-emissions allows a dynamic detection of the part-load boundary yielding a significant extension of the load range of the gas turbines.

Discussion

Predictive stability margins have mainly been verified in the controlled environment of a laboratory setup[16, 24, 29]. This work shows that the precursor proposed in previous work[40] functions fruitfully in the field. The method is shown to robustly identify the proximity of the azimuthal mode of interest before the amplitude of thermoacoustic oscillations significantly rises. The linear approach of the method allows the bandwidth around the acoustic eigenmode to be isolated from other dynamics in frequency domain, such as blade passing frequencies from the compressor and turbine blades.

Contribution

As the lead author I wrote the manuscript and led the review process. The actual turn-down experiments were performed by the on-site co-authors: J. Becker, J. Gerhard and J. Niedermeier. Results of the Bachelor thesis of M. Häringer on the particular subject have been utilized for the present work. Thanks to R. Widhopf-Fenk and J. Hermann, the stability margin algorithm was implemented and installed on site.

4.5 In Situ Identification Strategy of Thermoacoustic Stability in Annular Combustors

D. Rouwenhorst, J. Hermann and W. Polifke, *International Journal of Spray and Combustion Dynamics*, vol. 10(4): pp. 351-361. DOI: 10.1177/1756827718799043. Peer reviewed, Scopus-Listed.
Reproduced on page 82.

Summary

In this publication the output-only identification method for the state-space model is tested on a laboratory scale annular combustor, with varying flame-to-flame distance. In particular when the flames are close together, strong eigenvalue splitting is identified, resulting in distinct decay rates as well as frequencies. For this case, the decay rates of the system develop in a non-monotonic way for increasing equivalence ratio. It is observed that identification parameters have a considerable influence on the result for experimental data. In contrast, the difference between the least square fitting and the subspace identification methods is rather small.

Discussion

The dynamics of the experimental setup has been investigated in detail [49, 50]. Using a baffle, the symmetry can be broken forcing a standing wave solution and adding more baffles the mode can be dampened [9]. Even the symmetric setup without baffles shows some symmetry breaking, seen by the coupling of CW and ACW waves in limit cycle. This work shows that eigenvalue splitting also occurs before instability, especially in case of small flame separation distances. Eigenvalue splitting of a symmetric annular test-rig during stable operation has not been demonstrated before.

Contribution

As lead author, I performed the analysis and wrote the manuscript. The experiments were carried out by N. Worth and J. Dawson, who kindly shared the measurement results for the analysis. Jakob Hermann and Wolfgang Polifke were involved from the formulation of the work to submission of the manuscript,

Comment

A first (peer reviewed) version of the manuscript was published in the proceeding of the *1st Global Power and Propulsion Forum*[41].

Erratum

An error occurred in the scaling of the ordinate of Figure 7. The damping ratios need to be divided by 200 π in order to agree with the damping ratios in the other figures.

Bibliography

[1] K. Balasubramanian and R. Sujith. Thermoacoustic instability in a Rijke tube: Non-normality and nonlinearity. *Phys. Fluids*, 20:044103, 2008.

[2] M. Bauerheim, M. Cazalens, and T. Poinsot. A theoretical study of mean azimuthal flow and asymmetry effects on thermo-acoustic modes in annular combustors. *Proceedings of the Combustion Institute*, 35(3):3219–3227, 2015. ISSN 1540-7489. doi: 10.1016/j.proci.2014.05.053.

[3] P. Berenbrink and S. Hoffmann. Suppression of Dynamic Combustion Instabilities by Passive and Active Means. In *Int'l Gas Turbine and Aeroengine Congress & Exposition, rmASME Paper*, 2000-GT-0079, pages 7–7, Munich, Germany, 2000. ASME.

[4] R. Blumenthal, A. Tangirala, R. Sujith, and W. Polifke. A systems perspective on non-normality in low-order thermoacoustic models: Full norms, semi-norms and transient growth. *Int. J. Spray Combust. Dyn.*, 9(1):19–43, 2017. doi: 10.1177/1756827716652474.

[5] C. Bourquard and N. Noiray. Stabilization of acoustic modes using Helmholtz and Quarter-Wave resonators tuned at exceptional points. *J. Sound Vib.*, 2019.

[6] L. Crocco. Aspects of Combustion Stability in Liquid Propellant Rocket Motors Part1: Fundamentals. Low frequency instability with monopropellants. *Journal of the American Rocket Society*, 21(6):163–178, 1951. doi: 10.2514/8.4393.

[7] L. Crocco and S. I. Cheng. *Theory of Combustion Instability in Liquid Propellant Rocket Motors*. Number 8 in AGARDograph. Butterworths Science Publication, 1956.

[8] F. E. C. Culick. *Unsteady Motions in Combustion Chambers for Propulsion Systems*. Number AC/323(AVT-039)TP/103 in RTO AGARDograph AG-AVT-039. AGARD / NATO, 2006.

[9] J. R. Dawson and N. A. Worth. The effect of baffles on self-excited azimuthal modes in an annular combustor. *Proceedings of the Combustion Institute*, 35(3):3283–3290, 2015. ISSN 15407489. doi: 10.1016/j.proci.2014.07.011.

[10] T. Emmert, S. Bomberg, and W. Polifke. Intrinsic Thermoacoustic Instability of Premixed Flames. *Combustion and Flame*, 162(1):75–85, 2015. ISSN 0010-2180. doi: 10.1016/j.combustflame.2014.06.008.

[11] S. Evesque and W. Polifke. Low-Order Acoustic Modelling for Annular Combustors: Validation and Inclusion of Modal Coupling. In *Int'l Gas Turbine and Aeroengine Congress & Exposition*, ASME GT-2002-30064, Amsterdam, NL, 2002. doi: 10.1115/GT2002-30064.

[12] S. Evesque, W. Polifke, and C. Pankiewitz. Spinning and Azimuthally Standing Acoustic Modes in Annular Combustors. In *Proc. 9th AIAA/CEAS Aeroacoustics Conf., Paper AIAA 2003-3182, 12–14 May 2003, Hilton Head, South Carolina*, AIAA 2003-3182, Hilton Head, S.C., U.S.A., 2003.

[13] J. E. Ffowcs Williams and M. S. Howe. The Generation of Sound by Density Inhomogeneities in Low Mach Number Nozzle Flows. *Journal of Fluid Mechanics*, 70(03):605–622, Aug. 1975. ISSN 1469-7645. doi: 10.1017/S0022112075002224.

[14] G. Ghirardo, J. Moeck, and M. Juniper. Stability criteria for standing and spinning waves in annular combustors. In *Proceedings of the ASME Turbo Expo 2015: Turbine Technical Conference and Exposition*, GT2015-43127, Montreal, Quebec, Canada, June 2015. ASME.

[15] F. Giuliani, A. Lang, K. Johannes Gradl, P. Siebenhofer, and J. Fritzer. Air Flow Modulation for Refined Control of the Combustion Dynamics Using a Novel Actuator. *Journal of Engineering for Gas Turbines and Power*, 134(2):021602–021602–8, Dec. 2011. ISSN 0742-4795. doi: 10.1115/1.4004147.

[16] H. Gotoda, Y. Shinoda, M. Kobayashi, Y. Okuno, and S. Tachibana. Detection and control of combustion instability based on the concept of dynamical system theory. *Physical Review E*, 89(2):022910, Feb. 2014. doi: 10.1103/PhysRevE.89.022910.

[17] G. A. Gottwald and I. Melbourne. Testing for chaos in deterministic systems with noise. *Physica D: Nonlinear Phenomena*, 212(1):100–110, 2005.

[18] M. A. Heckl. Active Control of the Noise from a Rijke Tube. *Journal of Sound and Vibration*, 124(188):117–133, 1988. doi: 10.1016/S0022-460X(88)81408-1.

[19] M. A. Heckl. Non-linear Acoustic Effects in the Rijke Tube. *Acustica*, 72:63–71, 1990.

[20] M. Hoeijmakers, V. Kornilov, I. Lopez Arteaga, P. de Goey, and H. Nijmeijer. Intrinsic Instability of Flame-Acoustic Coupling. *Combustion and Flame*, 161(11):2860–2867, Nov. 2014. doi: 10.1016/j.combustflame.2014.05.009.

[21] M. P. Juniper. Triggering in thermoacoustics. *Int. J. Spray Combust. Dynamics*, 4(3), 2012. doi: 10.1260/1756-8277.4.3.217.

[22] J. J. Keller, W. Egli, and J. Hellat. Thermally Induced Low-Frequency Oscillations. *Zeitschrift für angewandte Mathematik und Physik (ZAMP)*, 36(2):250–274, 1985. doi: 10.1007/BF00945460.

[23] U. Krüger, J. Hüren, S. Hoffmann, W. Krebs, and D. Bohn. Prediction of Thermoacoustic Instabilities With Focus on the Dynamic Flame Behavior for the 3A-Series Gas Turbine of Siemens KWU. In *Volume 2: Coal, Biomass and Alternative Fuels; Combustion and Fuels; Oil and Gas Applications; Cycle Innovations*, ASME 99-GT-111, page V002T02A016, Indianapolis, Indiana, USA, June 1999. American Society of Mechanical Engineers. doi: 10.1115/99-GT-111.

[24] T. Lieuwen. Online Combustor Stability Margin Assessment Using Dynamic Pressure Data. *Transactions of the ASME*, 127:478–482, 2005.

[25] T. Lieuwen and V. Yang, editors. *Combustion Instabilities in Gas Turbine Engines: Operational Experience, Fundamental Mechanisms, and Modeling*, volume 210 of *Progress in Astronautics and Aeronautics*. AIAA, 2005. ISBN 1-56347-669-X.

[26] E. N. Lorenz. Deterministic Nonperiodic Flow. *Journal of the atmospheric sciences*, 20: 130–141, Jan. 1963.

[27] S. Mariappan, R. I. Sujith, and P. J. Schmid. Experimental investigation of non-normality of thermoacoustic interaction in an electrically heated Rijke tube. *International Journal of Spray and Combustion Dynamics*, 7(4):315–352, 2015. doi: 10.1260/1756-8277.7.4.315.

[28] D. Mejia, M. M. Brebion, and L. Selle. On the experimental determination of growth and damping rates for combustion instabilities. *Combustion and Flame*, 169:287–296, July 2016. ISSN 0010-2180. doi: 10.1016/j.combustflame.2016.05.004.

[29] V. Nair and R. I. Sujith. Multifractality in combustion noise: Predicting an impending combustion instability. *Journal of Fluid Mechanics*, 747:635–655, May 2014. ISSN 0022-1120, 1469-7645. doi: 10.1017/jfm.2014.171.

[30] V. Nair, G. Thampi, S. Karuppusamy, S. Gopalan, and R. I. Sujith. Loss of Chaos in Combustion Noise as a Precursor of Impending Combustion Instability. *International Journal of Spray and Combustion Dynamics*, 5(4):273–290, Dec. 2013. ISSN 1756-8277. doi: 10.1260/1756-8277.5.4.273.

[31] V. Nair, G. Thampi, and R. I. Sujith. Intermittency route to thermoacoustic instability in turbulent combustors. *Journal of Fluid Mechanics*, 756:470–487, Oct. 2014. ISSN 0022-1120, 1469-7645. doi: 10.1017/jfm.2014.468.

[32] N. Noiray and B. Schuermans. Deterministic quantities characterizing noise driven Hopf bifurcations in gas turbine combustors. *International Journal of Non-Linear Mechanics*, 2012.

[33] N. Noiray, M. Bothien, and B. Schuermans. Investigation of azimuthal staging concepts in annular gas turbines. *Combustion Theory and Modelling*, 15(5):585–606, 2011. doi: 10.1080/13647830.2011.552636.

[34] J.-F. Parmentier, P. Salas, P. Wolf, G. Staffelbach, F. Nicoud, and T. Poinsot. A simple analytical model to study and control azimuthal instabilities in annular combustion chambers. *Combustion and Flame*, 159(7):2374–2387, July 2012. ISSN 0010-2180. doi: 10.1016/j.combustflame.2012.02.007.

[35] J. W. S. Rayleigh. The Explanation of Certain Acoustical Phenomena. *Nature*, 18:319–321, 1878. doi: 10.1038/018319a0.

[36] S. W. Rienstra and A. Hirschberg. An Introduction to Acoustics. Technical Report IWDE 92-06, Eindhoven University of Technology, 2018.

[37] P. L. Rijke. Notiz über eine neue Art, die in einer an beiden Enden offenen Röhre enthaltene Luft in Schwingungen zu versetzen. *Annalen der Physik*, 183(6):339–343, Apr. 1859. ISSN 00033804, 15213889. doi: 10.1002/andp.18591830616.

[38] D. Rouwenhorst, J. Hermann, and W. Polifke. Online monitoring of thermoacoustic eigenmodes in annular combustion systems based on a state space model. In *Proceedings of ASME 2016 Turbo Expo: Turbomachinery Technical Conference & Exposition*, GT2016-56671, Seoul, Korea, 2016. ASME. doi: 10.1115/GT2016-56671.

[39] D. Rouwenhorst, J. Hermann, and W. Polifke. Bifurcation study of azimuthal bulk flow in annular combustion systems with cylindrical symmetry breaking. In *Thermoacoustic Instabilities in Gas Turbines and Rocket Engines*, GTRE-010, Garching, Germany, May 2016.

[40] D. Rouwenhorst, J. Hermann, and W. Polifke. Online Monitoring of Thermoacoustic Eigenmodes in Annular Combustion Systems Based on a State-Space Model. *J Eng Gas Turb Power*, 139(2), 2017. doi: doi:10.1115/1.4034260. Originally published as GT2016-56671.

[41] D. Rouwenhorst, J. Hermann, and W. Polifke. In Situ Identification of Thermoacoustic Stability in Annular Combustors. In *1st Global Power and Propulsion Forum*, GPPF-2017-10, Zürich, Switzerland, Jan. 2017.

[42] A. Saurabh and C. O. Paschereit. Combustion Instability in a Swirl Flow Combustor With Transverse Extensions. page V01BT04A057, June 2013. doi: 10.1115/GT2013-95732.

[43] J. R. Seume, N. Vortmeyer, W. Krause, J. Hermann, C. Hantschk, P. Zangl, S. Gleis, D. Vortmeyer, and A. Orthmann. Application of Active Combustion Instability Control to a Heavy Duty Gas Turbine. *J. Eng. for Gas Turbines and Power*, 120:721–726, 1998.

[44] N. V. Stadlmair, T. Hummel, and T. Sattelmayer. Thermoacoustic Damping Rate Determination From Combustion Noise Using Bayesian Statistics. *Journal of Engineering for Gas Turbines and Power*, 140(11):111501, 2018. doi: 10.1115/1.4038475.

[45] L. Strobio Chen, S. Bomberg, and W. Polifke. Propagation and Generation of Acoustic and Entropy Waves Across a Moving Flame Front. *Combustion and Flame*, 166:170–180, Apr. 2016. doi: 10.1016/j.combustflame.2016.01.015.

[46] F. Takens. *Detecting Strange Attractors in Turbulence*. Springer, 1981.

[47] G. Walz, W. Krebs, S. Hoffmann, and H. Judith. Detailed Analysis of the Acoustic Mode Shapes of an Annular Combustion Chamber. *J. of Engineering for Gas Turbines and Power*, 124(3):3–9, 2002. originally published as 99-GT-113.

[48] P. Wolf, G. Staffelbach, L. Y. M. Gicquel, J.-D. Müller, and T. Poinsot. Acoustic and Large Eddy Simulation studies of azimuthal modes in annular combustion chambers. *Combustion and Flame*, 159(11):3398–3413, Nov. 2012. ISSN 0010-2180. doi: 10.1016/j.combustflame.2012.06.016.

[49] N. A. Worth and J. R. Dawson. Self-excited circumferential instabilities in a model annular gas turbine combustor: Global flame dynamics. *Proceedings of the Combustion Institute*, 34(2):3127 – 3134, 2013.

[50] N. A. Worth and J. R. Dawson. Modal dynamics of self-excited azimuthal instabilities in an annular combustion chamber. *Combustion and Flame*, 160(11):2476–2489, Nov. 2013.

Appendix

Reprints of Original Publications

This section contains reprints of the original publications. Permission to reprint for this purpose is obtained from the publisher where required. Note that the publications contain their own nomenclatures or symbol definitions that might slightly deviate from the nomenclature at the start of this dissertation.

ICSV 21
13-17 July, 2014, Beijing/China

The 21st International Congress on Sound and Vibration

13-17 July, 2014, Beijing/China

ON THE PERFORMANCE OF STABILITY MARGIN MEASURES FOR THERMOACOUSTIC INSTABILITIES IN TURBULENT COMBUSTION SYSTEMS

Driek Rouwenhorst, Jakob Hermann, Roel Müller

IfTA Ingenieurbüro für Thermoakustik GmbH, 82194 Gröbenzell, Germany,
e-mail: driek.rouwenhorst@ifta.com

Wolfgang Polifke

Lehrstuhl für Thermodynamik, Technische Universität München, 85747 Garching, Germany

Recently, the search for a stability margin quantity has been extended to the field of nonlinear time series analysis, yielding a set of measures showing a smooth transition between the stable and unstable regime of a turbulent combustion system. So far, the performance of these measures to presage instability has been tested on a few laboratory setups, without mutual comparison of the different approaches. In this work a variety of measures are tested on a laboratory scale burner for validation and comparison. An atmospheric, partially premixed methane-fueled bluff-body stabilized burner is operated at 20 kW, showing stable and limit cycle oscillation operation for varying equivalence ratio. Focus is on an early and robust detection of an impending instability, suitable for on-line monitoring. Two data sets of acoustic pressure are considered, with different acoustic damping. Monotonicity and unambiguity of the stability margins are investigated. Additionally a surrogate data analysis is conducted, showing evidence of a nonlinear underlying dynamical system. However, these nonlinearities are found to have no significant influence on the predictions by methods that are based on nonlinear time series analysis.

1. Introduction

Gas combustion technology is changing significantly, mainly because of environmental considerations and new market requirements. With lean combustion NO_x emissions are reduced substantially [1]. Near the lean blow-off limit of a combustor, the heat release rate responds fiercer to equivalence ratio fluctuations, increasing the flame response to acoustical perturbations [2]. Moreover, design considerations for lean combustors often lead to lower acoustic damping and enhanced coupling conditions between the flame and the acoustic field.

Renewable energy sources contribute substantially to the energy supply. From the conventional power generation plants, gas turbine installations are most capable of flexible operation, required to compensate for the weather dependent power coverage of wind and solar power. Increased flexibility entails increased excursions through the operating parameter space of the gas turbine, where thermoacoustically unstable regions can be encountered.

Currently, an important role is reserved for the gas turbine operator, monitoring and steering the combustion process. Besides the set operating parameters and resulting conditions, high frequently

sampled pressure and acceleration signals are usually available as well. Changes in spectral distribution can be assessed to foretell an instability based on experience.

More sophisticated methods have been proposed to obtain a stability margin, of which the first passive approach (i.e. without excitation) was proposed by Lieuwen in 2005 [3]. In his method an effective damping coefficient ζ is determined for the acoustic eigenfrequencies, utilizing the combustion noise as natural excitation of the system. The damping coefficient is obtained by fitting the exponential decay rate of the autocorrelation function of a filtered signal acquired from the thermoacoustic system.

The inherent nonlinearity of turbulent combustion systems with (delayed) acoustic feedback, led researcher to seek for measures that are able to respond to the nonlinear characteristics of combustion signals. These methods quantify the amount of chaos in the time series. Stable combustion is characterized by the chaotic signal of the turbulent flame. As the system approaches the stability limit, deterministic acoustics start to dominate the signal, until a limit cycle emerges. The degree of determinism in the signal is found to progressively increase towards limit cycle oscillation [4].

In 2011 Gotoda et al. [5] used a method to extract the determinism in a time series recorded from a swirl combustor. In a later publication this measure, named 'translation error', is explicitly referred to as a potential stability margin measure [6]. Simultaneously nonlinear methods have been explored at the Department of Aerospace Engineering at the IITM in Chennai, India. Nair et al. [4] proposed to use a chaos test developed by Gottwald et al. [7] for combustion characterization. Moreover, Nair stressed that several other measures appear suitable as smooth stability margins, including measures from the Recurrence Quantification Analysis (RQA) [8]. Most recently the multifractal signature in combustion noise at the onset of instability is investigated [9].

Absence of mutual comparison and application of the measures on different combustion systems makes it unclear which measure is most suitable to foretell thermoacoustic instabilities. The benefit of applying nonlinear time series analysis has not been clearly demonstrated either.

In this work four proposed stability margin measures have been tested: Lieuwen's damping coefficient, translation error, Gottwald's 0-1 test and RQA Determinism. The methods are mutually compared. Moreover, the results have been compared to the publications in which the measures have been proposed (not available for RQA Determinism). For details about the methods and their settings, the reader is referred to the above references.

Two slightly different acquired data sets have been put to the test, distinguished by their acoustic damping. Both sets show limit cycle oscillation and stable operation for a changing equivalence ratio. A surrogate data analysis algorithm is applied to validate whether the results of the applied methods can actually be assigned to the nonlinear features of the considered time series.

2. Experimental setup

Measurements were performed on a laboratory burner, designed to be prone to thermoacoustic instability [10]. The geometry is sketched in figure 1. Air enters the combustor at the base of the plenum. Methane is injected from small holes on the bottom sides of the prismatic triangular bluff-body, into the air flow. The partially premixed flame is anchored on top of this bluff-body flame holder. The combustion chamber is a long liner, with poorly damped longitudinal acoustic eigenmodes.

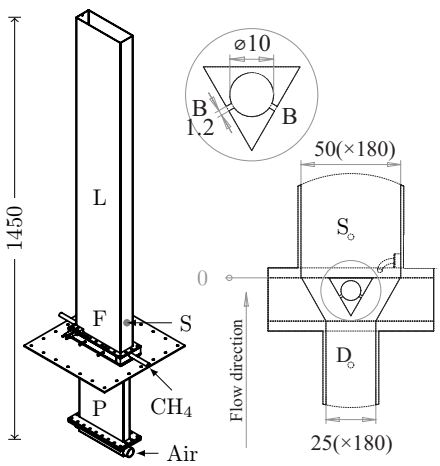

Figure 1: Burner geometry and close up of the bluff-body. Dimensions in mm. P: Plenum, F: Flame, L: Liner, B: Fuel injection holes, S: Pressure sensor, D: Damping orifices (⌀=4)

The pressure transducer is positioned in a water-cooled holder fixed in the liner, approximately 12 cm above the bluff-body location. This ensures the sensor collects the pressure to which the flame is subjected up to high frequencies. Measurement holes with a diameter of 4 mm are located along both sides of the burner. The holes 12 cm upstream of the flame holder have been opened to increase the damping in the second case.

The methane flow is fixed by a valve, such that 20 kW (lower heating value) thermal power is obtained in case of complete combustion. The airflow is controlled manually in order to vary the air excess ratio λ. Data of the operating conditions are collected approximately once a second, while pressure oscillations are sampled with 5120 Hz using a piezoelectric pressure transducer. The instability manifested is the first longitudinal mode (quarter-lambda mode) with $f_d \approx 100$ Hz.

It has to be noted that the flame at the bluff-body was not anchored properly. Temperature distributions suggest that at one side of the burner, the flame was located below the bluff-body. This indicates an unintended recirculation and a three-dimensional flow field. For the current investigation this complication of the simple thermodynamic system is not considered detrimental.

3. Nonlinear time series analysis

Turbulent combustion noise is an inherently nonlinear phenomenon, therefore it seems logical to apply techniques that respond to nonlinear dynamics, in characterizing a thermoacoustic system excited by a turbulent flame.

3.1 Phase space reconstruction

The first step consists of the reconstruction of a phase space. For a single measured time series this is done on basis of Takens' time delay *embedding theorem* [11]. It states that a phase space of dimension D_0 can be reconstructed for every dynamic system by generating the position vectors $\mathbf{X}$ by time delayed values of signal $x(t)$.

$$\mathbf{X}(i, D_0) = [x(t_i), x(t_i + \tau), ..., x(t_i + (D_0 - 1)\tau)] \tag{1}$$

Two parameters, τ and D_0 have to be fixed appropriately for the reconstruction.

3.1.1 Time delay

The time delay τ is chosen on basis of the average mutual information in this work [12]. The first minimum in the mutual information is considered the optimal time delay. This way the delayed vector locally shares minimal information with the original counterpart, while the time delay still falls well within the dominant time scale of the dynamics. The mutual information for stable combustion at $\lambda = 2.8$ yields an optimal time delay of $\tau = 2.54$ ms. This corresponds to a phase shift of $\pi/2$ of the dominant longitudinal acoustic mode (±100Hz). Note that the exact choice of τ is not very critical, and other determination methods yield approximately the same delay for the current data.

3.1.2 Embedding dimension

A *False Nearest Neighbour* method is applied to determine the dimension at which the embedding can be truncated. Embedding a dynamical system in a too high dimension can be compared to investigating a photograph from all sides, while looking at it from the front gives all the information of interest. In practice, noise in the time series will cause the points to spread over infinite dimensions in phase space, therefore a truncation criterion will have to be used.

The *False Nearest Neighbour* method of Cao [13] is adapted in this work, which makes use of two parameters E_1 and E_2.

$$E_1(D) = \frac{E(D+1)}{E(D)} \qquad \text{and} \qquad E_2(D) = \frac{E^*(D+1)}{E^*(D)} \tag{2}$$

The first parameter is based on E, a measure related to false crossings of trajectories in phase space. When trajectories cross in phase space, the intersection point has two possible dynamical states and therefore the embedding dimension of that phase space was too low. E^* is an error norm of a simple nonlinear predictor. The predictor sets the future value of a point to the corresponding value of the closest point in phase space. For a detailed description of the parameters the reader is referred to the publication of Cao [13]. When the parameter E_1 becomes independent of the embedding dimension, there would be no benefit to increase the dimension and the minimum embedding dimension D_0 is found. When E_2 is unity for all dimensions, the time series is a random distribution rather than coming from a high-dimensional system.

The Cao parameters for stable operation ($\lambda = 2.8$) are presented in figure 2 for 3.2 seconds of recorded data. The parameter E_1 slowly converges to unity, not giving a clear attractor dimension where the system could be truncated. Setting a threshold at for instance $E_1 = 0.95$, it could be asserted that most of the dynamics is captured in a 9-dimensional space.

3.2 Surrogate data analysis

Surrogate data analysis can be used to confirm or reject a hypothesis on the underlying dynamics of a time series [14]. Nair et al. [4] rejected the hypothesis that combustion noise is random uncorrelated noise, by creating randomly shuffled surrogate data sets. That there is *some* determinism in combustion noise should actually be no surprise. The question we have to ask is whether nonlinear behaviour can be demonstrated, in order to justify the use of a nonlinear framework. To this end the *Amplitude Adjusted Fourier Transform* (AAFT) algorithm is applied [15]. The algorithm is suitable to the null hypothesis that the data come from a linear Gaussian process, whether or not observed through a nonlinear measurement function.

The above determination of the minimal embedding dimension did not return a satisfying result. Ideally a dimension is found, clearly discriminating a dominant attractor from background dynamics and noise. The slow convergence of E_1 does not give this opportunity. As E_1 is supposed to respond to the attractor characteristics of the nonlinear time series, this parameter is an interesting candidate to investigate with the AAFT Surrogate data method.

3.2.1 Amplitude Adjusted Fourier Transform algorithm

In the AAFT algorithm, the phases of the real data series are randomized in Fourier domain. In general this will yield a data set with a different probability density function (pdf) of the amplitude in time domain. By iteratively enforcing the amplitude distribution and power spectrum of the real data set, the AAFT surrogate data is obtained after convergence. This algorithm ensures surrogate data sets can be discriminated from the real data neither by its amplitude distribution nor by its power spectrum, yet the dynamics have been randomized by scrambling the phase of the spectrum. The geometrical structure of an attractor will be destroyed, yielding a dimension of the order of the amount of data points considered.

When a chosen statistic of the real series falls outside of a certain confidence interval of the surrogate values, the hypothesis of an underlying linear process can be rejected. The Cao parameters are relevant candidates to affirm or negate the hypothesis since they are meant to quantify a nonlinear characteristic of the time series [15].

The result of the surrogate data analysis has been added in figure 2. The mean of 25 surrogates is shown, including 2σ deviations as an approximate 95% confidence interval. Both E_1 and E_2 fall on top of the confidence band of their surrogates counterparts. Even though it is known that the underlying physics are nonlinear, the hypothesis can not be rejected with these parameters. This means that for all we know, the combustion noise might as well be driven by a linear Gaussian process. It appears that a dimension found with the Cao method is not related to a specific shape of the

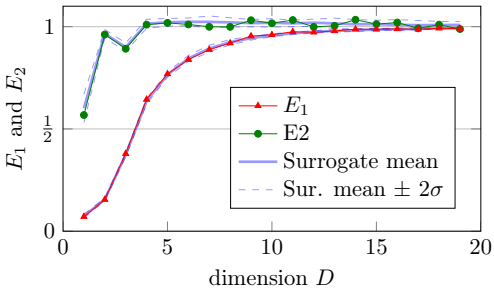

Figure 2: Cao parameters for real and surrogate data (window size = 3.2 s)

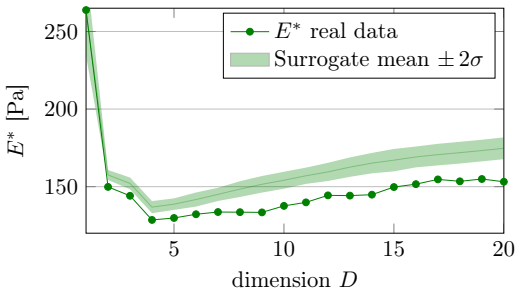

Figure 3: E^* prediction error for real and surrogate data (window size = 3.2 s)

reconstructed attractor, but is solely determined by the power spectrum and/or amplitude distribution of the signal.

The Cao parameters are ratios for increasing dimension, which seems to obscure the absolute difference between the real and surrogate data of the underlying parameters E and E^*. If the analysis is applied on E^* directly, the null hypothesis can be rejected with rather high confidence, see figure 3. For every $D \geq 2$ the real data even falls outside of a 4σ-band (> 99% confidence) around the surrogate mean values. The minimum value of E^* is found at $D = 4$, meaning that an embedding in 4D yields best predictive power. This can be explained by the fact that a prediction from a higher dimension uses an additional pressure sample further back in time, reducing the weight of the point closest (in the time series) to the value to be predicted.

4. Results

The four stability margin measures are applied to dynamic pressure time series obtained from the methane burner. Parameters for the phase space reconstruction are fixed on basis of the findings in section 3.1 and 3.2. The time delay is set to 2.54 ms and the dimension to $D_0 = 5$. Note that the latter is chosen on basis of the nonlinear predictor E^* rather than the Cao parameters. The criterion for D_0 is taken as the location of the minimum of E^* in the intermittent region.

4.1 Data sets

Two data sets are recorded along the same operating line of the bifurcation parameter. In the second run two access orifices in the plenum chamber were opened, resulting in increased damping for the low acoustic frequencies of the burner. This added damping results in effective suppression of thermoacoustic instabilities; when more orifices were opened, no limit cycle oscillation established in the studied parameter space.

The burner was operated for several minutes at $\lambda > 3$, to warm up the system and reach a steady combustion state. Subsequently data was acquired while the air flow was slowly reduced until the rich combustion limit ($\lambda \approx 0.5$) of the burner. Significant intermittency in the pressure signal is found for $\lambda < 1.6$, and transition to limit cycle occurs at $\lambda \approx 1.1$. At stoichiometric operation ($\lambda = 1$) the combustion process is unstable. Lowering λ further causes a flame to become anchored on top of the open end of the burner, resulting in an undesired (stable) combustion solution.

The limit cycle oscillations occur at slightly higher λ in the damped data set. Furthermore, amplitudes are somewhat lower as a result of the increased damping. The biggest difference is found in the intermittent region. Where the first data set shows constant humming with amplitude variation, the damped data set is quite silent with short, high amplitude bursts.

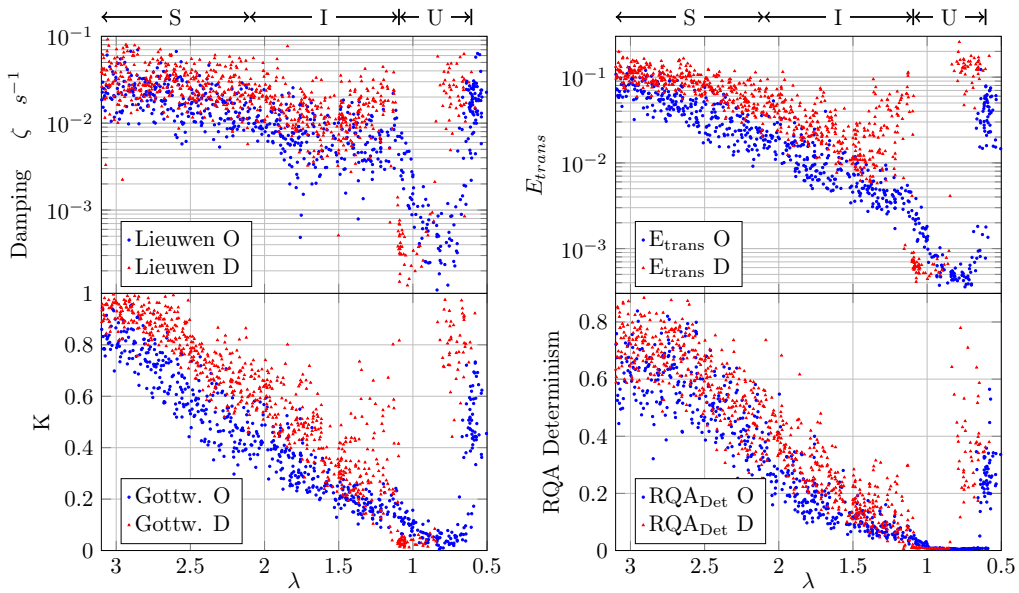

Figure 4: Stability margin results of both original (O) and damped (D) case, for the four investigated measures for slowly descending λ. Time windows of 0.8 seconds (4096 data points). Thermoacoustic state abbreviated to S(table), I(ntermittent) and U(nstable)

4.2 Response of the measures

The measures are applied to windows of 4096 data points, corresponding to 0.8 seconds with the current sample rate. An overlap of the windows of 50% is used. In order for the measures to extract useful information, enough points should be available in the windows to guarantee that the underlying dynamics can be captured. On the other hand a quick characterization of the system is required for on-line monitoring of the measures. A time delay of more than a second in a control loop is considered to become a significant impediment for operating flexibility. The slope of the bifurcation parameter is $\mathrm{d}\lambda/\mathrm{d}t \approx -0.01\,\mathrm{s}^{-1}$, such that the process can be assumed quasi-stationary.

Both the analysis of the original data series (O) and the damped series (D) are shown simultaneously in figure 4. A first overall impression of the results is that the measures clearly respond to a change in the equivalence ratio, however, a lot of variation in values for the measures is encountered. The damped data set generally results in higher values, as to be expected for more stable operation.

For both cases, the damping coefficient does not show a very clear trend throughout the intermittent region, but only discriminates limit cycle oscillation clearly. Strikingly the path towards the unstable region is not a monotonic decreasing function for the damped data set. The order of magnitude of the damping coefficient and the general behaviour of this measure agree with the original work by Lieuwen [3]. The fluctuations found in this work are much more pronounced, but the signal length considered and amount of averages are not mentioned by Lieuwen.

The logarithm of the translation error is found to be predominantly linear with respect to λ for the first data set. Transition from high amplitude intermittency to limit cycle oscillation is characterized by a further drop to a constant value. Tachibana et al. [6] found a more clear transition between stable and unstable operation, comparing their translation error with a damping coefficient based on the peak width of the considered frequency. This observation (made for a swirl combustor) is now shown to hold for the bluff-body combustor in this work. In this statement it is assumed that damping coefficient estimates from peak width and autocorrelation decay rate yield qualitatively similar results.

The Gottwald test and RQA Determinism show a relatively smooth, monotonic decay towards instability. Comparing the results for the Gottwald test with the work of Nair shows that the stability characteristics of the combustors are quite different. In figure 4 it is found that the measures change over the entire domain of allowable equivalence ratios. The combustor used by Nair yields $K = 1$ (stable, chaotic signal) for most of the parameter space and drops only shortly before instability. A connoted threshold of 0.9 would not work on the burner in this investigation, since it would unnecessarily exclude a large part of the operating window.

Due to the change in the characteristics of the intermittent region, the set with added damping does not show a monotonic change in the translation error towards instability. The translation error even strongly suggests that the system is getting away from instability just before the transition to limit cycle oscillation. The Gottwald test has some large outliers that claim a chaotic and thus stable system in the intermittent region. The RQA Determinism measure is least misled by the intermittent behaviour in the damped data set.

This example with a subtle change in boundary conditions (added damping) shows that a monotonic decrease towards instability is not always found. Therefore a specified threshold cannot guarantee a certain margin between the considered operating point and the onset of instability. Different conditions lead to different behaviour in the intermittent region between stable and unstable operation that is characterized by the measure.

All methods investigated in this work scarcely respond to scrambling of the data by the AAFT algorithm. Differences found are of the same magnitude as those found for the linear damping coefficient, and do not contribute to the performance of the methods.

5. Conclusion

Combustion noise has a very high – if not infinite – dimension, making an unequivocal choice for an embedding dimension impossible. Surrogate data tests show that the improved *False Nearest Neighbour* method developed by Cao does not give valuable results for combustion noise. The same embedding dimension is suggested for any time series with equal power spectrum and amplitude distribution, confuting the ability of this method to find a sufficient embedding dimension based on the dynamics of the underlying nonlinear system.

Although the average value of a measure at a certain state results in a relatively smooth curve from stable to unstable, large fluctuations are found between measurements at a fixed value of the bifurcation parameter. These fluctuations result from the chaotic dynamics, having time scales that are not sufficiently small with respect to the considered time window. The fluctuations can be reduced by increasing the window length or smoothening the values afterwards. Inevitably this results in a longer time lag in determining the corresponding value of the measure.

Compared to the damping coefficient proposed by Lieuwen, the methods based on nonlinear time series analysis show a smoother decay towards instability. Determination of an unambiguous effective acoustic damping based on combustion noise excitation appears to be difficult. Moreover intermittency complicates the determination of a proper damping coefficient. This lack of performance is not the result of the linear theory which it is based on, since the same conclusions would be drawn when all methods are applied to AAFT surrogate data sets. The introduction of nonlinear time series analysis in the search for a stability margin is beneficial because it opens a new library of methods that obviously can also be applied to predominantly linear systems. Attempting to quantify chaos simply yields less relative spread in the results, in comparison to the quantification of acoustic damping.

By changing the acoustic boundary conditions it is shown that a small system modification can have quite a large influence on the bifurcation behaviour of the dynamical system. The damped time series shows different behaviour in the intermittent regime, which is characterized by the measures.

A successful stability margin should be insensitive to different transitions to instability, otherwise no quantitative critical value of the measure exists that should not be passed.

If a quantitative critical threshold value for the stability margin cannot be found, instability can still occur "out of the blue". Measures as those investigated in this work can therefore only serve as an additional decision making tool for the operator. A stability margin measure that is applicable under different conditions should be fundamentally based on knowledge about the transitional behaviour and thus on the underlying complex dynamics of the specific thermoacoustic system.

ACKNOWLEDGEMENTS: The presented work is part of the Marie Curie Initial Training Network Thermo-acoustic and aero-acoustic nonlinearities in green combustors with orifice structures (TANGO). We gratefully acknowledge the financial support from the European Commission under call FP7-PEOPLE-ITN-2012.

REFERENCES

[1] Correa, S. M. (1992) A review of NO_x formation under gas-turbine combustion conditions. *Combustion Science and Technology*, **87**, 329–362.

[2] Lieuwen, T. and Zinn, B. T. (1998) Theoretical investigation of combustion instability mechanisms in lean premixed gas turbines. *AIAA paper*, **98-0641**.

[3] Lieuwen, T. (2005) Online combustor stability margin assessment using dynamic pressure data. *Transactions of the ASME*, **127**, 478–482.

[4] Nair, V., Thampi, G., Karuggusamy, S., Gopalan, S., and Sujith, R. I. (2013) Loss of chaos in combustion noise as a precursor of impending combustion instability. *International journal of spray and combustion dynamics*, **5**, 273–290.

[5] Gotoda, H., Nikimoto, A. H., Miyano, T., and Tachibana, S. (2011) Dynamic properties of combustion instability in a lean premixed gas-turbine combustor. *Chaos*, **21**.

[6] Tachibana, S., Fukumoto, A., Kanai, K., Yoshida, S., Suzuki, K., Sato, T., and Gotoda, H. (2013) Characteristics of dynamic pressure data and flame structures in an unstable lean premixed combustor with mixture inhomogeneity. *n^3l - International Summer School and Workshop on Non-Normal and Nonlinear Effects in Aero- and Thermoacoustics*.

[7] Gottwald, G. A. and Melbourne, I. (2005) Testing for chaos in deterministic systems with noise. *Physica D*, **212**, 100–110.

[8] Nair, V., Thampi, G., and Sujith, R. I. (2013) Intermittent bursts presage the onset and of instability in turbulent combustors. *n^3l - International Summer School and Workshop on Non-Normal and Nonlinear Effects in Aero- and Thermoacoustics*.

[9] Nair, V. and Sujith, R. I. (2014) Multifractality in combustion noise and predicting an impending combustion instability. *J. Fluid Mech.*, **747**, 635–655.

[10] Kosztin, B., Heckl, M., Müller, R., and Hermann, J. (2013) Thermo-acoustic properties of a burner with axial temperature gradient: Theory and experiment. *International journal of spray and combustion dynamics*, **5**, 67–84.

[11] Takens, F. (1981) Detecting strange attractors in turbulence. *Dynamical Systems and Turbulence, Warwick 1980, Lecture Notes in Mathematics*, **898**, 366–381.

[12] Abarbanel, H. D. I., Brown, R., Sidorowich, J. J., and Tsimring, L. S. (1993) The analysis of observed chaotic data in physical systems. *Reviews of Modern Physics*, **65**, 1331–1392.

[13] Cao, L. (1997) Practical method for determining the minimum embedding dimension of a scalar time series. *Physica D*, **110**, 43–50.

[14] Theiler, J., Eubank, S., Longtin, A., Galdrikian, B., and Farmer, J. D. (1992) Testing for nonlinearity in time series: the method of surrogate data. *Physica D*, **58**, 77–94.

[15] Schreiber, T. and Schmitz, A. (1997) Discrimination power of measures for nonlinearity in a time series. *Physical Review E*, **55**, 5443–5447.

Online Monitoring of Thermoacoustic Eigenmodes in Annular Combustion Systems Based on a State-Space Model

D. Rouwenhorst
IfTA Ingenieurbüro für Thermoakustik GmbH,
Gröbenzell 82194, Germany
e-mail: driek.rouwenhorst@ifta.com

J. Hermann
IfTA Ingenieurbüro für Thermoakustik GmbH,
Gröbenzell 82194, Germany

W. Polifke
Professur für Thermofluiddynamik
Fakultät für Machinenwesen,
Technische Universität München,
Garching 85747, Germany
e-mail: polifke@tfd.mw.tum.de

Thermoacoustic instabilities have the potential to restrict the operability window of annular combustion systems, primarily as a result of azimuthal modes. Azimuthal acoustic modes are composed of counter-rotating wave pairs, which form traveling modes, standing modes, or combinations thereof. In this work, a monitoring strategy is proposed for annular combustors, which accounts for azimuthal mode shapes. Output-only modal identification has been adapted to retrieve azimuthal eigenmodes from surrogate data, resembling acoustic measurements on an industrial gas turbine. Online monitoring of decay rate estimates can serve as a thermoacoustic stability margin, while the recovered mode shapes contain information that can be useful for control strategies. A low-order thermoacoustic model is described, requiring multiple sensors around the circumference of the combustor annulus to assess the dynamics. This model leads to a second-order state-space representation with stochastic forcing, which is used as the model structure for the identification process. Four different identification approaches are evaluated under different assumptions, concerning noise characteristics and preprocessing of the signals. Additionally, recursive algorithms for online parameter identification are tested.
[DOI: 10.1115/1.4034260]

Introduction

Thermoacoustic stability in combustion systems remains a major concern in industrial applications. As industry moves toward lean premixed combustion, the susceptibility of combustion systems to the problem of combustion instability has increased. Potential problems with thermoacoustic feedback often cannot be ruled out in the design phase of a combustion system. Common practice is to define a safe operational window upon commissioning, in which combustion parameters can be changed without risking thermoacoustic instability. However, increased requirements for flexible power generation, efficiency, and emission reduction demand a wider operational window.

One promising strategy is to monitor the combustion system continuously, by assessing the prevalent stability margin of the thermoacoustic modes. The first such output-only identification method, quantifying the decay rate of the autocorrelation function of an acoustic time series, was proposed in 2005 by Lieuwen [1]. More recently, methods from the field of dynamical system theory and chaos theory, suitable for nonlinear dynamics, have been adapted [2–4]. Instead of representing a linear decay rate, precursors quantify how structured (or chaotic) the dynamics is, on basis of a representative time series.

In annular combustion systems, acoustic waves can travel around the combustion chamber and plenum annulus without experiencing severe obstructions. Although the azimuthal waves propagate through an environment that is far from quiescent, the attenuation of these waves is relatively low, making azimuthal modes the major concern regarding thermoacoustic stability in annular combustion systems, such as heavy-duty annular gas turbines. As a result, annular combustion systems have been studied quite extensively, from low-order mathematical descriptions to a costly large eddy simulation, see Refs. [5–7] to name just a few. In addition, active control strategies have been proposed, based on a network model description of an annular combustor [8]. Annular test rigs are quite rare, yet some valuable experimental results are available [9]. Considering pure azimuthal acoustic modes, two eigenmodes are associated with each (positive integer) azimuthal mode order m. Fundamentally, the modes are degenerate, i.e., they have the same eigenvalue. For various reasons, including azimuthal bulk flow and azimuthally distributed heat release characteristics, the eigenvalues can become nondegenerate. When the split strength of the eigenvalue pair is of the magnitude of their decay rates, the nondegeneracy of the system cannot be neglected.

Measurable precursors that presage thermoacoustic instability are generally developed and tested on axial laboratory combustors, in which the acoustic field can be considered geometrically fixed. Annular combustion systems do not have the convenience of a priori knowledge on the azimuthal mode shapes. A dense distribution of sensors around the circumference would be required to assess uniquely both the temporal and spatial dynamics of the acoustic field in the annulus. Assuming azimuthal acoustics with a constant speed of sound and exploiting the phase information of measured signals, it can be shown that a minimum of two sensors would be required to solve for the modal contributions. Previously mentioned monitoring methods use a single input signal from the thermoacoustic system and would therefore suffer a dependency on measurement position. To illustrate this dependency, consider a standing wave solution where a single sensor could be located in one of the acoustic nodes, in which the modal fluctuations would not be registered.

The objective of this work is to develop an online monitoring strategy, specifically designed for annular combustion systems. The monitoring algorithm, based on acoustic measurements, should constantly be able to quantify the stability of the thermoacoustic modes. Such quantification would allow an operator or operating system to maintain a safe margin from instability under the prevailing conditions, including the machine state, ambient

Contributed by the Combustion and Fuels Committee of ASME for publication in the Journal of Engineering for Gas Turbines and Power. Manuscript received June 20, 2016; final manuscript received July 7, 2016; published online September 13, 2016. Editor: David Wisler.

Copyright © 2017 by ASME

Downloaded From: https://gasturbinespower.asmedigitalcollection.asme.org/ on 09/23/2016 Terms of Use: http://www.asme.org/about-asme/terms-of-use

and operating conditions. By slowly changing the system parameters under stable operating conditions, the influence on the system stability can be inferred. Using this strategy would help to optimize operation conditions with respect to required power output, efficiency, and pollution emission, while limiting the risk of entering into a state of thermoacoustic limit cycle. A model structure based on low-order modeling is proposed, which can be used for online stability estimation and works by identification of the decay rates and mode shapes of azimuthal eigenmodes.

A low-order model closely related to the models found in Refs. [10,11] is described. The model captures the key dynamics of the system in the form of a state-space model with two complex state variables, which shows traveling, standing, and mixed acoustic field solutions. Assuming that the thermoacoustic coupling is predominantly linear in the stable regime, a stochastically forced state-space model structure can be used to estimate the decay rates of the potentially split eigenvalues, belonging to a certain order of azimuth. In the Low-Order Modeling of Annular Thermoacoustics section, the low-order thermoacoustic model is introduced and evaluated. Subsequently, the identification methods are tested on surrogate time series. Special focus is on robust online monitoring of signals, including recursive implementations of the methods on finite time windows for quasi-steady dynamics.

Low-Order Modeling of Annular Thermoacoustics

Modal dynamics of annular thermoacoustics often show predominant standing or traveling wave behavior. In limit cycles, this can be observed clearly in both experiment and modeling even though the process noise results in some spread in the observed modal behavior [9,12]. Preferences for certain mode shapes are also present in the stable regime, although strongly obscured by process and measurement noise. To identify the stability and mode shapes of a thermoacoustic system, a model structure that captures the key dynamics with the least amount of parameters is pursued. The objective, therefore, is to describe the different azimuthal mode shapes using the simple model possible.

In the combustion chamber annulus, 1D plane wave propagation is modeled in the azimuthal direction and expanded in a Fourier series. A mean azimuthal bulk flow and global damping are included in the azimuthal acoustic description. Heat release is modeled by an $n-\tau$ model, relating heat release fluctuations to the axial velocity fluctuations in premixing ducts which supply fuel to the combustion chamber. Velocity fluctuations are driven solely by the fluctuating pressure difference between the plenum and the combustion chamber. This corresponds to a side branch in an acoustic network (applied in Ref. [13] as an example), in which the cross-sectional area of a branch is very small compared to the cross-sectional area of the annulus. Heat release forms an acoustic source according to the Rayleigh criterion, closing the thermoacoustic feedback mechanism. Heat release parameters can be prescribed locally, as a function of the azimuth. The azimuthal mode orders in the model (i.e., the azimuthal Fourier components that form the acoustic field) are orthogonal and are individually considered as such.

Acoustics. One-dimensional acoustics are fully described by two Riemann invariants F and G traveling with the speed of sound in the positive and negative directions of the coordinate, respectively. In the azimuthal coordinate system of an annulus, any shape of the two invariants can be suitably expressed as a Fourier series. The mth Fourier coefficient is the contribution to the acoustic variable of azimuthal mode order m. A modal contribution $\hat{p}_m$ to the acoustic pressure field $\hat{p}$ is then given by a clockwise ($\hat{F}_m$) and anticlockwise ($\hat{G}_m$) traveling wave amplitude. Refer to the sketch of an annular combustor in Fig. 1 for graphical support. The hat on a variable denotes that it is a complex quantity

$$\hat{p}_m(\theta,t) = \hat{F}_m e^{im(\omega_0 t-\theta)} + \hat{G}_m e^{im(\omega_0 t+\theta)} \tag{1}$$

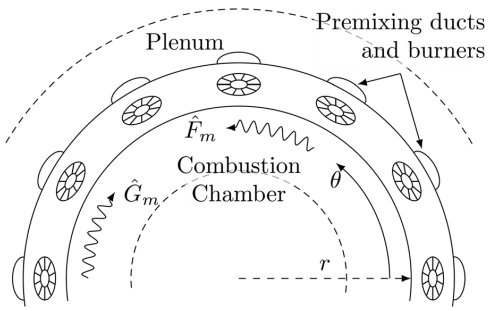

Fig. 1 Sketch of an annular combustor with 1D acoustic waves $\hat{F}_m$ and $\hat{G}_m$ in the combustion chamber. Premixing ducts of the burners connect the combustion chamber with the plenum.

The modal eigenfrequencies of the annulus are the azimuthal mode order m times the fundamental frequency ω_0. The complex amplitudes $\hat{F}_m$ and $\hat{G}_m$ can change slowly over time as a result of an azimuthal bulk flow velocity v_θ and a global acoustic attenuation rate ζ, which can be considered as a simple description of acoustic losses

$$\begin{aligned} \frac{1}{\hat{F}_m}\frac{\partial \hat{F}_m}{\partial t} &= imv_\theta - \zeta \\ \frac{1}{\hat{G}_m}\frac{\partial \hat{G}_m}{\partial t} &= -imv_\theta - \zeta \end{aligned} \tag{2}$$

The azimuthal flow causes a direction-dependent wave propagation velocity. Although v_θ is considered here as a bulk flow velocity, other physical phenomena might also contribute to a direction-dependent wave propagation velocity.

Premixing Ducts. Premixed fuel enters the annular combustion chamber through premixing ducts, as shown in Fig. 2. The ducts, which connect the combustion chamber with a plenum, are assumed to be narrow and acoustically compact with respect to the considered azimuthal wavelengths. According to the 1D momentum equation, a pressure difference between the annuli induces a plug flow in the fuel lines. In this work, the pressure fluctuations in the plenum are set to zero as a boundary condition. The (uniform) axial particle velocity $\hat{u}_x$ in the premixing duct causes the heat release fluctuations in the next subsection

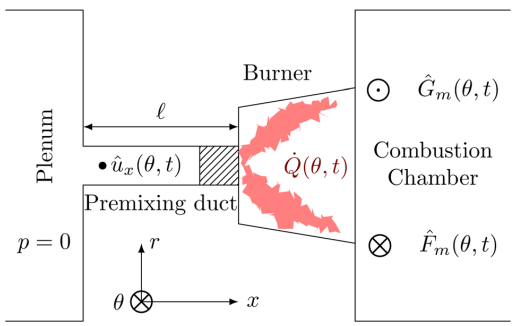

Fig. 2 Section view showing the premixing duct with reference velocity $\hat{u}_x$ for the heat release model. The combustion zone is subject to the pressure fluctuations in the combustion chamber, but secluded for azimuthal particle velocity.

Downloaded From: https://gasturbinespower.asmedigitalcollection.asme.org/ on 09/23/2016 Terms of Use: http://www.asme.org/about-asme/terms-of-use

$$\hat{u}_x(\theta,t) = \frac{-1}{\rho_c}\int \frac{\mathrm{d}\hat{p}_m}{\mathrm{d}x}\,\mathrm{d}t \approx \frac{i}{m\omega_0\rho_c\ell}\hat{p}_m(\theta,t) \tag{3}$$

Newly introduced variables are the cold fuel density ρ_c and premixing duct length ℓ and the low azimuthal Mach number assumption $M_\theta = v_\theta/\omega_0 \ll 1$ is applied to obtain the right-hand side of Eq. (3). The expected order of magnitude for the burner impedance $\hat{Z}_m$ given in Eq. (4) is 0.1 for the first few mode numbers

$$\hat{Z}_m = \frac{\hat{p}_m}{\rho_0 c\hat{u}_x} = \frac{-i\rho_c m\ell}{\rho_0 R} \tag{4}$$

In this equation, the speed of sound c is rewritten to the product of the radius R and fundamental frequency ω_0 of the annulus. Note the appearance of a density ratio between the supplied fuel ρ_c and the combustion gases ρ_0 in the combustion chamber. The acoustic response of a side branch to azimuthal waves for unity and very low burner impedance can be found in Ref. [14]. The axially induced particle velocity $\hat{u}_x$ is of interest here and follows the azimuthal acoustic pressure passively. Note that coupling is easily included by setting the impedance in Eq. (4) such that it matches the coupled acoustic field, leading to a description with coupled plenum, burner, and combustion chamber (PBC).

Heat Release Model. An $n-\tau$ model has been adapted to describe the heat release in the annular combustion chamber. The heat release fluctuations in the combustion chamber are locally prescribed by $\dot{Q} \propto n\hat{u}_x(t-\tau)$. Physically, it can be explained as fuel split modulations in the premixing duct being convected to the flame front, or to pulsating mass flow at the burners due to the axial particle velocity. The interaction index n is scaled to a real dimensionless amplification factor N using Eq. (3), yielding the heat release based on pressure fluctuations: $\dot{Q}_m \propto N\hat{p}_m(t-\tau)$. Note that this amplification factor includes the effect of the burner impedance. Choosing another acoustic boundary condition that describes the coupling with the plenum simply yields another (possibly complex) value for N

$$\dot{Q}_m(\theta,t) = \frac{2i\omega_0 N(\theta)}{(\gamma-1)m}\hat{p}_m\big(\theta, t-\tau(\theta)\big) \tag{5}$$

One strategy to control thermoacoustic stability is to install burners with different characteristics, or feeding some burners with a different fuel mixture. To mimic a so-called staging effect, the flame response strength N is a function of the circumference, written as a harmonic expansion with coefficients N_k and corresponding angles θ_k

$$N(\theta) = N_0 + 2\sum_{k=1}^{\infty} N_k \cos(k\theta - k\theta_k) \tag{6}$$

The time delay τ can also be varied azimuthally. A continuous description of the heat release characteristics around the combustor circumference has been used, rather than modeling a discrete set of individual burners. Note that breaking of the azimuthal uniformity does not have to result from a staging strategy. It can also be present unintentionally, due to varying fuel line lengths connecting the main fuel supply to their respective premixing ducts, for example, which affects their acoustic impedances.

Rayleigh Criterion. For a 1D annular geometry, the acoustic equations with heat release source leads to a differential equation for the total sound energy E

$$\frac{DE}{Dt} = \frac{\gamma-1}{\gamma p_0}A_{cc}R\oint \dot{Q}p\,\mathrm{d}\theta \tag{7}$$

In order to keep the model simple, the heat release location is kept fixed, despite the azimuthal particle velocity and bulk velocity in the combustion chamber.

System of Equations Assembly. Evaluating the change in acoustic energy of the wave pair belonging to a mode order and substituting Eqs. (1) and (2) into Eq. (7) yield a linear system of ordinary differential equations. Coupling between the waves is established through the heat release response

$$\dot{\mathbf{q}} = \mathbf{M}\mathbf{q} \tag{8}$$

In the above equation, the state vector $\mathbf{q} = [\hat{F}_m \quad \hat{G}_m]^T$ contains the acoustic variables, and the 2×2 system matrix $\mathbf{M}$ includes all system parameters. So that, only the slow amplitude and phase modulations are described, and fast dynamics with time scales corresponding to an acoustic period or smaller have been eliminated from the system of equations by integrating over an acoustic period. This averaging can be justified for $|\lambda_{1,2}| \ll m\omega_0$, where $\lambda_{1,2}$ are the two eigenvalues of the system matrix $\mathbf{M}$. By requiring that the amplitude modulations of $\hat{F}_m$ and $\hat{G}_m$ are slow compared to the corresponding eigenfrequency, this has been assumed implicitly in the model description.

Uniform Time Delay. If the time delay τ is uniform around the circumference, the system matrix $\mathbf{M}$ is given by the following equation, with $\varpi^{\pm} = m(\omega_0 \pm v_\theta)$:

$$\mathbf{M} = \begin{bmatrix} \frac{i\omega_0}{m}N_0 e^{-i\varpi^+\tau} + imv_\theta - \zeta & \frac{i\omega_0}{m}N_{2m}e^{2im\theta_{2m}-i\varpi^-\tau} \\ \frac{i\omega_0}{m}N_{2m}e^{-2im\theta_{2m}-i\varpi^+\tau} & \frac{i\omega_0}{m}N_0 e^{-i\varpi^-\tau} - imv_\theta - \zeta \end{bmatrix} \tag{9}$$

Averaging contributions around the circumference eliminates all products of orthogonal harmonics, such that only N_0 and N_{2m} of the flame response strength expansion in Eq. (6) remain. This shows that burners do not have to be considered individually and only their average and the effect on one spatial basis function have to be accounted for. Simple analytic expressions for the eigenvalue problem can be obtained, revealing a pair of eigenvalues that are typically nondegenerate

$$\lambda_{1,2} = \frac{i\omega_0}{m}\left(N_0\cos(mv_\theta\tau) \pm N_{2m}\sqrt{1-\eta^2}\right)e^{im\omega_0\tau} - \zeta \tag{10}$$

$$\eta = \frac{m^2 v_\theta}{i\omega_0 N_{2m}}e^{im\omega_0\tau} - \frac{N_0}{N_{2m}}\sin(mv_\theta\tau) \tag{11}$$

The real part of the eigenvalues is the growth rate of the modes, whereas the imaginary part contains the deviation from the average acoustic modal frequency $m\omega_0$

$$\begin{aligned} \alpha_{1,2} &= -\Re(\lambda_{1,2}) \\ \omega_{1,2} &= m\omega_0 + \Im(\lambda_{1,2}) \end{aligned} \tag{12}$$

Eigenvectors of the system with two degrees-of-freedom, are fully defined by the ratio $\upsilon = \hat{F}/\hat{G}$

$$\upsilon_{1,2} = (i\eta \pm \sqrt{1-\eta^2})e^{2im\theta_{2m}-imv_\theta\tau} \tag{13}$$

Nonuniform Time Delay. When the heat release time delay τ is also a function of the circumference, the integral over the circumference cannot be evaluated in the general case

$$\mathbf{M} = \begin{bmatrix} \Gamma_0^+ + imv_\theta - \zeta & \Gamma_2^- \\ \Gamma_2^+ & \Gamma_0^- - imv_\theta - \zeta \end{bmatrix} \tag{14}$$

Downloaded From: https://gasturbinespower.asmedigitalcollection.asme.org/ on 09/23/2016 Terms of Use: http://www.asme.org/about-asme/terms-of-use

Table 1 Parameters used for the simulation of the acoustic time series, yielding a system in the mixed regime, i.e., possessing both standing and traveling wave characteristics

m	ω_0	ζ	$m\omega_0\tau$	$N_0\omega_0$	$N_{2m}\omega_0$	θ_{2m}	v_θ
2	200π	100	$2\pi/3$	200	20	0	-3
—	rad/s	s^{-1}	—	rad/s	rad/s	rad	rad/s

For given distributions of N and τ, the integrals Γ as defined in Eq. (15) need to be evaluated

$$\Gamma_k^{\pm} = \frac{i\omega_0}{2\pi m}\oint N(\theta)e^{\mp ikm\theta - i\varpi^{\pm}\tau(\theta)}\,\mathrm{d}\theta \tag{15}$$

Model Validation. The low-order thermoacoustic model introduced in this work is compared to ATACAMAC [11,15], an annular thermoacoustic network model. In ATACAMAC, the combustor is modeled by burner ducts in which the combustion is described by acoustic jump conditions, also based on an $n-\tau$ formulation. The burner ducts joint with annular duct sections, forming the annular geometry. A plane wave solution describes the transfer function across the ducts. An analytic estimation of the eigenvalue problem is found by a Taylor expansion of the system around the acoustic eigenfrequency of the annulus, yielding the decay rate and thermoacoustic frequency of the considered mode order.

Validation Case. The example system in Ref. [11] is considered, which is a combustor with four burners, two of which share a variable delay τ_1 in the heat release model, ordered in the pattern 1212. The first azimuthal mode order is considered as a function of τ_1 and v_θ, fixing $\tau_2 = 2.21$ ms, $\zeta = 0$, and all other system parameters listed in Ref. [11] (Table 1).

The discrete set of burners can be described with the use of the Dirac delta functions before evaluation of the integrals in Eq. (14). For comparison between the two models, the acoustic contribution of the burner duct length in ATACAMAC is eliminated. Moreover, a correction factor matching the impedance ratio between the hot and cold domain was required, because in ATACAMAC the heat is released in the cold domain. Following these adjustments, the model results are identical, apart from the mixed regime (i.e., nonzero v_θ and $\tau_1 \neq \tau_2$) where small discrepancies are discerned. The frequency and decay rate versus τ_1 for both models are shown in Fig. 3 for the (mixed) case with $v_\theta/\omega_0 = M_\theta = 0.01$, according to Eq. (12) in this work and Eq. (18) in Ref. [11]. The Taylor expansion of the ATACAMAC model matrix around the acoustic eigenfrequency yields a discontinuity in its roots, visible at $m\omega_0\tau_1/2\pi = 0.8$. Close to the point where the eigenfrequencies are equal, both roots result in a positive decay rate α, seen by two markers at this location.

It is concluded that the two models predict the exact same key features as a result of variable heat release and azimuthal bulk velocity. Both low-order models show that deviations from a uniform and quiescent annular thermoacoustic system cause split eigenvalues for a given mode order. The present model starts with continuous flame response distributions, such that the general effect of system parameters can be evaluated, without specifying the amount of burners and their characteristics. If desired, a discrete set of burners could be represented by a corresponding continuous description as shown in this validation case. Moreover, the model described here is more reliable in the mixed region, since it returns continuous eigenvalue solutions.

From a monitoring perspective, it is key that the dynamics can be described by a state-space representation in Eq. (8) with two complex state variables, independent of system parameters and the amount of burners.

Annular System Identification

Due to the complex coupling of physical phenomena, an accurate prediction of the thermoacoustic stability of a combustor is not straightforward, even when accurate descriptions of the geometry and flame response measurements are available. Moreover, the behavior can change with extend variables, such as weather conditions, transient heating of the system, etc. Uncertainties in model parameters can have a significant influence on the stability, see, for example, Ref. [16]. For optimal operational flexibility, the thermoacoustic state of the system is best evaluated online, i.e., during operation. For satisfactory identification, a model structure is required, describing the relevant physics with a limited amount of free parameters. Evaluating the decay rate of the autocorrelation function of an acoustic sensor as in Ref. [1] proves to be insufficient in case of eigenvalue splitting.

The simplest explanatory model structure in this case would have two degrees-of-freedom, describing the evolution of two complex acoustic amplitudes around the combustor circumference, as found in the thermoacoustic model described in the first part of this work. In this section, possibilities to identify matrix M, or its characteristics, are evaluated. The model for the time series s at the sensor locations follows a state-space representation with stochastic input

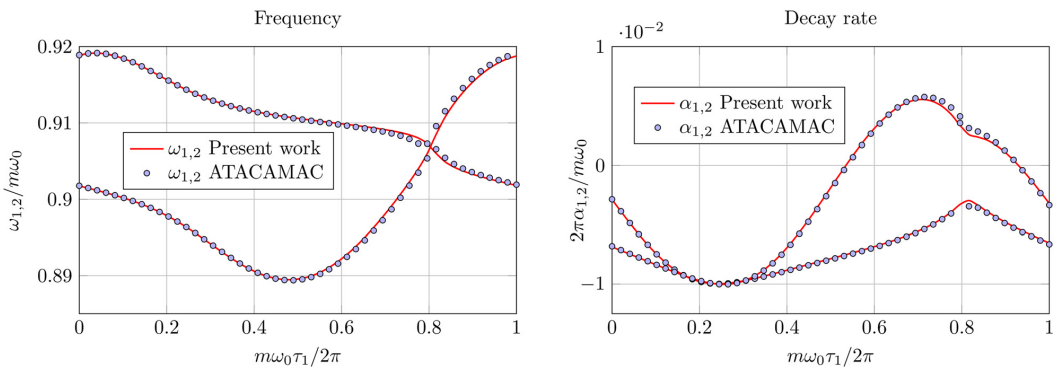

Fig. 3 Comparison of the current model with the analytic (linearized) ATACAMAC model. Eigenfrequencies and decay rates of a system with burner pattern 1212 for variable time delay τ_1. Both solutions coincide very well after enforcing the same conditions, noting the small deviations around $m\omega_0\tau_1/2\pi = 0.8$.

Downloaded From: https://gasturbinespower.asmedigitalcollection.asme.org/ on 09/23/2016 Terms of Use: http://www.asme.org/about-asme/terms-of-use

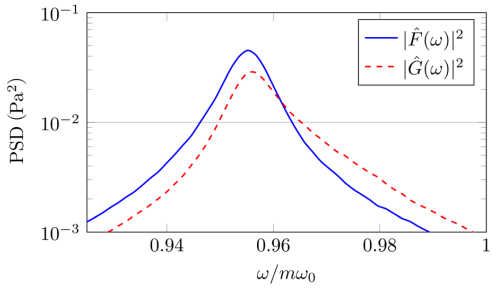

Fig. 4 Modal peak in the power spectral density of clockwise and anticlockwise waves of the surrogate time-series data generated by Eq. (17)

$$\begin{aligned}\dot{\mathbf{q}} &= \mathbf{M}\mathbf{q} + \mathbf{w}_\mathbf{q} \\ \mathbf{s} &= \mathbf{C}\mathbf{q} + \mathbf{w}_\mathbf{s}\end{aligned} \tag{16}$$

The matrix $\mathbf{C}$ is the output matrix relating the analytic sensor output $\mathbf{s}$ to the two modal amplitudes in the state vector $\mathbf{q}$. Heat release fluctuations in the turbulent combustion process perturb the system through $\mathbf{w}_\mathbf{q}$, while $\mathbf{w}_\mathbf{s}$ denotes measurement noise on the sensor channels.

System parameters listed in Table 1 that define $\mathbf{M}$ are chosen as the order of magnitude that can be expected in a heavy-duty annular gas turbine. The time delay of the flame is set so that a positive feedback between acoustics and heat release occurs. Subsequently, the response strength is chosen so that the system approaches marginal stability. Moderate nonuniformity $N_{2\mathbf{m}}$ and bulk velocity v_θ are included to have a mixed system with nondegenerate eigenvalues. The resulting thermoacoustic system features two eigenvalues with decay rates $\alpha_{1,2} = [\,5.7 \quad 21.1\,]\,\mathrm{s}^{-1}$ and respective eigenfrequencies $f_{1,2} = [\,191 \quad 193\,]\,\mathrm{Hz}$.

Time Series Generation. Identification methods have been tested on surrogate time-series data, generated by the model description in Eq. (16). The stochastic differential equation for $\mathbf{q}$ is numerically integrated using the Euler–Maruyama scheme given in Eq. (17), generating 100 min of data. Stochastic forcing $\boldsymbol{\varepsilon}^\mathbf{q}$ and sensor noise $\boldsymbol{\varepsilon}^\mathbf{s}$ are discrete time series of Gaussian processes

$$\begin{aligned}\mathbf{q}_{\mathbf{j}+1} &= (\mathbf{M}\Delta t + \mathbf{I})\mathbf{q}_\mathbf{j} + \sqrt{\Delta t}\boldsymbol{\varepsilon}^\mathbf{q}_\mathbf{j} \\ \mathbf{s}_\mathbf{j} &= \mathbf{C}\mathbf{q}_\mathbf{j} + \boldsymbol{\varepsilon}^\mathbf{s}_\mathbf{j}\end{aligned} \tag{17}$$

Relatively large time-steps of $\Delta t = 10^{-4}$ s are used for the integration, which is possible as only slow amplitude changes are described. Real-time signals are constructed for sensor positions $\boldsymbol{\theta}_\mathbf{s} = [\,0 \quad \pi/8 \quad \pi/3\,]^T$, with a sampling frequency of $f_s = (4\Delta t)^{-1} = 2.5$ kHz. The signals are divided into 100 segments of 1 min, which are analyzed individually by the identification methods introduced in section Identification Results. The power spectral densities of the clockwise and anticlockwise traveling waves are shown in Fig. 4. Spectral analysis of a sensor output, which is some linear combination of these two spectra, does not suggest that two eigenmodes with different decay rates underlie the time series.

Identification Methods. A set of four different output-only modal identification methods have been tested on the segments of simulated time series. A brief description of the methods is given below. As the slow dynamics are of interest, the spectrum of a window was shifted toward the origin by $m\omega_0$ as a preconditioning step. Only accounting for the (originally) positive frequencies yields an analytic time signal relative to the expected frequency, upon back transformation to the time domain.

Stochastic Subspace Identification. Stochastic subspace identification (SSI) is a time-domain method, identifying exactly a state-space structure as Eq. (16). Both an observability matrix and a controllability matrix are identified, which are the matrices $\mathbf{M}$ and $\mathbf{C}$, respectively, under some (nonsingular) linear transformation. A balanced stochastic realization algorithm based on LQ decomposition is adapted [17], explained more thoroughly in Ref. [18], including an implementation algorithm. In this specific method, it is not possible to prescribe matrix $\mathbf{C}$, which is known for a given mode order and sensor locations.

Least Squares. When the sensor noise can be neglected, matrix M can be determined simply by least-squares fitting (LSQ) of the two equation lines in Eq. (17). First state vector $\mathbf{q}$ is determined by the pseudoinverse of $\mathbf{C}$, using the known (or determined) mode order m. Subsequently, also $(\mathbf{M}l/f_s + \mathbf{I})$ is estimated by least squares, evaluating $\mathbf{Q}_{1\to J-l}/\mathbf{Q}_{1+l\to J}$ over a window with length J, where matrix $\mathbf{Q}$ is formed by horizontal concatenation of $\mathbf{q}_j$

$$\mathbf{Q}_{1\to J} = [\,\mathbf{q}_1 \quad \mathbf{q}_2 \quad \cdots \quad \mathbf{q}_{J-1} \quad \mathbf{q}_J\,] \tag{18}$$

Note that the latter least-squares fitting is based on a time-step $l/f_s = 4l\Delta t$, in which l is a free to choose integer identification parameter. The eigenvalues of $\mathbf{M}$ are found by

$$\mathrm{eiv}(\mathbf{M}) = \frac{f_s}{l}\log(\mathrm{eiv}(\mathbf{M}l/f_s + \mathbf{I})) \tag{19}$$

Eigenvector Ratio. Instead of identifying the entire system matrix, just the eigenvector ratio (EVR) can be identified. The (normalized) time derivative of the wave ratio $\dot{\upsilon}/\upsilon$ can be written as a quadratic equation in υ using the differential system Eq. (16): $\dot{\upsilon}/\upsilon = \boldsymbol{\xi}\mathbf{X}$, where $\mathbf{X} = [\,\upsilon \quad 1 \quad \upsilon^{-1}\,]^T$ and $\boldsymbol{\xi}$ represents a vector with the polynomial coefficients to be identified. Eigenvalues of the system have the property $\dot{\upsilon} = 0$; therefore, the roots of $\boldsymbol{\xi}$ provide the eigenvector ratios $\upsilon_{1,2}$. The coefficient vector $\boldsymbol{\xi}$ is fitted over time using a weighted least-squares approach. Weighing by |FG| is applied to avert strong outliers caused by the singularities at zero wave amplitudes. Once the eigenvectors are determined, the signals can be projected on its eigenbasis, and the decay rate and frequency can be estimated from the corresponding autocorrelation functions in the time domain.

Fourier Domain Decomposition. In Fourier domain decomposition (FDD), singular value decomposition is performed on the power spectral density matrix of the signals at the modal frequency. The singular vectors contain the (approximate) eigenvectors of the system. For the details of the method, the interested reader is referred to Ref. [19]. The frequency is picked by finding the maximum of the power spectra, introducing some uncertainty, especially for the least dominant eigenmode. Again, the decay rate and frequency are found from the autocorrelations of the projected modal dynamics.

Identification Results. The surrogate data were identified under different assumptions, regarding the driving combustion noise $\mathbf{w}_q$ and measurement noise $\mathbf{w}_s$. Additionally, the consequences of applying a bandpass filter around the modal peak were evaluated. Results are presented for an academic and a practical case. Elimination of the fast dynamics allows for larger time-steps in the estimation of $\dot{\mathbf{q}}$. This strategy is beneficial in case of limited high-frequency excitation and/or the application of a bandpass filter that eliminates high frequencies. Methods are performed on the 100 windows independently to get a statistical mean and variance of the estimated parameters.

Academic Case. In the academic case, there is no measurement noise $\boldsymbol{\varepsilon}^\mathbf{s}$, nor any signal filtering applied. The state-space model is numerically integrated with Gaussian white noise $\boldsymbol{\varepsilon}^\mathbf{q}$ as driving force, with unit variance. It is tried whether the methods are able

Downloaded From: https://gasturbinespower.asmedigitalcollection.asme.org/ on 09/23/2016 Terms of Use: http://www.asme.org/about-asme/terms-of-use

Table 2 Table with average estimated decay rates α_1 and α_2, using the different identification methods based on 100 surrogate data segments. Standard deviations are given in parenthesis. Shaded cells failed the test for being an unbiased estimated.

	Theory[a]	SSI	LSQ	EVR	FDD
Academic case					
α_1	5.54	5.57(0.4)	5.54(0.3)	5.60(0.4)	5.52(0.4)
α_2	21.03	21.1(0.8)	21.1(0.7)	20.8(1.2)	21.4(0.8)
Practical case					
α_1	5.54	5.63(0.3)	4.79(0.3)	5.57(0.4)	5.51(0.4)
α_2	21.03	21.1(0.7)	17.9(0.6)	19.9(1.5)	21.3(0.8)

[a]Deviation from Eq. (10) due to the discrete differentiation of $\dot{\mathbf{q}}$.

to recover the correct system characteristics, especially the modal decay rates, listed on the top of Table 2. Although the results are rather close to the theoretical values overall, it is worth mentioning that the second mode identified by FDD (shaded cell) failed the statistical test hypothesizing that the estimate is unbiased, using a 95% confidence interval. All methods are accurate for the first (least stable) eigenmode, and the uncertainties (standard deviations) are similar.

Practical Case. Combustion noise features spatiotemporal correlations, mainly due to the heat release response to turbulent structures in the fuel flow. A second time series is generated to evaluate the identification under forcing by colored noise. The power spectral density of $\boldsymbol{\varepsilon}^{\mathbf{q}}$ is prescribed by Eq. (20), representing a noise spectrum with a power-law energy fall-off for $\omega \gg \omega_c$

$$\mathrm{E}\left[\left|\boldsymbol{\varepsilon}^{\mathbf{q}}(\omega)\right|^2\right] \propto \frac{1}{1+(\omega/\omega_c)^{3/2}+(\omega/\omega_c)^{-3/2}} \tag{20}$$

This serves as a generic function, since the actual noise power spectrum will depend on multiple parameters related to geometry, flow conditions, and the combustion process. Important is the decrease of excitation power for high frequency. The characteristic frequency is chosen $\omega_c = 600\pi$.

White noise is added to the sensor signals $\mathbf{s}$, representing measurement noise $\boldsymbol{\varepsilon}^{\mathbf{s}}$. The standard deviation of this Gaussian noise is set to 10% of the standard deviation of the signal. For the identification of a modal peak, it might be necessary to filter out dynamics dominating at other frequencies. A brick-wall bandpass filter is applied on the signals from 150 to 250 Hz.

It is found that LSQ is affected most, by both the measurement noise and the bandpass filter. In determining the change of $\mathbf{q}$, the time delay (l/f_s) should be large enough when a bandpass filter is applied; otherwise, the filter characteristics dominate the result. This time delay is typically taken 12 ms in the identification algorithms. The results for the practical case, found at the bottom of Table 2, are clearly less accurate compared to the academic case. The uncertainties, on the other hand, hardly changed.

Online Monitoring of Decay Rates. In this part, the capability of the methods is tested, to monitor the stability of a system that changes in time. To monitor a combustion process online, it is important that the results become available directly with limited calculation costs. Instead of waiting for sufficient data for parameter estimation, recursive methods can be applied that constantly update knowledge about the system on which the estimates are based. With help of a forgetting factor, weight can be put on the most recent measurements, allowing slow changes of the underlying dynamics to be followed.

Windows of 1024 data points (≈0.4 s) have been analyzed by the methods, resulting in imprecise and biased parameter estimation based on a single window. The recursive approach is imperative to obtain an unbiased estimation over a longer period.

Cycle Description. In the parameter space of the thermoacoustic model, a cycle is defined in a span of 10 min. The bulk velocity and nonuniformity parameter have been varied slowly, leaving the other settings as in Table 1. A time series with slowly changing system parameters according to the parameterization in Eq. (21) was generated. In the first 3 min, the bulk velocity v_θ linearly changes from 0 to −60 rad/s. As v_θ reverted in the following 3 min, the geometrical nonuniformity coefficient N_{2m} rose from 0 to 15 s^{-1}. From 6 to 9 min, N_{2m} vanished again to return to the degenerate state found at the start of the cycle, with the remaining minute spent at rest. In this cycle, the system crosses through traveling, mixed, and standing mode behavior, respectively. This test may also be useful to find identification problems under specific system conditions

$$\begin{aligned} v_\theta(t) &= -60+|t/3-60| \quad 0<t<360 \\ N_{2m}(t) &= 15-|t/12-30| \quad 180<t<540 \end{aligned} \tag{21}$$

Noise characteristics and bandpass filtering are applied according to the practical case described in the subsection Identification Results.

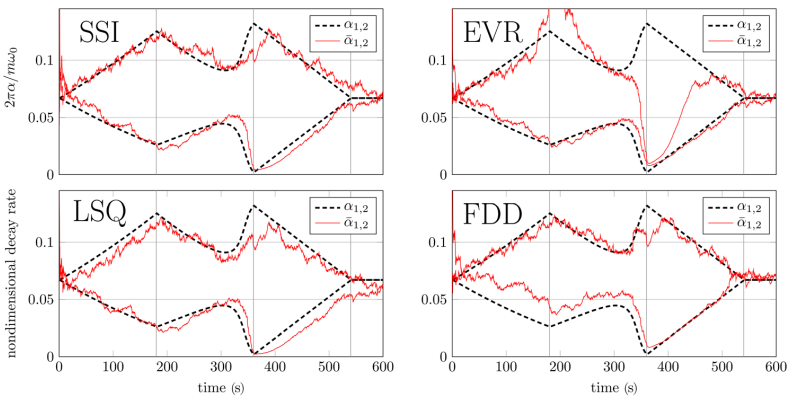

Fig. 5 Online identified decay rates $\bar{\alpha}_{1,2}$ of the thermoacoustic system during slow parameter variation. Theoretical decay rates $\alpha_{1,2}$ following from the prescribed parameters by Eq. (12) are given in dashed lines.

Downloaded From: https://gasturbinespower.asmedigitalcollection.asme.org/ on 09/23/2016 Terms of Use: http://www.asme.org/about-asme/terms-of-use

Monitoring Results. The stability monitoring results are shown in Fig. 5, in which the estimated dynamic decay rates are compared to the theoretical split decay rates (thick dashed lines). The forgetting factor is set to 0.975, as a tradeoff between noise suppression and the ability to follow the slowly changing dynamics. All methods can be calculated in a fraction of the physical time, about a few seconds for the 10 min of data. Therefore, regarding computational costs, all methods are considered viable candidates for online monitoring.

The main challenge for the parameter estimation is the passage between 300 and 400 s, where the eigenmodes change from dominantly traveling waves to standing wave solutions. The trajectory through the mixed regime ends with a steep decrease of the decay rate. As future data are unavailable, the past data are used for smoothing, meaning that estimated parameters lag behind the physical state.

SSI and LSQ have very similar estimates, with LSQ showing a slight bias toward lower decay rates, observed also in the steady practical case. When the splitting is strong, EVR has problems in estimating the mode with high decay rate, although it may be noted that this most stable mode is of limited interest for stability monitoring. Potentially hazardous is the overestimating of the first mode by FDD. The changing of the eigenfrequencies is expected to cause the troubles in FDD, in which the power spectral density matrix is updated recursively. Determination of the decay rate by means of the autocorrelation function always yields a bias toward stability for a decay rate approaching zero. SSI and LSQ do not suffer this drawback and could in principle also identify negative decay rates. In practice when the decay rate becomes negative, the thermoacoustics would saturate quickly to limit cycle behavior, from which point the linear stability of this new dynamic state is determined.

Conclusions

A low-order model for azimuthal thermoacoustic modes in annular combustion systems has been introduced, which shows dynamics observed in practice, such as the possibility to have dominant standing or traveling wave behavior. A continuous description of the flame characteristics around the azimuth yields analytic solutions, which can be useful to assess staging strategies without going into the detail of individual burner positioning, for example. It has been observed that splitting of eigenvalues can influence the stability of the system significantly and should thus be accounted for in monitoring strategies. Two complex wave amplitudes are the lowest amount of state variables required (per mode order) to describe the key features in the dynamics. To monitoring a peak in the spectrum of an annular combustor, at least two sensors around the azimuth must be adapted in order to identify split eigenvalues. A state-space representation is proposed as model structure in order to apply output-only modal identification on annular combustors.

Online monitoring of the resulting decay rates serves as a physical and quantitative stability margin. Frequency and mode shape information can help to find more robust combustor configurations or operating conditions. Four different identification methods are evaluated as candidates for online monitoring of the modal decay rates. All four methods return a reasonable indication of the system stability and considering computational costs found to be utilizable online.

Stochastic subspace identification performed better than the other methods, as it is suited to identify the exact model structure. A drawback for this method is that not all system knowledge can be exploited, since the mode order cannot be prescribed. This may cause interference with dynamic behavior not accounted for in the modeling, such as axial modes in the combustion chamber. Although a bias should be expected under practical conditions, least squares of the matrix coefficients (LSQ) functions robustly when used for monitoring a slowly changing thermoacoustic system. The volume of system data stored for recursive updating of LSQ is slightly lower compared to SSI, as well as the amount of computational operations per window. In contrast to SSI, the mode order is prescribed for an investigated frequency range. For these reasons, a least-squares implementation might be preferred over SSI in monitoring industrial annular combustion systems.

Decay rate estimation based on the autocorrelation yields biased estimates when marginal stability is approached, forming the main disadvantage for methods such as EVR and FDD.

Acknowledgment

The presented work is part of the Marie Curie Initial Training Network Thermo-acoustic and aero-acoustic nonlinearities in green combustors with orifice structures (TANGO). We gratefully acknowledge the financial support from the European Commission under call FP7-PEOPLE-ITN-2012.

Nomenclature

A_{cc} = cross-sectional area of the annular combustion chamber
$\mathbf{C}$ = state-space output matrix
$\mathrm{E}[\cdot]$ = expected value
$\hat{F}$ = acoustic wave amplitude traveling along θ-coordinate
f_s = sampling frequency
G = acoustic wave amplitude traveling against θ-coordinate
i = imaginary unit $\sqrt{-1}$
$\mathbf{I}$ = identity matrix
m = azimuthal mode number
$\mathbf{M}$ = thermoacoustic system matrix
n = heat release interaction index
N = heat release response strength
$\hat{p}$ = acoustic pressure in the annulus
$\mathbf{q}$ = state-space vector
$\dot{Q}$ = heat release rate per cubic meter
r = radial coordinate
R = radius of the annular combustion chamber
$\mathbf{s}$ = acoustic sensor output
t = time
v_θ = azimuthal bulk velocity, rad/s
x = axial coordinate
α = decay rate
γ = ratio of specific heats
Δt = discrete time-step
ε = discrete Gaussian noise
ζ = acoustic attenuation
θ = azimuthal coordinate
λ = system eigenvalue
τ = heat release time delay
υ = eigenvector ratio

References

[1] Lieuwen, T., 2005, "Online Combustor Stability Margin Assessment Using Dynamic Pressure Data," ASME J. Eng. Gas Turbines Power, **127**(3), pp. 478–482.
[2] Nair, V., Thampi, G., Karuppusamy, S., Gopalan, S., and Sujith, R., 2013, "Loss of Chaos in Combustion Noise as a Precursor of Impending Combustion Instability," Int. J. Spray Combust. Dyn., **5**(4), pp. 273–290.
[3] Nair, V., and Sujith, R., 2014, "Multifractality in Combustion Noise: Predicting an Impending Combustion Instability," J. Fluid Mech., **747**, pp. 635–655.
[4] Gotoda, H., Shinoda, Y., Kobayashi, M., Okuno, Y., and Tachibana, S., 2014, "Detection and Control of Combustion Instability Based on the Concept of Dynamical System Theory," Phys. Rev. E, **89**(2), p. 022910.
[5] Evesque, S., and Polifke, W., 2002, "Low-Order Acoustic Modelling for Annular Combustors: Validation and Inclusion of Modal Coupling," ASME Paper No. GT-2002-30064.
[6] Campa, G., Camporeale, S., Guaus, A., Favier, J., Bargiacchi, M., Bottaro, A., Cosatto, E., and Mori, G., 2011, "A Quantitative Comparison Between a Low Order Model and a 3D FEM Code for the Study of Thermoacoustic Combustion Instabilities," ASME Paper No. GT2011-45969.
[7] Staffelbach, G., Gicquel, L. Y. M., Boudier, G., and Poinsot, T., 2009, "Large Eddy Simulation of Self Excited Azimuthal Modes in Annular Combustors," Proc. Combust. Inst., **32**(2), pp. 2909–2916.

Downloaded From: https://gasturbinespower.asmedigitalcollection.asme.org/ on 09/23/2016 Terms of Use: http://www.asme.org/about-asme/terms-of-use

[8] Morgans, A. S., and Dowling, A. P., 2007, "Model-Based Control of Combustion Instabilities," J. Sound Vib., **299**(1–2), pp. 261–282.
[9] Worth, N. A., and Dawson, J. R., 2013, "Modal Dynamics of Self-Excited Azimuthal Instabilities in an Annular Combustion Chamber," Combust. Flame, **160**(11), pp. 2476–2489.
[10] Noiray, N., Bothien, M., and Schuermans, B., 2011, "Investigation of Azimuthal Staging Concepts in Annular Gas Turbines," Combust. Theory Modell., **15**(5), pp. 585–606.
[11] Bauerheim, M., Cazalens, M., and Poinsot, T., 2015, "A Theoretical Study of Mean Azimuthal Flow and Asymmetry Effects on Thermo-Acoustic Modes in Annular Combustors," Proc. Combust. Inst., **35**(3), pp. 3219–3227.
[12] Noiray, N., and Schuermans, B., 2013, "On the Dynamic Nature of Azimuthal Thermoacoustic Modes in Annular Gas Turbine Combustion Chamber," Proc. R. Soc. A: Math. Phys. Eng. Sci., **469**(2151), p. 20120535.
[13] Krüger, U., Hüren, J., Hoffmann, S., Krebs, W., and Bohn, D., 1999, "Prediction of Thermoacoustic Instabilities With Focus on the Dynamic Flame Behavior for the 3A-Series Gas Turbine of Siemens KWU," ASME Paper No. 99-GT-111.
[14] Blimbaum, J., Zanchetta, M., Akin, T., Acharya, V., O'Connor, J., Noble, D. R., and Lieuwen, T., 2012, "Transverse to Longitudinal Acoustic Coupling Processes in Transversely Excited Flames," Spring Technical Meeting of the Central States Section of the Combustion Institute.
[15] Parmentier, J.-F., Salas, P., Wolf, P., Staffelbach, G., Nicoud, F., and Poinsot, T., 2012, "A Simple Analytical Model to Study and Control Azimuthal Instabilities in Annular Combustion Chambers," Combust. Flame, **159**(7), pp. 2374–2387.
[16] Ndiaye, A., Bauerheim, M., and Nicoud, F., 2015, "Uncertainty Quantification of Thermoacoustic Instabilities on A Swirled Stabilized Combustor," ASME Paper No. GT2015-44133.
[17] Tanaka, H., and Katayama, T., 2003, "Stochastic Subspace Identification Via 'LQ Decomposition'," IEEE Conference on Decision and Control, Dec. 9–12, Vol. 4, pp. 3467–3472.
[18] Katayama, T., 2005, *Subspace Methods for System Identification. Communications and Control Engineering*, Springer-Verlag, London.
[19] Brincker, R., Zhang, L., and Andersen, P., 2000, "Output-Only Modal Analysis by Frequency Domain Decomposition," International Conference on Noise and Vibration Engineering, ISMA25, Vol. 2, pp. 717–723.

Downloaded From: https://gasturbinespower.asmedigitalcollection.asme.org/ on 09/23/2016 Terms of Use: http://www.asme.org/about-asme/terms-of-use

International journal of spray and combustion dynamics

Original Research Article

International Journal of Spray and Combustion Dynamics
0(0) 1–14
© The Author(s) 2017
Reprints and permissions:
sagepub.co.uk/journalsPermissions.nav
DOI: 10.1177/1756827717715858
journals.sagepub.com/home/scd
SAGE

Bifurcation study of azimuthal bulk flow in annular combustion systems with cylindrical symmetry breaking

Driek Rouwenhorst[1], Jakob Hermann[1] and Wolfgang Polifke[2]

Abstract

In annular combustion systems, azimuthal thermoacoustic modes manifest themselves predominantly as travelling or standing waves. Several phenomena can influence the modal behaviour of annular thermoacoustics. To monitor the stability of azimuthal thermoacoustics in industrial installations, a better understanding of the dynamics is required to correctly interpret online measurements. In this work, thermoacoustic eigensolutions of annular combustion systems are investigated, using a low-order analytic model. Heat release fluctuations are considered as a weak source term for a given acoustic eigenmode. The fluctuating heat release is modelled as a linear feedback to the local acoustics, in which the feedback response is a function of the azimuthal coordinate, causing cylindrical symmetry breaking. A bifurcation map is generated as a function of azimuthal mean flow velocity around the annulus. It is shown that a pitchfork bifurcation exists, separating standing wave and travelling wave solutions. Due to the interaction with non-uniform thermoacoustic feedback, an azimuthal flow with a low Mach number can significantly influence the system stability. Close to the bifurcation point, the non-normal nature of the dynamic system can induce a considerable gain of acoustic energy and yield more predictable time traces. These findings address the influence of non-normality, when applying a linear damping rate, acoustic amplitude or entropy-based quantity with the intent to monitor combustion dynamics in an annular combustion system.

Keywords

Thermoacoustics, stability analysis, transient growth, annular combustor, analytic modelling

Date received: 22 September 2016; accepted: 29 May 2017

1 Introduction

The risk of encountering a thermoacoustic instability in combustion systems increases under lean combustion conditions and a progressively variable power demand, as more renewable resources supply to the grid. A thorough understanding of the thermoacoustic feedback loop and the resulting measured dynamic signals is required for efficient control or monitoring strategies. In particular, the complex dynamics in annular gas turbines has not yet been fully understood. Complex conjugate wave pairs exist in the annulus as a result of the rotational symmetry, allowing for standing waves, travelling waves and combinations thereof. Fundamentally, the two azimuthal waves corresponding to an azimuthal mode number have repeated eigenvalues and form an eigenspace in linear stability analysis. Breaking of the cylindrical symmetry, either geometric or in the flame response, will typically lead to split eigenvalues. An example is a structural element in the annulus, causing reflections of azimuthal waves, leading to standing wave behaviour. Another example is single damaged burner with deviant feedback characteristics, which causes the standing wave in its orientation to have a different decay rate than the wave in orthogonal orientation. Considering the acoustics from the fixed coordinate system, an azimuthal flow also splits the eigenvalues, as the convection of the acoustic field causes a Doppler shift in the

[1]Research and Development, IfTA GmbH, Gröbenzell, Germany
[2]Department of Mechanical Engineering, Technische Universität München, München, Germany

Corresponding author:
Driek Rouwenhorst, IfTA Ingenieurbüro für Thermoakustik GmbH
Industriestr. 33, Gröbenzell 82194, Germany.
Email: driek.rouwenhorst@ifta.com

Creative Commons CC BY-NC: This article is distributed under the terms of the Creative Commons Attribution-NonCommercial 4.0 License (http://www.creativecommons.org/licenses/by-nc/4.0/) which permits non-commercial use, reproduction and distribution of the work without further permission provided the original work is attributed as specified on the SAGE and Open Access pages (https://us.sagepub.com/en-us/nam/open-access-at-sage).

frequency. Similar physics involving degenerate eigenvalue pairs are found in structural dynamics, such as eigenmodes in bladed disc assemblies. A study of Ewins shows the splitting of eigenmodes due to cylindrical symmetry breaking as a result of the mistuning of rotor blades.[1]

In this work, the interaction between azimuthal flow and cylindrical symmetry breaking is analysed analytically. The latter promotes standing wave behaviour as depicted before in the provided examples, whereas the former counteracts the formation of standing wave solutions by rotating the acoustic field with respect to the gas turbine. Upon commissioning of a gas turbine cylindrical symmetry cannot be guaranteed, because manufacturing margins and installation will for example cause some deviations in acoustic impedance from burner to burner. Wear, fouling and replacement of parts will add to the symmetry breaking. Regarding the azimuthal flow, no restriction is present in this direction. Azimuthal flow has been demonstrated both experimentally and numerically and is generally attributed to a co-swirling burner configuration. Wolf et al.[2] for example reports a bulk velocity exceeding an azimuthal Mach number of 1%, based on an extensive LES-simulation. Referring to the monitoring of combustion dynamics, it is of interest how the wave structures, amplitudes, decay rates and frequencies behave, when symmetry breaking and azimuthal flow are present simultaneously. The solution regimes (regarding standing and travelling wave structures) resulting from these effects have been recognized in Bauerheim et al.;[3] however, the interaction has not been investigated in detail. In the work of Noiray et al.,[4] the effect of nonlinear and non-uniform heat release response strength is investigated. The Fourier component C_{2n} of the non-uniformity was found to be responsible for the eigenvalue splitting. The effect of an azimuthal bulk flow was not considered.

The objective of the work is to investigate the transitional region between predominantly standing and travelling waves, in the parameter space spanned by symmetry breaking and azimuthal flow velocity. This is achieved by considering linear coupling between those phenomena in a low order description of the physical problem. The transition regime is characterized by a bifurcation, as a function of the relative strength of the two phenomena. The effect of non-normality of the linear system close to the bifurcation point is highlighted, as it turns out to have a significant influence on the statistical properties of the thermoacoustic amplitude under stochastic forcing. A small supplementary investigation is carried out to better understand the frequency split between clockwise (CW) and anticlockwise (ACW) acoustic waves. This phenomenon is often attributed to a mean flow around the annulus, that establishes when co-rotating swirl burners are used, but the details of this process are still unresolved.

The article consists of five sections, starting with this introduction. The next section treats the azimuthal flow and symmetry breaking in more detail, including the introduction of an effective source of azimuthal flow. The third section describes the modelling approach for the thermoacoustics, before the results are presented in 'Results: Feedback based on axial velocity' section. The final section concludes the work to be followed by references and three appendices with detailed derivations of used equations and the nomenclature.

2 Azimuthal flow and cylindrical symmetry breaking

In this section, the way the two phenomena, azimuthal flow and cylindrical symmetry breaking, can arise in annular combustion systems is explored. It is expected that effects causing symmetry breaking, including a non-uniform geometry and heat release response, cause split eigenvalues with standing wave eigenvectors. Azimuthal flow results in split eigenfrequencies for travelling wave eigenvectors, where it should be noted that the acoustic field is still degenerate in a coordinate system rotating with the mean flow.

A supplementary numerical investigation is carried out to understand the influence of a two-dimensional transverse velocity field. It demonstrates that a split in frequency of CW and ACW waves is not only related to a mean azimuthal velocity, but also to the gradient of azimuthal velocity with respect to the radial coordinate.

2.1 Azimuthal flow

In most annular combustion systems, flow around the annulus is not restricted in either the combustion chamber, or the plenum. In the axial direction, there is a constant flow of fresh and burnt gases that can reach high velocities at certain positions. It is to be expected that (depending on the operating conditions) some net momentum transfer in azimuthal direction occurs, for example, at the compressor exit in the plenum of the combustion chamber of a gas turbine or at the swirl burner in the combustion chamber. Experimental evidence of different acoustic propagation velocities in the opposing azimuthal directions can be found in Worth and Dawson[5] for varying burner separation distances. This has been wrongly attributed to a mean azimuthal flow alone,[2,5] as more than one phenomenon can be responsible for this split in frequencies.

The frequency splitting occurs when co-rotating swirl burners are used, however, co-rotating swirlers are expected to cause a velocity gradient, rather than

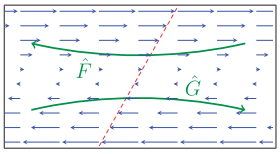

Figure 1. Refraction of acoustic waves in a velocity gradient. The direction of refraction depends on the direction of acoustic propagation and the refraction radius depends on the ratio of the velocity gradient and the speed of sound.

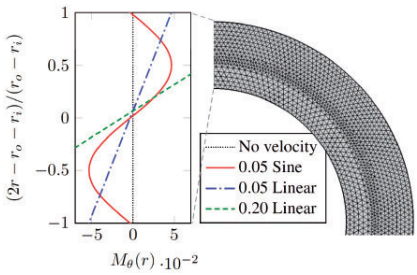

Figure 2. Tested azimuthal velocity profiles as a function of the radius. A quarter of the mesh used for the computation is shown on the right side.

a mean velocity. Therefore, it is investigated in this work whether a velocity gradient can also cause a split in the effective propagation speed between CW and ACW travelling waves. It is posed that a gradient of azimuthal velocity with respect to the radial coordinate, which refracts the acoustic waves as shown in Figure 1. A shear flow in an annulus refracts waves in one azimuthal direction towards the centre of the annulus. The wave in the other direction is constantly refracted towards the outer wall. A radially distributed azimuthal velocity field can be expected in annular combustion systems when co-rotating swirlers are used, refer to Bourgouin et al.[6] for a cold flow velocity field downstream of a swirl burner. Acoustic refraction can also be expected as a result of temperature gradients; however, this would affect the two waves in opposite direction identically, causing no split between the frequencies.

To demonstrate eigenvalue splitting as a result of a gradient of azimuthal velocity in the radial direction (refer to Figure 2), a 2D annular geometry with a ratio between the outer and inner radius of $r_o/r_i = 1.5$ is considered. Over the width of the annulus azimuthal velocity profiles are prescribed, without bulk flow contribution, as it would just add a known frequency split. A linear and harmonic profile with a peak to peak azimuthal Mach number of $M_{p2p} = 0.1$ is used. Additionally, a linear profile with a peak to peak of

Table 1. Increment of the eigenfrequencies as a result of azimuthal velocity gradients, with respect to frequency in the quiescent case ω_a. The first two mode orders m are given.

Velocity profile	m	$\omega_{cw}/\omega_a - 1$	$\omega_{acw}/\omega_a - 1$
No velocity	1	0	0
0.05 Sine	1	$-7.3 \cdot 10^{-3}$	$10.7 \cdot 10^{-3}$
0.05 Linear	1	$-8.6 \cdot 10^{-3}$	$11.0 \cdot 10^{-3}$
0.20 Linear	1	$-19.9 \cdot 10^{-3}$	$57.8 \cdot 10^{-3}$
No velocity	2	0	0
0.05 Sine	2	$-6.7 \cdot 10^{-3}$	$10.0 \cdot 10^{-3}$
0.05 Linear	2	$-8.0 \cdot 10^{-3}$	$10.2 \cdot 10^{-3}$
0.20 Linear	2	$-18.5 \cdot 10^{-3}$	$53.9 \cdot 10^{-3}$

$M_{p2p} = 0.4$ has been tested. The velocity in the latter case is too high to be expected in practice, but this case is used for analytical validation as the refraction radius is equal to the radius of the annulus. Acoustic solutions are obtained by solving the linear Euler equations numerically. COMSOL FEM software was used to obtain a solution in time domain, in which streamline diffusion was applied for stabilization. A quarter of the mesh is shown in Figure 2, together with the three prescribed velocity profiles. It must be noted that the velocity profiles include a small offset, in order to force the mean flow (integrated over the radial coordinate) to be zero.

The influence of the velocity profiles on the eigenfrequencies of azimuthal orders $m = 1$ and $m = 2$ are given in Table 1. The eigenfrequencies ω_{cw} and ω_{acw} correspond to a CW and an ACW travelling wave, respectively. It is concluded that waves that are refracted towards the centre of the annulus (which are CW waves for the used profiles in Figure 2), experience a decreased frequency. This can be explained by a loss of the radial wave number. When the refraction radius is equal to the radius of the annulus, plane wave propagation is obtained (in polar coordinates), with the lowest possible frequency, as the radial wave number is zero. The waves refracted away from the centre have an increased frequency. The lower frequency of the 0.20 linear velocity profile corresponds to the plane wave propagation in the polar coordinate frame, which is used for validation of the results. The theoretical frequency for this plane wave, normalized by the analytical solution without flow (quiescent solution, available in terms of Bessel functions), yields $\omega_{cw}/\omega_a - 1 = -19.7 \cdot 10^{-3}$. Table 1 shows that the theoretically and numerically found results deviate with 1% and 6%, for mode order 1 and 2, respectively. As this investigation is merely meant to demonstrate the existence and the order of magnitude of this phenomenon, such deviations are considered acceptable.

For $m = 1$ and a peak to peak azimuthal Mach number of $M_{p2p} = 0.1$, a difference in frequency of almost $0.02\omega_1$ is observed, which can be translated to an 'effective azimuthal Mach number' of $M_\theta \approx 0.01$. This investigation shows that a velocity gradient in the azimuthal flow can cause a significant split in wave propagation speed between the two directions. Despite this result, all possible effects that cause an apparent azimuthal bulk flow are represented by the angular bulk flow velocity v_θ in the remaining sections of this work, i.e. bulk flow is used as a paradigm for a split in the acoustic propagation velocity of opposing waves.

2.2 Cylindrical symmetry breaking

For fixed wavenumbers in the spatial directions, including a nonzero azimuthal mode order m, the acoustic field in an annulus is described by two complex amplitudes. A one-dimensional representation of azimuthal acoustics can be described by characteristic waves $\hat{F}$ and $\hat{G}$ for the ACW and CW acoustic propagation, respectively.

$$\hat{p}(\theta, t) = \hat{F}e^{i\omega_a t - im\theta} + \hat{G}e^{i\omega_a t + im\theta} \tag{1}$$

When the pure travelling waves $\hat{F}$ and $\hat{G}$ have identical amplitudes, they form a standing wave around the circumference. In case of cylindrical symmetry (where geometry and parameters are invariant under angular rotation), the system manifests a pair of degenerate eigenvalues. Through non-uniformities in azimuthal direction the eigenvalues can split, i.e. lose the degeneracy. When the acoustic waves partially reflect at a certain angular location, the opposing waves couple and tend to form standing wave solutions. One could think of a slight constriction in azimuthal direction, caused by a structural element. The eigenvalues will be different for the standing waves with the structural element in the pressure node and the orthogonal wave with the element in the pressure antinode. A constriction mainly splits the eigenfrequencies,[7] but can also split the decay rate.

Similarly, acoustic sources (or sinks) varying with the azimuth can cause eigenvalue splitting. In particular, heat release fluctuations in response to acoustic perturbations form such an acoustic source. Examples of eigenvalue splitting through a non-uniform heat release response include retrofitting of burner parts at some location(s), designed to reduce the heat release response strength. When instability still occurs, it is most likely to develop perpendicular to the retrofitted burner(s). The alternating use of two burner types could be applied in an annular combustor (see the patent of Joos and Polifke[8]), in such a way that a smoother overall flame response that is less prone to instabilities, is obtained. In such case, the chosen burner pattern influences the splitting strength and therefore the stability of the system, as pointed out by Berenbrink and Hoffman.[9]

Unintended azimuthal non-uniformities are likely to be present in industrial applications, for example, clogged fuel injection holes, deviations in acoustic impedance of the fuel injections and acoustic reflections from supporting structures. In this work, it is implied that the eigenvalue splitting is caused by a non-uniform flame response, but it might as well be of acoustic nature.

3 Modelling approach

The acoustics is described by a three-dimensional solution, satisfying the Helmholtz equation in an annulus, with two azimuthal wave amplitudes as free variables. The acoustic solution is convected passively with an azimuthal bulk flow. Axial flow is not considered, as it does not seem to influence the dynamic solution.[10] As in the work of Noiray et al.,[4] heat release fluctuations are continuously modelled over the azimuth of the annulus, rather than considering discrete burner locations. Local acoustic fluctuations result in heat release fluctuations at the corresponding angular location, through a linear flame response description. The heat release acts as a source to the acoustic pressure fluctuations, described on a Fourier basis over the azimuth.

A linear heat release response to acoustics perturbations is used, since the dynamic behaviour in the stable regime is sought, i.e. before exponential growth and saturation to a limit cycle occurs. It is assumed here that the magnitude of combustion noise does not cause a significant nonlinear response. Although saturation and limit cycle behaviour fall outside the scope of this work, initial growth rate and transient growth effects can still be studied in the unstable regime. Also, it is assumed that instantaneous growth rates and the angular bulk velocity are small compared to the considered eigenfrequency under all circumstances, such that time scales of amplitude modulations can be separated from the time scale of an acoustic cycle. This allows to average the equations over the acoustic cycles, resulting in compact analytic expressions. In this section, it will be shown that the resulting system of equations is a state space model with two complex degrees of freedom per degenerate acoustic eigensolution. The dynamic behaviour of this system is well suited for analytical evaluation.

3.1 Acoustic field

Thermoacoustics can be described by a sum of independent eigenmodes, based on solutions of the acoustic

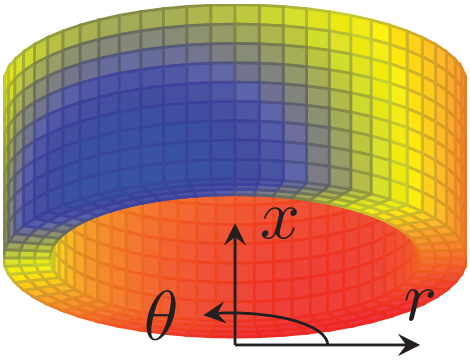

Figure 3. Example of an acoustic field of first azimuthal mode order, which could be described by equation (2).

field. Assuming that one modal solution of the 3D acoustic pressure field $\hat{p}$ with frequency ω_a is separable in the following way,

$$\hat{p}(\tilde{\mathbf{x}}, t) = \psi(x, r)\phi(\tilde{\theta})e^{i\omega_a t} \tag{2}$$

The spatial function $\psi(x, r)$ is assumed to be known, fulfilling the wave equation for given longitudinal and radial boundary conditions in the annular combustion chamber. An example pressure field described by equation (2) is shown in Figure 3 for a generic annular geometry. Azimuthal dependency $\phi(\tilde{\theta})$ is not fully determined, as the periodic boundary condition merely enforces a continuous solution around the circumference.

$$\phi(\tilde{\theta}) = \hat{F}e^{-im\tilde{\theta}} + \hat{G}e^{im\tilde{\theta}} = \mathbf{b}^T\mathbf{z} \tag{3}$$

In equation (3), the vector $\mathbf{z} = [\hat{F} \quad \hat{G}]^T$ contains the two Riemann invariants as free acoustic parameters, while $\mathbf{b} = [e^{-im\tilde{\theta}} \quad e^{im\tilde{\theta}}]^T$ contains their respective azimuthal basis functions. These basis functions satisfy the periodic boundary condition for a domain with uniform acoustic properties in the azimuthal direction for a positive definite azimuthal mode number m. The azimuthal coordinate $\tilde{\theta}$ is defined relative to the angular rotation $v_\theta t$, since the acoustics are passively convected by the flow field. In the fixed coordinate system of the combustor, the acoustics is obtained by substitution of $\tilde{\theta} = \theta - v_\theta t$.

Equation (2) is the fundamental solution of a 3D acoustic field in a cylindrically symmetric geometry with azimuthal bulk flow. Choosing the amplitudes $\hat{F}$ and $\hat{G}$, standing, travelling and mixed solutions can be constructed. The two amplitudes and complex angles give four free variables, explaining the variety of possible wave structures.

The slow evolution of the acoustic amplitudes $\hat{F}$ and $\hat{G}$, as a result of global acoustic damping ζ and thermoacoustic feedback, is governed by equations (4).

$$\begin{aligned} \frac{\mathrm{d}}{\mathrm{d}t}\hat{F} &= -\zeta\omega_a\hat{F} + \kappa\oint \dot{Q}(\hat{F}, \hat{G})\hat{F}\mathrm{d}\theta \\ \frac{\mathrm{d}}{\mathrm{d}t}\hat{G} &= -\zeta\omega_a\hat{G} + \kappa\oint \dot{Q}(\hat{F}, \hat{G})\hat{G}\mathrm{d}\theta \end{aligned} \tag{4}$$

The damping ratio is assumed to be small ($\zeta \ll 1$), such that the time scale of natural decay is long compared to the eigenfrequency. For brevity, the global damping ζ is ignored in this work, because it only superimposes on the eigenvalues of the thermoacoustic system. Heat release fluctuations $\dot{Q}$ are excited by the acoustics and form a source term in the acoustic equations, which is discussed in the following subsection. The proportionality constant κ is related to the volume of the acoustic domain and the ratio of specific heats.

3.2 Thermoacoustic feedback

Weak thermoacoustic feedback is added to the acoustic mode to find the combined dynamics. The thermoacoustic feedback is considered as small linear perturbations to the acoustic field, which justifies the performed separation in equation (2) of the acoustic time scale and the time scale with which the azimuthal acoustic field ($\phi(\tilde{\theta})$) changes. Dynamics dominated by the time scale of the combustion, such as intrinsic thermoacoustic instability,[11] are not considered.

The Rayleigh criterion states that acoustic energy is generated when heat release fluctuations $\dot{Q}$ are in phase with the pressure fluctuations. The growth of the acoustic mode in consideration is obtained by integrating over the volume in which the heat is released. Using $\star$ to denote the complex conjugate, the following equation can be derived (see Appendix 1).

$$\frac{\mathrm{d}\mathbf{z}}{\mathrm{d}t} = \kappa\oint \mathbf{b}^\star\dot{Q}\mathrm{d}\theta - v_\theta\left(\mathbf{b}^\star \cdot \mathbf{z} \cdot \frac{\mathrm{d}\mathbf{b}}{\mathrm{d}\tilde{\theta}}\right) \tag{5}$$

This equation describes the time derivative of the two acoustic amplitudes in $\mathbf{z}$, resulting from the fluctuating heat release and an angular velocity. Prevailing methods for the modelling of heat release fluctuations assume a linear response to the acoustics at the burners, for low perturbation amplitudes. Examples are the flame transfer function and the sensitive time lag model.[12] Considering the response at the acoustic eigenfrequency ω_a only, these methods are in essence

identical. A general linear heat release response to the two acoustic waves can be written as

$$\kappa\dot{Q}(\theta) = \mathbf{b}^T\left(\left[\,\hat{C}^F(\theta) \quad \hat{C}^G(\theta)\,\right]^T\cdot\mathbf{z}\right) \tag{6}$$

in which the complex-valued coefficients $\hat{C}^F$ and $\hat{C}^G$ represent the amplitude and phase of the heat release response to the respective waves in $\mathbf{z}$. These response coefficients are a function of the azimuth in case of non-uniform heat release, causing cylindrical symmetry breaking. Apart from the heat release, the coefficients can also include acoustic effects, such as attenuation and reflections. Combining the linear heat release response in equation (6) with the acoustic modal growth equation (5) yields a thermoacoustic system of ordinary differential equations.

$$\frac{\mathrm{d}\mathbf{z}}{\mathrm{d}t} = \oint\begin{bmatrix} \hat{C}^F + imv_\theta & \hat{C}^G e^{2im\theta} \\ \hat{C}^F e^{-2im\theta} & \hat{C}^G - imv_\theta \end{bmatrix}\mathrm{d}\theta\mathbf{z} \tag{7}$$

From the integration of the system matrix over the azimuthal coordinate, it can be directly deduced that the diagonal only depends on the average of $\hat{C}^F$ and $\hat{C}^G$. On the other hand, the antidiagonal is only sensitive to coefficient $2m$ of the azimuthal Fourier decomposition of $\hat{C}^F$ and $\hat{C}^G$. This can be verified by recognizing that an integral of the form $\oint \exp(ik\theta)\mathrm{d}\theta$ is zero for any nonzero integer k, because of the orthogonality of harmonic functions with different amounts of integer periods. Describing the coupling coefficients $\hat{C}$ as Fourier series over the azimuth allows the integration to be performed directly, by inserting the Fourier component that eliminates the harmonic dependency with respect to the azimuthal coordinate.

$$\hat{C}(\theta) = \sum_{k=-\infty}^{\infty} \hat{c}_k e^{ik\theta} \tag{8}$$

The coefficient $\hat{c}_0$ corresponds to the mean thermoacoustic feedback strength that influences the overall thermoacoustic stability. Equal to the C_{2n} coefficient in the work of Noiray et al.,[4] $\hat{c}_{2m}$ causes the eigenvalue pair of azimuthal mode order m to split. In this work, the coefficient is merely scaled differently, and it is complex, to cover heat release non-uniformities in both strength and phase. Physically, this means that standing wave eigenvalue splitting of a mode with azimuthal order m is only expected when the broken cylindrical symmetry has a non-zero Fourier component $2m$ around the circumference.

The azimuthal description of the thermoacoustic dynamics reduces to a complex second-order system of ODE's per azimuthal mode order. In Bauerheim et al.,[3] this solution structure was also found, modelling the heat release with an $n-\tau$ model.

$$\frac{\mathrm{d}\mathbf{z}}{\mathrm{d}t} = \begin{bmatrix} \hat{c}_0^F + imv_\theta & \hat{c}_{-2m}^G \\ \hat{c}_{2m}^F & \hat{c}_0^G - imv_\theta \end{bmatrix}\mathbf{z} \tag{9}$$

The coupling coefficients $\hat{c}_k$ can be a function of the frequency to be solved for, for example in the case of an $n-\tau$ model, where the phase linearly decreases with frequency.

$$\dot{\mathbf{z}} = \mathrm{M}(\omega)\mathbf{z} \tag{10}$$

The system matrix M describes the coupling between the two (complex) acoustic degrees of freedom, including thermoacoustic interaction. Under additional flame response assumptions, the coupling coefficients can be specified in more detail, as demonstrated in Rouwenhorst et al.[13] for an $n-\tau$ flame model.

3.3 Solution strategy

The eigenvalues $\lambda_{1,2}$ of M prescribe the temporal evolution of the amplitude of the eigensolutions with multiplier $\exp(\lambda_{1,2}t)$. The real part of the eigenvalues describes the growth rate, of which the sign determines the stability of the mode. The imaginary part causes a frequency deviation with respect to the acoustic eigenfrequency ω_a.

In order to come to an analytic eigensolution of the system in equation (10), the system matrix must be independent of the frequency. When this is not the case, the characteristic equation of $\mathrm{M}(\omega)$ is a transcendent equation for the eigenvalues (or complex frequency) that must be solved numerically. For small frequency dependency, however, using constant coupling values belonging to the frequency ω_a will yield accurate solutions.

The imaginary part of an eigenvalue of the system matrix M represents the frequency deviation $\Delta\omega$ from the acoustic eigenfrequency ω_a. When the coefficients $\hat{C}(\omega)$ are smooth and hardly change on the interval $[\omega_a - \Delta\omega < \omega < \omega_a + \Delta\omega]$, the frequency dependency can be neglected.

$$\left|\frac{\Delta\omega}{\hat{C}}\frac{\mathrm{d}\hat{C}}{\mathrm{d}\omega}\Big|_{\omega_a}\right| \ll 1 \tag{11}$$

As $\Delta\omega$ is of the order of $|\hat{C}|$, it can be stated that the derivative of the coupling parameters with respect to the frequency should be much smaller than one. Hence, the condition $\mathrm{d}\hat{C}/\mathrm{d}\omega \ll 1$ should be fulfilled at

the acoustic eigenfrequency in order to study the analytical solutions.

4 Results: Feedback based on axial velocity

In this section, further simplifications and assumptions are made in order to come to compact analytical expressions that enable to present the interaction between symmetry breaking and azimuthal bulk flow. Heat release fluctuations, due to vortical structures and equivalence ratio modulations, are usually attributed to the axial particle velocity (see Paschereit et al.,[14] for example). When axial particle velocity is held responsible for the fluctuating heat release, the thermoacoustic system is a function of the pressure fluctuations and independent of the azimuthal particle velocity. Assuming also that the coupling constants are (locally) independent of the frequency ($\mathrm{d}\hat{C}/\mathrm{d}\omega = 0$), the coupling parameters are identical ($\hat{C}^F = \hat{C}^G = \hat{C}$). These assumptions are made only to obtain a compact analytic eigensolution.

$$\frac{\mathrm{d}\mathbf{z}}{\mathrm{d}t} = \begin{bmatrix} \hat{c}_0 + imv_\theta & \hat{c}_{-2m} \\ \hat{c}_{2m} & \hat{c}_0 - imv_\theta \end{bmatrix} \mathbf{z} \tag{12}$$

This system of differential equations, a function of mv_θ and the Fourier components of $\hat{C}(\theta)$, is used as the starting point of the analytic parameter study performed in this work. The eigensolution found is:

$$\lambda_{1,2} = \hat{c}_0 \pm \sqrt{\hat{c}_{2m}\hat{c}_{-2m} - m^2 v_\theta^2} \tag{13}$$

In equation (13), it is visible how azimuthally varying heat release characteristics and azimuthal velocity split the eigenvalues $\lambda_{1,2}$ of the thermoacoustic system. The ratios of $\hat{F}$ and $\hat{G}$ corresponding to the eigenvectors, named $\nu_{1,2}$, are also readily obtained.

$$\nu_{1,2} = \frac{imv_\theta}{\hat{c}_{2m}} \pm \frac{1}{\hat{c}_{2m}}\sqrt{\hat{c}_{2m}\hat{c}_{-2m} - m^2 v_\theta^2} \tag{14}$$

The influence of the model parameters on the acoustic eigensolution and their interaction will now be explained in detail. From the eigensolution, it can be seen that the interacting parameter groups are mv_θ, i.e. azimuthal velocity with respect to the azimuthal wave length, and the cylindrical symmetry breaking strength S. As the azimuthal velocity with respect to the wave length, mv_θ is a good parameter for azimuthal velocity, equations (13) and (14) suggest that

$$S = \sqrt{\hat{c}_{2m}\hat{c}_{-2m}} \tag{15}$$

is a proper candidate to define as the symmetry breaking strength.

4.1 Uniform feedback $\hat{c}_0$ only ($mv_\theta = S = 0$)

This case corresponds to a setup with perfect cylindrical symmetry under quiescent conditions, i.e. no azimuthal flow. Without azimuthal non-uniformity of the thermoacoustic feedback response and no bulk velocity, the eigenvalues of the system are simply given by the constant feedback strength $\hat{c}_0$ on the diagonal of the system matrix. With repeated eigenvalues, the system is degenerate (i.e. solutions are defined by the eigenspace spanned by $\hat{F}$ and $\hat{G}$). This means that any linear combination of the two waves is an eigensolution, covering standing, travelling and mixed modes. The growth rate and frequency difference as a function of $\arg(\hat{c}_0)$ are the cosine and sine function, respectively.

4.2 Azimuthal flow mv_θ, with $S = 0$

This case corresponds to the theoretical setup with perfect cylindrical symmetry but now with an azimuthal flow through the annulus. Considering only azimuthal bulk flow, the same degenerate solution is found, now rotating with the mean flow. The rotation is visible in the imaginary split eigenvalues by $\pm imv_\theta$ for $\hat{F}$ and $\hat{G}$, respectively, in equation (13).

4.3 Cylindrical symmetry breaking S, with $mv_\theta = 0$

This case corresponds to a setup with quiescent flow conditions, but with a broken cylindrical symmetry that causes S to be non-zero. The symmetry breaking can be caused either by reflections (e.g. structural element) or a non-homogeniety in heat release response (e.g. clogged gas orifice in a burner). A pair of standing waves evolves as a result of the symmetry breaking, with eigenvalues that are split by S, as defined in equation (15). When S has a real contribution, a saddle point is formed by two orthogonal standing waves, one with positive and one with negative feedback. It can be understood that the azimuthal order $2m$ of $\hat{C}(\theta)$ causes this splitting, as it excites the $2m$ antinodes of these standing waves, respectively. In Figure 4, the growth rate and frequency are shown as a function of $\arg(S)$, which is the phase between the acoustic pressure and heat release rate. This phase is directly related to the phase of a flame transfer function, which is often used to describe the heat release response to acoustic excitation.

4.4 Interaction between mv_θ and S

This case corresponds to the general situation in practical systems, where azimuthal velocity and symmetry breaking are expected to coexist. As both mv_θ and S appear in the root in the eigensolution equations (13) and (14), some interaction takes place, shaping the

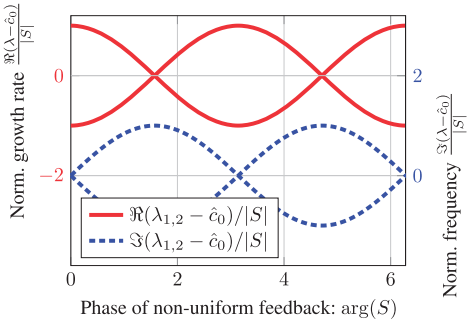

Figure 4. Effect of the phase of the non-uniform feedback $\arg(S)$ on the eigenvalues of the thermoacoustic system, without angular bulk velocity v_θ. Normalization by the cylindrical asymmetry strength $|S|$.

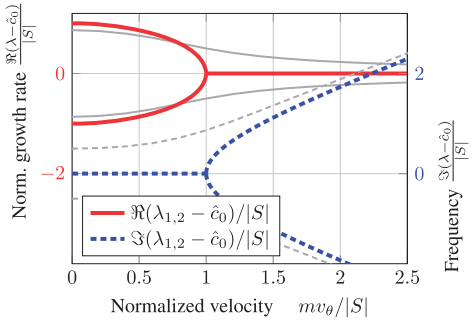

Figure 5. Normalized effect of the interaction between mv_θ and cylindrical symmetry breaking S on the eigenvalues of the thermoacoustic system, with $\arg(S) = 0$. In gray thin lines, the result for $\arg(S) = \pi/6$.

modal solutions. What the eigenmodes look like is not directly clear from the analytic expressions. The interaction in this intermediate regime can be understood qualitatively as follows; the azimuthal feedback non-uniformity tries to develop a standing wave solution, but the bulk velocity constantly rotates the acoustic field away from its standing wave angle. Two new equilibria will therefore evolve, given by the full eigensolution. The interaction is most pronounced when the two effects are of similar magnitude; $|S| \approx |mv_\theta|$. In the regime where $|mv_\theta/S| \ll 1$, solutions are predominantly standing waves, whereas $|mv_\theta/S| \gg 1$ is better characterized as travelling waves.

The velocity term can cancel out the eigenvalue splitting as a result of the symmetry breaking strength. An important observation is that only limited azimuthal velocity is required for noticeable changes in the stability analysis. Instability is most likely to occur in strongly underdamped (thermo)acoustic eigenmodes, say with a damping ratio of the order $\zeta = \mathcal{O}(10^{-2})$. Azimuthal velocity can potentially change the stability with strength mv_θ, therefore azimuthal Mach numbers of the same order $M_\theta = \mathcal{O}(10^{-2})$ are already relevant in the presence of cylindrical symmetry breaking.

4.5 Bifurcation point

The case where $\hat{c}_{2m} = \hat{c}^\star_{-2m}$ is of most interest, because the feedback contributes optimally to the real part of the eigenvalues and thus to the system stability. Physically, this occurs when the non-uniform part of the feedback response $\hat{C}(\theta)$ is real, i.e. the non-uniform heat release response acts in phase with acoustic pressure oscillations. The symmetry breaking S is real and the feedback phase is constant around the azimuth. The bifurcation diagram with mv_θ as the bifurcation parameter forms a unit circle and unit parabola for the growth rate and frequency difference, respectively, when normalized by $|S|$ (see Figure 5). Without azimuthal velocity, two standing wave solutions in orthogonal orientations are found, with pure positive and negative feedback. In a phase portrait, this solution is represented by a saddle point (shown in Figure 6(a)). As a mean flow is introduced, the splitting of the growth rate decreases and simultaneously the eigenvectors lose their mutual orthogonality. A bifurcation point at $|mv_\theta| = S$ emerges as the discriminant in the root of the dynamical solutions crosses zero. At this point, the two eigenvectors coincide, as Figure 6(e) suggests. In other words, the eigenvectors are linearly dependent and the system matrix is defective. For comparison, a case with complex S is shown in Figure 5 (thin gray lines) that does not cross the bifurcation point. In that case, the feedback partially acts on the frequency, preventing the discriminant in the eigensolution (equations (13) and (14)) to become zero.

The bifurcation point as shown in Figure 5 can be dangerous during the operation of an annular combustion system. As the bifurcation parameter varies a little, the stability can abruptly change near the bifurcation point.

4.6 Non-normal growth

In the case of non-normality, especially, coinciding eigenvectors, perturbations to the system can experience transient amplification. When the system has a nonlinear response to the amplitude, an instability can be triggered even though the system is fixed point stable at zero amplitude. Non-normal growth has been studied in thermoacoustic systems, based on modelling[15] as well as experiments.[16] In this section, non-normal growth in annular combustion systems is demonstrated in the bifurcation point of the model

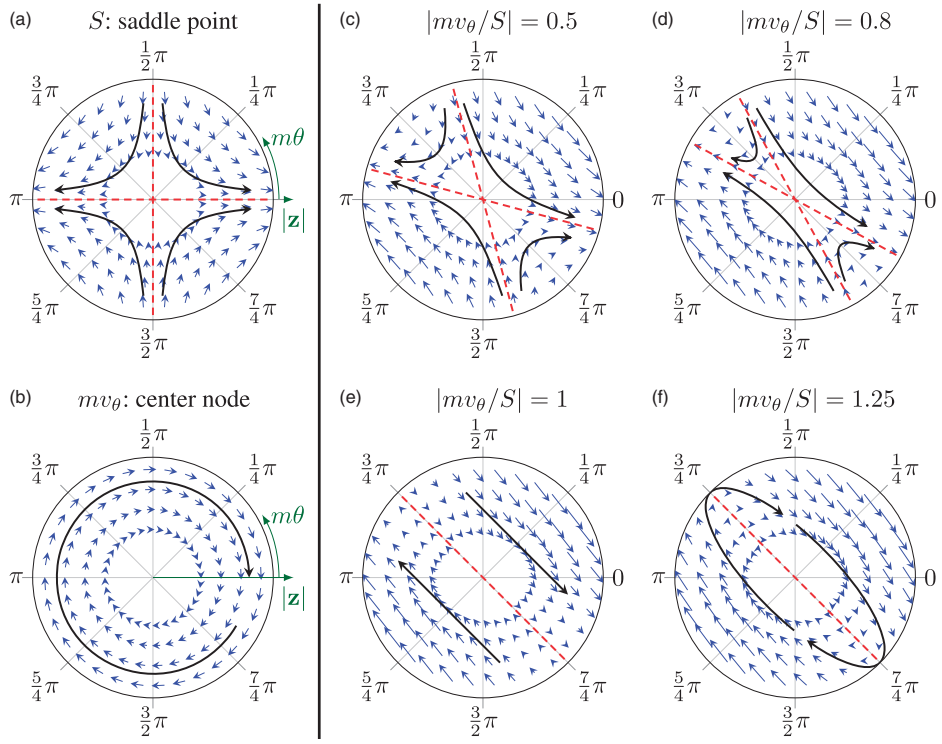

Figure 6. Phase portraits of the thermoacoustic system for real azimuthal symmetry breaking S, in the vector space of two orthogonal standing waves. Vectors show the tangents of possible dynamic trajectories, of which a few options are plotted by curved arrows. Eigenvectors are shown as dashed lines passing through the origin. The acoustic amplitude $|\mathbf{z}(t)|$ is represented by the radial distance to the origin and the angular orientation $m\theta$ of the standing wave can be read from the angle in the phase portrait. (a) A real azimuthal asymmetry S results in a saddle point, with an unstable standing wave with orientation $m\theta = 0$ and a stable standing wave at $m\theta = \pi/2$. (c,d) Increasingly adding azimuthal velocity – a centre node shown in (b) – brings the eigenvectors together. In the bifurcation point (e), a neutrally stable improper node is found, with coinciding eigenvectors. (f) For higher velocities, the standing wave solutions are convected by the flow, rather than being kept in place by the cylindrical symmetry breaking. A contribution of $\hat{c}_0$ could be included by superposing a star node, influencing the overall stability.

system. Due to the annular geometry, the amplitude amplification can occur at a single mode order revealing an insightful physical mechanism behind the transient growth.

The dynamic solution of the defective system matrix takes the form

$$\mathbf{z}(t) = 2S\left(Ate^{\hat{c}_0 t} + Be^{\hat{c}_0 t}\right)\mathbf{v} + Ae^{\hat{c}_0 t}\mathbf{w} \tag{16}$$

where v is the (repeated) eigenvector, while w is chosen as the standing wave orthogonal to v. Amplitudes A and B follow from initial conditions.

The term $Ate^{\hat{c}_0 t}$ causes the transient behaviour before the exponential decay sets in. Transient growth can occur only when the system would have been unstable in one orientation (saddle point), if there were no azimuthal bulk flow. From the solution in equation (16), the maximum transient growth can be obtained analytically (see Appendix 2). For $\Re(\hat{c}_0)^2 \ll S^2$, the time after which the maximum amplification occurs is approximately $t_{\max} = -1/\Re(\hat{c}_0)$. At this point, a maximum possible amplification ratio is reached of about

$$\frac{|\mathbf{z}(t)|}{|\mathbf{z}_0|} = \frac{-2S}{\Re(\hat{c}_0)e} \tag{17}$$

The transient growth is demonstrated for $S = mv_\theta = 10s^{-1}$ and a thermoacoustic decay of $\Re(\hat{c}_0) = -2s^{-1}$. The phase portrait of the dynamic system is shown in the top of Figure 7. The two thick lines represent the solutions that experience the maximum possible transient growth, starting on the unit circle. In the plot below this transient growth of the

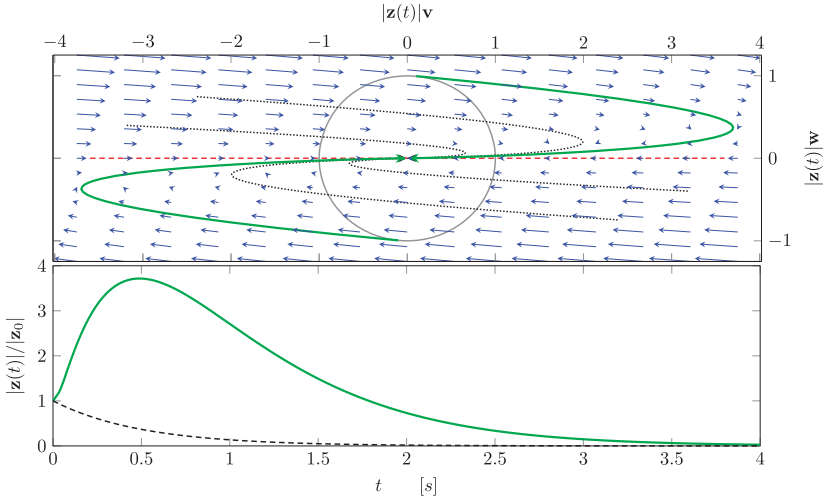

Figure 7. Transient growth of the acoustic amplitude in the bifurcation point of the system, with $S = mv_\theta = 10s^{-1}$ and $\lambda = \Re(\hat{c}_0) = -2s^{-1}$, starting from the initial conditions that lead to the maximum transient growth. Above, the evolution in the phase portrait (eigenvector aligned with the *x*-axis) shows the rotation of the acoustic field. Below, the growth is plotted as a function of time, compared to the case of normal decay (dashed line). The maximum growth amplification is accurately approximated by equation (17).

amplitude is shown as a function of time. A maximum amplitude amplification of 3.7 is reached as estimated by equation (17). This is equivalent to an amplification factor of over 13 for the acoustic energy.

Alternatively, the maximum amplification and the corresponding initial conditions can be found computationally (see for example Nagaraja et al.[17]). Using this approach, the same results have been found (not shown). For this specific low-order model, the amplification can be computed analytically at the bifurcation point. In this way, it has been found theoretically that infinite transient growth can be obtained for nonzero splitting strength and vanishing stability (refer to case $|mv_\theta/S| = 1$ in Figure 6(e), where a perturbation away from the eigenvector pair linearly grows to infinity, even though the system is marginally stable).

With help of the phase portrait representations, the transient behaviour of this system can be easily understood physically. A perturbation in an unstable orientation of the symmetry breaking will initialize exponential growth. In the phase portrait of Figure 7, these orientations are located in quadrant 1 (positive–positive) and quadrant 3 (negative–negative). The azimuthal flow then convects the growing amplitude around the circumference towards the stable orientation of the saddle node. The growth will eventually come to a halt and the perturbation will converge to the least stable eigenmode and decay accordingly.

4.7 Amplitude statistics under stochastic excitation

The maximum transient amplification shows what amplitude can be reached for an optimized initial condition. More interesting is what effect the non-normality of the system has on the characteristics under constant stochastic forcing. To investigate this, the system of equations (equation (12)) has been integrated numerically with white noise excitation, using the Euler–Mayurama scheme. The system is compared to the uncoupled, degenerate case (uniform heat release response) with the same set of eigenvalues $\Re(\lambda_{1,2}) = \Re(\hat{c}_0) = -2s^{-1}$. Part of the two time series that were subjected to the same excitation noise are shown in Figure 8. The average amplitude (RMS) of the non-normal system is found to be 5 times higher (25 times for the acoustic energy) than the degenerate system, which is higher than the maximum possible non-normal growth ratio. This result suggests it is more interesting to look at the integral of the amplitude over time for all initial conditions, rather than looking at the maximum possible amplification.

The probability density function of the Euclidean norm of four independent, normal distributed variables (two complex amplitudes) is given by the χ_4 distribution. The histogram of the bottom time series in Figure 8 shows that the χ_4 distribution accurately describes the probability of the amplitudes found for the uncoupled thermoacoustic system. For the

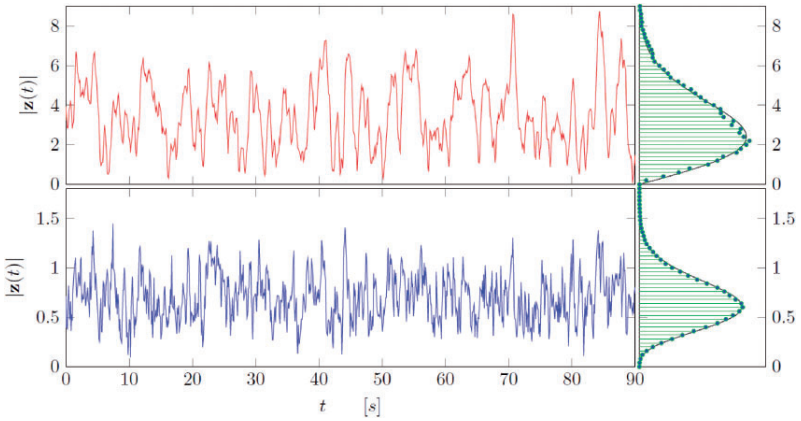

Figure 8. Time series of stochastically forced systems, with eigenvalues $\lambda_{12} = -2s^{-1}$. Above: bifurcation point; below: degenerate case (uncoupled). The RMS value of the non-normal system is 5 times higher compared to the degenerate case, both under unit forcing strength. Note the difference in amplitude histograms (based on 14 min) on the right, compared to χ_2 and χ_4 distributions (solid lines), respectively.

non-normal system matrix, however, the amplitude distribution is much better described by the χ_2 distribution, i.e. a process with only two independent variables. This result can be explained by the strong coupling of the waves (caused by the anti-diagonal in the system matrix, equation (12)), predominantly yielding standing waves under a preferred angular orientation. The latter distribution has a higher kurtosis than the former, which means that the observed peaks in the time series are relatively high with respect to the mean amplitude.

When monitoring a stochastically forced oscillating signal, the exponential decay of the autocorrelation function can normally be used to estimate the damping of the system.[18] Underlying assumption is that the oscillation comes from a dynamic system that can be described by a single damped harmonic oscillator. In the annular geometry, the dynamics is described by two coupled harmonic oscillators, which is why the damping cannot be obtained from the autocorrelation decay. Especially in this example with a strong non-normal system matrix, the autocorrelation function does not show a clear behaviour of exponential decay and the decay is much slower than expected from the eigenvalue pair. Moreover, this example shows that monitoring strategies that are meant to warn for unstable combustion dynamics, respond differently to the non-normal nature of the system, depending on the monitored quantity. Stability criteria based on acoustic amplitude and the entropy of the signal (see for example Sarkar et al.[19]) would indicate a significantly reduced stability margin for the non-normal system, compared to the normal system with identical damping rate.

5 Conclusions

An annular thermoacoustic system with both azimuthal bulk flow and non-uniform response can show highly interesting dynamics, even under linear assumptions. As the damping ratio is typically much smaller than one, it is found that small azimuthal Mach numbers can be relevant for the thermoacoustic stability through the interaction with azimuthal non-uniformities. Similar to the C_{2n} criterion in Noiray et al.,[4] specific Fourier components of the non-uniform heat release in the annulus are found to contribute to eigenvalue splitting, resulting in two orthogonal standing wave solutions. A concurrent split in the acoustic propagation velocity between CW and ACW waves, however, impairs the formation of standing wave solutions.

Solving the acoustic field numerically, it is demonstrated that a velocity gradient in the azimuthal flow, induced by co-rotating swirlers, cause a frequency split through the refraction of acoustic waves. This implies that a slowly rotating acoustic field does not prove the presence of an azimuthal bulk flow in the annulus. The split in frequency between ACW and AC waves is, against this new knowledge, conveniently expressed in terms of an effective azimuthal flow. The azimuthal flow can stabilize standing wave solutions that would otherwise be unstable as a result of a broken geometrical symmetry or non-homogeneous flame response. In reverse, a loss of azimuthal flow can cause a sudden decrease of thermoacoustic stability. As the effective azimuthal flow follows from operating conditions in a non-trivial way, instability can occur unexpectedly. Therefore, the coupling between the acoustic field and the azimuthal flow

field could be an important nonlinear phenomenon in thermoacoustics of annular gas turbines.

The type of eigenmode solution depends on the ratio between the azimuthal flow velocity per wavelength and the cylindrical asymmetry. When their strengths are of the same order of magnitude, both phenomena must be regarded in the stability analysis of annular thermoacoustic systems. When the ratio is close to one, the system can behave in a strongly non-normal manner. A bifurcation point exists where the system matrix is defective. It is shown analytically that the maximum transient growth in this point is infinite for vanishing system stability. This prove of transient growth for azimuthal modes, considering just a single mode order, comes with a comprehensible physical explanation; an azimuthal velocity rotates an acoustic field past angular orientations with varying instantaneous growth rates, modulating the amplitude transiently.

A non-normal system can yield significantly higher amplitudes when stochastic forcing is applied, compared to the degenerate counterpart with equal eigenvalues. This effective amplification under random excitation is considered more relevant than the maximum possible transient amplification ratio. The statistical moments of the acoustic amplitude also change as a result of the linear coupling between the waves. The increased peakedness of the amplitude should not be mistaken with intermittency due to nonlinearities. For the monitoring of combustion dynamics (such as amplitude, decay rate and instability precursors), it is valuable to know that azimuthal eigenmode pairs can behave non-normal and how typical monitoring quantities respond to this. It is shown that for constant damping rate (i.e. thermoacoustic stability), the acoustic amplitude and predictability of the time series can rise remarkably for increased non-normality.

Acknowledgements

The authors express their gratitude to Max Meindl for numerically solving the acoustic Euler equations. The presented work is part of the Marie Curie Initial Training Network Thermo-acoustic and aero-acoustic nonlinearities in green combustors with orifice structures (TANGO).

Declaration of Conflicting Interests

The author(s) declared no potential conflicts of interest with respect to the research, authorship, and/or publication of this article.

Funding

The author(s) disclosed receipt of the following financial support for the research, authorship, and/or publication of this article: We gratefully acknowledge the financial support from the European Commission under call FP7-PEOPLEITN-2012.

References

1. Ewins DJ. Vibration characteristics of bladed disc assemblies. *J Mech Eng Sci* 1973; 15: 165–186.
2. Wolf P, Staffelbach G, Gicquel LYM, et al. Acoustic and Large Eddy Simulation studies of azimuthal modes in annular combustion chambers. *Combust Flame* 2012; 159: 3398–3413.
3. Bauerheim M, Salas P, Nicoud F, et al. Symmetry breaking of azimuthal thermo-acoustic modes in annular cavities: A theoretical study. *J Fluid Mech* 2014; 760: 431–465.
4. Noiray N, Bothien M and Schuermans B. Investigation of azimuthal staging concepts in annular gas turbines. *Combust Theory Modell* 2011; 15: 585–606.
5. Worth NA and Dawson JR. Modal dynamics of self-excited azimuthal instabilities in an annular combustion chamber. *Combust Flame* 2013; 160: 2476–2489.
6. Bourgouin JF, Durox D, Schuller T, et al. Ignition dynamics of an annular combustor equipped with multiple swirling injectors. *Combust Flame* 2013; 160: 1398–1413.
7. Choe SY. *Investigation of a constricted annular acoustic resonator*. Master Thesis, Naval Postgraduate School, http://calhoun.nps.edu/bitstream/handle/10945/8575/investigationofc00choe.pdf (1997, accessed 8 June 2017).
8. Joos F, Polifke W and Ni A. Combustion device for generating hot gases, http://patft1.uspto.gov/netacgi/nph-Parser?patentnumber=6449951 (2002, accessed 8 June 2017).
9. Berenbrink P and Hoffmann S. Suppression of dynamic combustion instabilities by passive and active means. In: *International gas turbine and aeroengine congress & exposition*, 2000-GT-0079, ASME, Munich, pp.7–7.
10. Evesque S, Polifke W and Pankiewitz C. Spinning and azimuthally standing acoustic modes in annular combustors. In: *Proceedings of the 9th AIAA/CEAS aeroacoustics conference*, Paper AIAA 2003-3182, 12–14 May 2003, Hilton Head, South Carolina, AIAA 2003-3182, http://arc.aiaa.org/doi/pdf/10.2514/6.2003-3182 (2003, accessed 8 June 2017).
11. Emmert T, Bomberg S and Polifke W. Intrinsic thermoacoustic instability of premixed flames. *Combust Flame* 2015; 162: 75–85.
12. Crocco L and Cheng SI. *Theory of combustion instability in liquid propellant rocket motors*. London: Butterworths Science Publication, 1956, pp.021502-1–021502-8.
13. Rouwenhorst D, Hermann J and Polifke W. Online monitoring of thermoacoustic eigenmodes in annular combustion systems based on a state-space model. *J Eng Gas Turb Power* 2017; 139: 021502-1–021502-8.
14. Paschereit CO and Polifke W. Investigation of the thermoacoustic characteristics of a lean premixed gas turbine burner. In: *International gas turbine and aeroengine congress & exposition*, Stockholm, ASME 98-GT-582.
15. Juniper M. Triggering in the horizontal Rijke tube: Non-normality, transient growth and bypass transition. *J Fluid Mech* 2011; 667: 272–308.
16. Kim KT and Hochgreb S. Measurements of triggering and transient growth in a model lean-premixed gas turbine combustor. *Combust Flame* 2012; 159: 1215–1227.

17. Nagaraja S, Kedia K and Sujith RI. Characterizing energy growth during combustion instabilities: Singularvalues or eigenvalues? *Proc Combust Inst* 2009; 32: 2933–2940.
18. Lieuwen T. Online combustor stability margin assessment using dynamic pressure data. *Trans ASME* 2005; 127: 478–482.
19. Sarkar S, Chakravarthy SR, Ramanan V, et al. Dynamic data-driven prediction of instability in a swirl-stabilized combustor. *Int J Spray Combust Dyn* 2016; 8: 235–253.

Appendix 1

Derivation of equation (5): The Rayleigh criterion can be written as

$$\frac{1}{\gamma-1}\frac{\mathrm{D}}{\mathrm{D}t}(\hat{p}^\star\hat{p}) = \dot{Q}\hat{p}^\star + \dot{Q}^\star\hat{p} \tag{18}$$

Regarding the slow azimuthal dynamics

$$\frac{1}{\gamma-1}\frac{\mathrm{D}}{\mathrm{D}t}(\phi^\star\phi) = \dot{Q}\phi^\star + \dot{Q}^\star\phi \tag{19}$$

Seeking the complex growth of ϕ as a function of the heat release $\dot{Q}$, we can keep the following part

$$\phi^\star\frac{\mathrm{D}\phi}{\mathrm{D}t} = (\gamma-1)\dot{Q}\phi^\star \tag{20}$$

The equation has to hold for both amplitudes in $\mathbf{z}$ independently as the basis functions are orthogonal, so we can write

$$\frac{\mathrm{D}\mathbf{b}\cdot\mathbf{z}}{\mathrm{D}t} = (\gamma-1)\dot{Q} \tag{21}$$

writing out the total derivative

$$\mathbf{b}\cdot\frac{\mathrm{d}\mathbf{z}}{\mathrm{d}t} + v_\theta\left(\mathbf{z}\cdot\frac{\mathrm{d}\mathbf{b}}{\mathrm{d}\tilde{\theta}}\right) = (\gamma-1)\dot{Q} \tag{22}$$

to retrieve the effect on $\mathbf{z}$

$$\frac{\mathrm{d}\mathbf{z}}{\mathrm{d}t} = (\gamma-1)\mathbf{b}^\star\dot{Q} - v_\theta\left(\mathbf{b}^\star\cdot\mathbf{z}\cdot\frac{\mathrm{d}\mathbf{b}}{\mathrm{d}\tilde{\theta}}\right) \tag{23}$$

The average effect over the volume V can be written as

$$\frac{\mathrm{d}\mathbf{z}}{\mathrm{d}t} = (\gamma-1)V\oint\mathbf{b}^\star\dot{Q}\mathrm{d}\theta - v_\theta\left(\mathbf{b}^\star\cdot\mathbf{z}\cdot\frac{\mathrm{d}\mathbf{b}}{\mathrm{d}\tilde{\theta}}\right) \tag{24}$$

because the right-most term is not a function of θ. The volume and ratio of specific heats are combined in a single proportionality constant: $\kappa = (\gamma-1)V$

$$\frac{\mathrm{d}\mathbf{z}}{\mathrm{d}t} = \kappa\oint\mathbf{b}^\star\dot{Q}\mathrm{d}\theta - v_\theta\left(\mathbf{b}^\star\cdot\mathbf{z}\cdot\frac{\mathrm{d}\mathbf{b}}{\mathrm{d}\tilde{\theta}}\right) \tag{25}$$

Appendix 2

Derivation of equation (17): We have the solution in terms of two standing waves (equation (16))

$$\mathbf{z}(t) = 2S\left(Ate^{\hat{c}_0 t} + Be^{\hat{c}_0 t}\right)\mathbf{v} + Ae^{\hat{c}_0 t}\mathbf{w} \tag{26}$$

A solution that starts on a unit circle and reaches the maximum will start tangential to the unit circle and then grow. This means the first derivative of the acoustic energy is zero (and the second positive). The acoustic energy is

$$|\mathbf{z}^2(t)| = \left(4S^2(At+B)(A^\star t+B^\star) + AA^\star\right)e^{2\Re(\hat{c}_0)t} \tag{27}$$

We know that travelling waves decay with $-\Re\lambda$ without growing transiently (on a time scale longer than a cycle). Therefore, any travelling energy content would reduce the transient growth. For this reason, we reduce our search to real values for A and B. Derivative at $t=0$, starting on the unit circle: $A^2 + 4S^2B^2 = 1$

$$|\mathbf{z}^2|'_{t=0} = 4ABS^2 + \Re(\hat{c}_0) = 0 \tag{28}$$

Solutions for A and B are

$$A = \pm\sqrt{\frac{1}{2}\pm\frac{1}{2}\sqrt{1-\frac{\Re(\hat{c}_0)^2}{S}}} \tag{29}$$

$$B = \frac{\sqrt{1-A^2}}{2S} = \pm\sqrt{\frac{1}{8S^2}\mp\frac{1}{8S^2}\sqrt{1-\frac{\Re(\hat{c}_0)^2}{S^2}}} \tag{30}$$

One of the (positive and negative) solution pairs are the initial condition for maximum growth, whereas the other pair points to the conditions where the maximum amplitude is located. This can be deduced by looking at the second derivative of the acoustic energy. Inserting the found initial amplitudes in the derivative of acoustic energy, the time to the maximum amplitude can be solved for

$$\begin{aligned}&\frac{1}{2}|\mathbf{z}^2(t)|'e^{-2\Re(\hat{c}_0)t}\\&= 4S^2(A^2t(\Re(\hat{c}_0)t+1) + AB(2\Re(\hat{c}_0)t+1)) + \Re(\hat{c}_0)\end{aligned} \tag{31}$$

Solving the polynomial for the time t, the time t_{max} is found at which the maximum amplitude is reached

$$t_{max} = \frac{-1}{\Re(\hat{c}_0)}\sqrt{1 - \frac{\Re(\hat{c}_0)^2}{S^2}} \tag{32}$$

Backsubstitution of t_{max} and amplitudes A and B in equation (27) yield the maximum amplitude growth, given by

$$|\frac{\mathbf{z}}{\mathbf{z_0}}|_{max} = \frac{-\Re(\hat{c}_0)}{S}\frac{e^{-\sqrt{1-\frac{\Re(\hat{c}_0)^2}{S^2}}}}{1-\sqrt{1-\frac{\Re(\hat{c}_0)^2}{S^2}}} \tag{33}$$

Clearly for $S^2 = \hat{c}_{2m}\hat{c}_{-2m} \gg \Re(\hat{c}_0)^2$, this can be simplified to

$$|\frac{\mathbf{z}}{\mathbf{z_0}}|_{max} = \frac{-\Re(\hat{c}_0)}{eS}\frac{1}{\frac{\Re(\hat{c}_0)^2}{2S^2}} = \frac{-2S}{\Re(\hat{c}_0)e} \tag{34}$$

Appendix 3

Nomenclature

A, B	Acoustic amplitudes of the defective system
$\mathbf{b}$	Vector with acoustic amplitudes $\hat{F}$ and $\hat{G}$
$\hat{c}_k$	Fourier components of $\hat{C}(\theta)$
$\hat{C}(\theta)$	Azimuthal feedback strength distribution
$\hat{F}$	Anticlockwise travelling acoustic wave
$\hat{G}$	Clockwise travelling acoustic wave
m	Azimuthal mode order
M	Thermoacoustic system matrix
M	Mach number
$\dot{Q}(\theta)$	Fluctuating heat release
S	Cylindrical symmetry breaking strength
v_θ	Angular velocity
$\mathbf{v}, \mathbf{w}$	Standing wave vectors for the defective system
$\mathbf{z}$	Vector with azimuthal basis functions
ζ	Natural acoustic damping
$\tilde{\theta}$	Moving azimuthal coordinate $(\theta - v_\theta t)$
κ	Feedback proportionality constant
λ	Eigenvalue of the thermoacoustic system
ν	Eigenvector of the thermoacoustic system
$\phi(\theta)$	Acoustic field along the azimuthal coordinate
$\psi(x, r)$	Acoustic field along the axial and radial coordinates

Proceedings of ASME 2018 Turbo Expo: Turbomachinery Technical Conference & Exposition
GT2018
June 11-15, 2018, Lillestrøm, Norway

GT2018-75468

PART-LOAD LIMIT REDUCTION OF A FRAME 9E USING A PRECURSOR FOR COMBUSTION DYNAMICS

Driek Rouwenhorst*
Robert Widhopf-Fenk
Jakob Hermann
IfTA Ingenieurbüro für Thermoakustik GmbH
Gröbenzell, 82194, Germany
Email: driek.rouwenhorst@ifta.com

Matthias Häringer
Fakultät für Maschinenwesen
Technische Universität München
Garching, 85748, Germany
Email: haeringer@tfd.mw.tum.de

Julius Becker
Jürgen Gerhard
Julian Niedermeier
Service Technik und Produktion
SWM, Stadtwerke München
München, 81371, Germany

ABSTRACT

In a test campaign to lower the minimum part-load of a combined cycle plant, a series of turndown tests on two GE Frame 9E gas turbines with DLN1 combustor technology were carried out under premix operation by Stadtwerke München (SWM). It has been found that the load can be reduced significantly compared to the conventional turndown ratio, before either CO emissions or combustion dynamics form the limiting factor of the turndown test. To exploit this potential safely and operate the gas turbines close to these physical limits, emissions and combustion dynamics must be monitored online. The azimuthal thermoacoustic mode that is observed in the can-annular machines is monitored with the IfTA PreCursor, based on the online determination of the modal decay rate. For this method, the acoustic pressure is measured at the cans around the gas turbine circumference to observe the azimuthal acoustic propagation that is enabled by the cross-firing tubes between the cans. Using this strategy to monitor CO emissions and thermoacoustic stability in real-time, a reduction of the minimal part-load limit by approximately 20% is achieved for the considered gas turbines. In must-run situations without demand for electricity generation, the operating costs can be directly reduced by the fuel savings. As an additional benefit, SWM can offer a broader power reserve for grid stabilization on the energy market. This monitoring strategy has been fully implemented in the control system and first experiences of the extended part-load limit are currently being gathered.

*Address all correspondence to this author.

NOMENCLATURE

C Output matrix
M System matrix
q Acoustic amplitude vector
$\dot{q}$ Time derivative of q
s Analytic sensor output
w Stochastic realization

INTRODUCTION

Changing demands and low electricity prices in the European energy market require increased energy supply flexibility from gas turbine operators. Therefore, power plants that are able to adapt power generation to the electricity demand quickly over a broad load range, become increasingly competitive. Although load flexibility is an important design requirement nowadays, the main focus during prior gas turbine development was to achieve maximum efficiency at rated power. For existing gas turbine power plants, load flexibility can be achieved by extending the operating range under low-NO_x operation. The manufacturers provide upgrades for their fleets to increase operational flexibility, such as extending the range for the inlet guide vanes of Siemens G-class gas turbines [1] and upgrading the fuel staging for the GE Frame 9E gas turbines [2]. Upgrades by the original manufacturer generally come with a warranty. However, when operators try to enhance the flexibility of their gas turbines on their own behalf, this does not apply.

Copyright © 2018 by ASME

During the operation of two Frame 9E gas turbines by SWM, confidence grew that the machines might have more turndown potential than that which is guaranteed by GE and programmed in the control logic. Through careful exploration of off-design operating conditions outside of the regular operating window, an extension of the gas turbine flexibility, without the need to purchase upgrades or change gas turbine hardware, is sought. Potential issues related to the combustion process were expected, including a changed thermal load in the combustion chamber, thermoacoustic instabilities, lean blow-off, flashback and increased pollutant emissions. Turndown tests have shown that the lower boundary of the load of these particular gas turbines is limited either by CO-emissions or increasing amplitudes of combustion dynamics. Although short-term exceedance of CO-emissions can be compensated, unstable combustion dynamics should generally be avoided as this can cause structural damage. Prediction of operating conditions with unstable combustion dynamics is a promising strategy to avoid high amplitudes which would jeopardize reliable operation at reduced turndown ratios.

In this work, the combustion dynamic activity that emerges in the turndown tests below the conventional turndown ratio is shown. The monitoring strategy has been developed to extend the turndown ratio with the help of a precursor for thermoacoustic instabilities. Thermoacoustic precursors are tools to predict future high combustion dynamic amplitudes based on real-time measurements. These tools can be based on pattern recognition, in which a measure for the predictability of the time series is quantified [3–5] or based on an exponential decay rate of thermoacoustic eigenmodes [6, 7].

The successful implementation of a thermoacoustic precursor enables real-time monitoring of all relevant phenomena that limit the part-load ratio, which in turn allows safe gas turbine operation below the conventional turndown limit. Data from the commissioning of the gas turbines verifies the functioning of this monitoring strategy and shows that for these specific machines a reduction of the part-load limit of more than 20% is achievable.

COMBUSTION DYNAMICS

The interaction between the combustion process and the gas dynamics in the gas turbine is referred to as combustion dynamics or thermoacoustics. The flame causes acoustic disturbances through heat release fluctuations and the acoustic fluctuations in turn can modulate the flame. Turbulent combustion in the cans ensure a constant presence of pressure and velocity fluctuations, especially visible at resonance frequencies of the combustion chamber geometry. When the flame(s) and an acoustic mode in the gas turbine feature a positive feedback loop, the natural damping can be overcome, yielding a linearly unstable system in which the amplitudes quickly rise and saturate to establish limit cycle oscillations.

Monitoring Methods

The most common method to monitor combustion dynamics, is to look at the amplitude level of the oscillations directly. An amplitude threshold is specified, above which the gas turbine in not supposed to run. This method works well as long as the amplitude varies smoothly with the changing operating parameters and conditions. The latter is not true for a dynamic system containing a bifurcation (transition from stable operation to limit cycle oscillations), as the amplitude effectively jumps or rapidly increases to an elevated level. The amplitudes can be well below the threshold, however, a tiny change in load can cause a fierce violation of the threshold that requires immediate action. Because of hysteresis it might be the case that a reversal of the change that led to instability, does not result in stabilization. For these reasons, an unscheduled power down might have to be initiated.

More sophisticated monitoring methods attempt to quantify the margin to unstable operating conditions, as a prediction tool for future high amplitudes. They can be grouped in methods that quantify the degree of chaos or predictability and methods that identify a linear decay rate exponent based on a low order model of the oscillations. In this work the IfTA PreCursor is used, specifically designed to monitor azimuthal instabilities that occur in the gas turbines under consideration. In contrast to other available methods, this method uses several sensors around the circumference, required to properly capture the dynamics of azimuthal modes. Because the orientation of the mode shape is not known in advance and can rotate freely, at least two sensors must be installed to observe the amplitude and phase of the azimuthal mode shape (shown in Fig. 4). In this case it would have quite an influence for the degree of chaos/predictability whether a sensor is installed at can 5 or 8. Furthermore it is uncertain how methods that rely on the degree of chaos/predictability, respond to other sound sources in a real gas turbine, such as the sound emitted by the compressor blades. In methods like the IfTA PreCursor that use the identified decay rate of a specific mode as the stability margin, a bandpass filter is used to isolate the dynamics of that mode only, mitigating the influence of other (non-stochastic) sound sources.

IfTA PreCursor

The IfTA PreCursor for azimuthal combustion dynamics, is based on the identification of the decay rate of a thermoacoustic mode with known mode order. This mode order, the amount of wavelengths around the circumference, can be estimated from the frequency or inferred from synchronous measurements around the circumference. In this investigation, the instability is of the first mode order, as seen in the instantaneous pressure fluctuations in multiple cans during one oscillation cycle (refer to Fig. 4). The acoustic fluctuations with said wavelength propagate in clockwise and anticlockwise directions through the

Copyright © 2018 by ASME

cross-firing tubes around the circumference of the gas turbine. While these acoustic waves pass the burners, they influence the heat release, resulting in an acoustic source of the same wavelength that, in turn, feeds back to the acoustic waves. Together with acoustic losses, this feedback loop results in a growth or decay of the two waves, possibly as a function of their relative azimuthal positioning. Disregarding nonlinear interactions, such as a nonlinear flame response, these dynamics can be described mathematically by the state space representation in Eq. 1.

$$\begin{aligned} \dot{\mathrm{q}} &= \mathbf{M}\mathrm{q} + \mathrm{w_q} \\ \mathrm{s} &= \mathbf{C}\mathrm{q} + \mathrm{w_s} \end{aligned} \tag{1}$$

The first line describes how the two acoustic amplitudes in vector q grow or decay as a result of their own presence, through the linear system matrix **M**. On the second line, the output of acoustic sensors s is given by linear combinations of the two waves. An output matrix **C** with size $N \times 2$ relates the output of N sensors to the acoustic waves q, depending on the respective azimuthal sensor locations. The stochastic forcing of the thermoacoustic system $\mathrm{w_q}$ comes from the heat release fluctuations, caused by the turbulent combustion process. Acoustic fluctuations that don't fit to the prescribed mode order and sensor noise are contained in the output noise vector $\mathrm{w_s}$. The dynamics in the system matrix **M**, including the feedback response of the flames, is unknown. It is merely assumed that the dynamic system is linear and consists of two azimuthal waves. It must be noted that all variables in Eq. 1 are complex, i.e. convey phase information by means of an imaginary contribution. Therefore, **s** is the analytic representation of the actual sensor output.

With data from acoustic sensors at different circumferential positions, the system is observable, i.e. can be identified. Solving the eigenvalue problem of the system matrix **M** yields two decay rates and eigenfrequencies, with their corresponding eigenvectors. The IfTA PreCursor is proportional to the least stable eigenvalue, i.e. the smaller of the two identified decay rates. The eigenvector states the contribution of the two waves and therefore determines whether the decay rates correspond predominantly to standing or traveling waves. A more detailed description of the low-order thermoacoustic model and the identification methods can be found in Rouwenhorst et al. [7].

GAS TURBINE OPERATION

The gas turbines considered in this work are located in a power plant in the south of Munich operated by Stadtwerke München (SWM). A description of the power plant, gas turbines and their operating conditions are presented to put the investigation into perspective.

Power Plant

Electric power has been generated since 1899 at this plant site alongside the Isar river in Munich. These days, the plant consists of two combined cycles in 2x1 configuration, including supplementary firing possibilities. An important task of the plant is the cogeneration of district heat for a substantial part of the 800 km long piping system under the city streets. In the near future, a heat storage system will be installed and geothermal heat will be exploited to feed the continuously growing district heating network with a sustainable heat source. With a total installed electric power of 698 MW alongside a thermal power of 814 MW for district heating, this is one of the two major power plants in Munich.

Gas Turbines

In 2004, this power plant was expanded with a second combined cycle, consisting of two General Electric gas turbines and a Siemens steam turbine, all on independent axes. Both Frame 9E gas turbines, model PG9171E, are designed to generate a base load of 124MW electric under standard conditions. Combustion takes place in 14 annularly arranged combustor cans, connected to the turbine inlet by transition pieces. For ignition of the primary combustion zone, the cans are interconnected by cross-firing tubes. The combustors are equipped with Dry Low NO_x combustion systems (DLN1) [8], as a best available technology (BAT) for NO_x emission reduction, and are controlled by a Mark V control system [9]. The DLN combustion system achieves a low combustion temperature by premixing the combustion gases to meet stringent emission regulations, significantly lowering the formation of NO_x compared to non-premixed combustion systems. Premixed combustion is enabled in the regular operating range, whereas non-premixed combustion covers other operating conditions, e.g. during the start-up sequence, where increased NO_x emissions are tolerated temporarily, to ensure stable combustion.

Operational Considerations

The market price for power generation in Europe has shown a slight downward trend since the commissioning of the gas turbines. As natural gas is a relatively expensive fuel compared to coal, it is often not economically viable to operate gas turbines in base load. However, for grid stabilization, gas fired power plants are among the most suitable energy sources. With high ramp rates, power can be adjusted quickly to apply primary and secondary reserve control, provided the gas turbines are running and have the appropriate reserves at their disposal. The gas turbines are also used to protect the municipal 110kV grid, for example, to avoid stressing the coupling between the municipal grid and the high-voltage lines of transmission system operator TenneT, by compensating a drop-out of another plant. Together with the demand for district heating, these considerations lead to increased

Copyright © 2018 by ASME

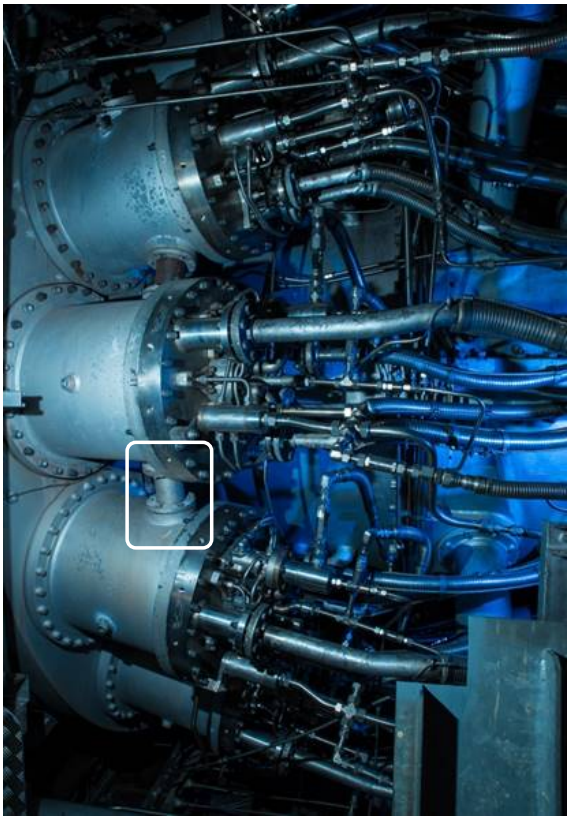

FIGURE 1. PICTURE OF THE FRAME 9E GT61 SHOWING THE COMBUSTOR CANS. MULTIPLE FUEL LINES ARE CONNECTED TO ENABLE A VARIETY OF DLN1 COMBUSTION MODES. A CROSS-FIRING TUBE IS HIGHLIGHTED, CONNECTING NEIGHBORING CANS

part-load operation hours in must-run situations. Under these circumstances, a low turndown rate is particularly lucrative, with lower fuel costs and an increased available power reserve.

Gas Turbine Control and Part-Load Restrictions

The Mark V control system is programmed to change the operation of the gas turbines according to the requested load. The main controls are the gas valves and the inlet guide vane (IGV) angle to change the air mass flow through the compressor. While controlling the load, the control system has to comply to various operating restrictions, for example the maximum allowable temperature in the combustion chamber to which the first turbine stage is exposed. There is also a restriction on the minimum combustion chamber temperature in which the gas turbines can be operated in premixed mode. When the temperature falls below this threshold, the combustion is automatically switched to non-premixed mode to ensure stable combustion. The latter restricts the turn-down rate, as the combustion becomes progressively leaner with decreasing load and thus the firing temperature decreases also. In non-premixed combustion modes, the NO_x emission restriction cannot be met, so a decision is required to either raise the load again and switch back to premixed combustion or turn off the gas turbine. The emission legislation in Germany prescribes a maximum NO_x emission level of $50 mg/m_N^3$ averaged over the day [10]. Half-hour averages may reach the twofold of this value, such that a short term outlier can be compensated within a reasonable time frame. The switching to non-premixed mode at low firing temperatures causes a minimal achievable load in premixed mode of about 50% base load [8] depending mainly on atmospheric conditions. The control temperature is not measured in the combustion chamber, but is a calculated reference temperature based on the exhaust gas temperature and compressor discharge pressure.

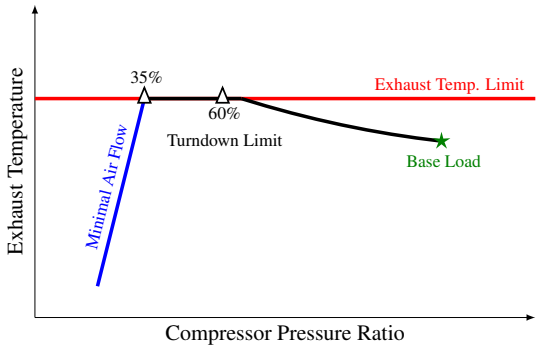

FIGURE 2. EXHAUST TEMPERATURE AS A FUNCTION OF THE COMPRESSOR PRESSURE RATIO ON FRAME 9E, AS A RESULT OF CONTROL CURVES AND PHYSICAL LIMITATIONS. REPRODUCTION OF FIGURE 7 IN ROMOSER ET AL. [2]

Physical Part-Load Restriction

The load of gas turbines in premixed mode is limited by the rather inflexible combustion process; the combustion itself must be stable and the resulting exhaust gas temperature and pollution levels are restricted. The inlet guide vanes (IGV's), in combination with inlet bleed heat system, allows a decrease in air mass flow, while the revolutions per minute remain constant at grid frequency. Figure 2 shows the turndown path of a frame 9E, in terms of exhaust temperature and compressor pressure ratio. In base load, the IGV's are open for a high air flow rate to the combustion chambers. Fuel is mixed with the air flow to achieve the

Copyright © 2018 by ASME

maximum allowable temperature at the first turbine stage, maximizing the efficiency of the gas turbine cycle. The IGV angle is controlled on the basis of the combustion chamber reference temperature, derived from the exhaust gas temperature and compressor pressure. At reduced load, the IGV's close accordingly to keep the equivalence ratio constant and temperature in the combustion chamber at its maximum. Because the compression ratio decreases for reduced loads, the Brayton cycle efficiency also decreases and the exhaust gas temperature increases to maintain constant firing temperature. At a certain part-load reduction level the control logic is based on the exhaust temperature limit rather than the combustion chamber reference temperature. From this point on, the IGV closes slower while reducing the load, so that the combustion becomes progressively leaner and the firing temperature reduces. After a further load reduction, the combustion chamber reference temperature drops below the threshold where the control system would reignite the primary combustion zone to leave the premixed combustion mode. This threshold is set, because flame stability and CO-emission compliance can't be guaranteed for all gas turbines under all possible conditions. When the load is reduced even further, the IGV reaches the most restricting angle setting and further air flow reduction is not possible. From this point on (around 35% part-load under standard conditions) the combustion process becomes progressively leaner, such that the gas turbine can only be operated with diffusion flames. The stretch between roughly 35% and 50% part-load is a region where premixed combustion is theoretically possible but not supported by the manufacturer, as phenomena such as combustion dynamics and formation of CO can inhibit continuous operation in this operating regime. The limit for CO emissions is 100 mg per normalized cubic meter exhaust gas, averaged over a production day. Within a half-hour time window, it is allowed to emit the double amount; 200 mg/m_N^3. This specific cogeneration plant has an additional local government restriction on the CO-emissions at a lower daily average of 90 mg/m_N^3.

LOAD REDUCTION TESTS

Load reduction tests were carried out on the pair of Frame 9E gas turbines to get an insight in the actual physical limiting phenomena and obtain an indication whether it is possible to safely reduce the prescribed part-load limit. This project was carried out by SWM, supported by IfTA GmbH with regard to the challenges presented by combustion dynamics. In addition to the existing gas turbine instrumentation, high-temperature dynamic pressure transducers were installed on the cans to measure the acoustic fluctuations in the combustion chambers.

Test Description

In an extensive test campaign, load reductions in premixed combustion mode were carried out on the GT61 and GT62 machines independently. The reference temperature threshold at which the control system switches off the premixed combustion mode was set to a lower temperature. At first, the turndown range between 35% and 50% has been explored cautiously with small load reduction steps. Subsequently, the part of this range in which the combustion turned out to be stable was tested dynamically, with the standard load ramp rates.

TABLE 1. ACHIEVED TURNDOWN RATIOS AND LIMITING PHENOMENA CO (CO-EMISSION LIMIT) AND CD (COMBUSTION DYNAMICS) OF THE PRESENTED TURNDOWN TESTS. TEST TD2C WAS PERFORMED DURING RECOMMISSIONING OF THE GAS TURBINES AFTER FULL IMPLEMENTATION OF THE MONITORING BASED TURN-DOWN EXTENSION

Turndown test	TD11	TD12	TD21	TD2C
Gas turbine	GT61	GT61	GT62	GT62
Original turndown*	50%	50%	50%	50%
Achieved turndown	37%	37%	42%	36%
Limited by	CO/CD	CO/CD	CO	CO/CD

* approximately, under standard atmospheric conditions.

Normally, the fuel split between the different injection points is optimized to yield minimal NO_x emissions at base load. This fuel split is not necessarily optimum for part-load conditions, therefore the load reductions were performed several times with varying fuel split settings. The fuel split tuning itself is not considered in this work, however, a selection of the tests is presented to show the setting of the precursor threshold and to validate its functionality. The test cases referred to are listed in Table 1.

Test Results

Figure 3 shows case TD11, with the load reduction of GT61 and the resulting acoustic amplitude in the combustor cans. At the start of the plot, the load is already reduced to 38% of the base load. At this point, the CO-emissions still comply to the regulations, although they have increased substantially. The combustion dynamics take place at lower frequencies in comparison to the combustion dynamics observed in base load, while the overall amplitude is low. Two further load reduction steps (less than one percentage point of load ratio reduction at a time), caused rapidly increasing pressure fluctuations at a specific frequency. Although amplitude and frequency are obfuscated in Fig. 3, it can be stated that prolonged operation with elevated oscillation amplitudes should be strictly avoided, due to possible hardware degradation. In this test, the CO-emissions crossed the $90 mg/m_N^3$ at the time period where high amplitude combustion dynamics occurred. In most cases, the thermoacoustic instability

Copyright © 2018 by ASME

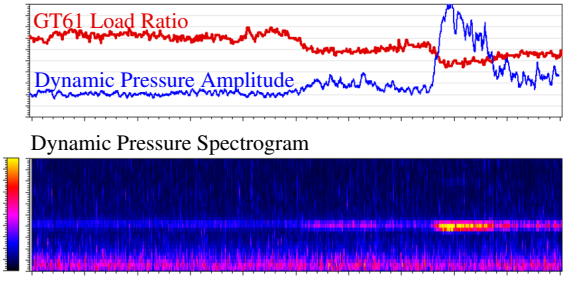

FIGURE 3. ACOUSTIC AMPLITUDE IN THE CANS DURING TURNDOWN TEST TD11. AXIS HAVE BEEN OBFUSCATED. THE TOP GRAPH SHOWS THE LOAD RATIO AND THE AMPLITUDE IN THE FREQUENCY BAND OF THE UNSTABLE THERMOACOUSTIC MODE. THE SPECTROGRAM IN THE LOWER GRAPH SHOWS THAT THE AMPLITUDE EMERGES AT A SPECIFIC FREQUENCY

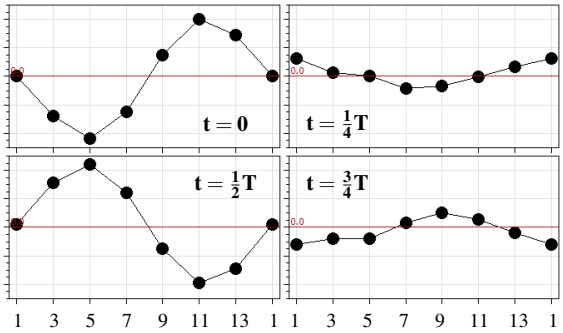

FIGURE 4. INSTANTANEOUS DYNAMIC PRESSURE AMPLITUDE AT EVERY SECOND CAN, SHOWING THE PHASE EVOLUTION OF A SINGLE CYCLE OF THE THERMOACOUSTIC EIGENMODE DURING COMBUSTION INSTABILITY DURING TURNDOWN TEST TD11

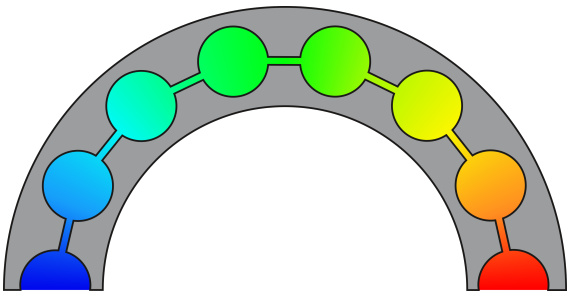

FIGURE 5. SKETCH OF THE ACOUSTIC PROPAGATION AROUND THE GAS TURBINE CIRCUMFERENCE, ENHANCED BY COMMUNICATION THROUGH THE CROSS FIRING TUBES

and the CO-limit were reached simultaneously, within the resolution of the performed load steps. Because a temporary breach of the daily emission limit can be compensated for, the priority is lower in comparison to the combustion dynamic instability. Unstable combustion dynamics form a real threat for the machine and therefore more attention to lowering the turndown ratio in regular operation is required. Because the combustion instability can occur earlier or later, depending on many factors, including atmospheric conditions, machine aging, assembly tolerances and fuel split, a significantly lower turndown ratio cannot be based on a single set of turndown tests.

Influence of Fuel Split The fuel split of the DLN combustor distributes the fuel over injectors in the first and second combustion zone, mainly influencing the flame shape and the quality of the premixing of the fuel. It has been established (evidence not included in this work) that the fuel split influences whether the combustion dynamics or the CO-emissions form the limiting factor for the minimum turndown. On GT61, the standard fuel split setting (minimizing NO_x at base load) causes both operating limits to occur almost simultaneously, forming the optimal fuel split for extended turndown as well.

Comparison of the GT's Although the GT61 and GT62 are identically engineered, the turndown tests were performed on both machines. With the experience from the GT61, the GT62 was tested with a reduced selection of sensors in case TD21. Qualitatively, the GT62 showed similar results, with both CO-emissions and combustion dynamics forming a restriction for the part load limit. A remarkable difference between two gas turbines is that the GT62 could achieve a minimal emission-conform load ratio of about 42%, whereas the GT61 could be operated down to around 37%. This shows that even identically constructed machines can behave significantly different during operation, which indicates that large safety margins must be taken into account when defining a fixed turndown ratio for a fleet of gas turbines, even of the same model. One hypothesis for the difference between the machines is that the combustion chamber reference temperature is no longer an accurate representation of the firing temperature, meaning that the GT62 is controlled to run leaner than supposed. This observed difference suggests individually set turndown ratios for the two gas turbines should be applied, ideally with constant monitoring to account for changes to stability limits.

Observed Combustion Dynamics

The unstable combustion dynamic mode observed in Fig. 3 has such low frequency that the corresponding wave length is too large to correspond to an acoustic mode in the individual combustor cans. The explanation is found by analyzing the phase-

Copyright © 2018 by ASME

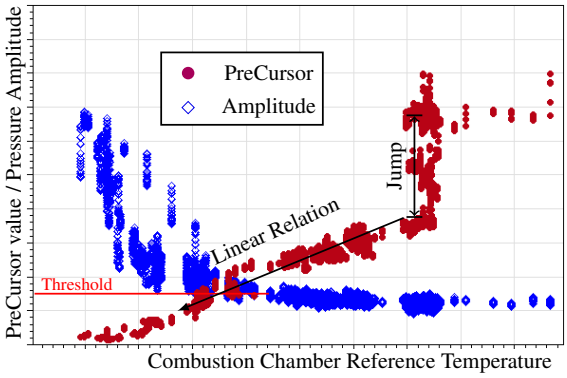

FIGURE 6. PRECURSOR AND ACOUSTIC AMPLITUDE AS A FUNCTION OF THE COMBUSTION CHAMBER REFERENCE TEMPERATURE IN TEST TD11. DURING A LOAD REDUCTION THE REFERENCE TEMPERATURE EVENTUALLY DECREASES. NEAR THE OPERATIONAL LIMIT, A SUDDEN INCREASE IN AMPLITUDE IS OBSERVED. THE PRECURSOR DEPENDS RELATIVELY LINEAR ON THE REFERENCE TEMPERATURE, WHICH MAKES IT SUITABLE FOR CONTROL PURPOSES. THE JUMP IN THE STABILITY IS CAUSED BY A CHANGE IN FUEL SPLIT. THE PRECURSOR THRESHOLD WAS DETERMINED ON BASIS OF THIS FIGURE

synchronization of the measured oscillations between multiple cans. Figure 4 shows the instantaneous dynamic pressure at every second combustor can during the period of elevated oscillation amplitudes. The four graphs, taken from a single cycle, show that the oscillations in the cans are synchronized and form an azimuthal mode shape, approaching the behavior of a standing wave of the first azimuthal mode order. Figure 5 shows an impression of the acoustic field around the gas turbine circumference, requiring communication between the cans. The cross-firing tubes, one of which is highlighted in Fig. 1, enable this azimuthal acoustic wave propagation. Additionally, some acoustic communication between cans may take place directly behind the compressor outlet and in front of the first turbine stage.

Precursor Threshold

The precursor was tested on the turndown data presented in Fig. 3 and 4 (TD11) based on a set of dynamic pressure transducers around the circumference of GT61. Figure 6 shows the result, as a function of the calculated combustion chamber reference temperature. Although the amplitude shows a sudden increase at low firing temperatures, the precursor decreases approximately linearly. Moreover, the value can be interpreted as a quantitative prediction of the stability margin, since marginal-stability will occur when the precursor reaches zero. The stability margin for combustion dynamics is determined by precursor threshold, which has been defined on the basis of Fig. 6 (i.e. case TD11).

That the stability of the combustion dynamics is not just a function of the firing temperature can be seen from the jump in the precursor at constant combustion chamber temperature. Here the fuel split was changed with constant IGV and load and thus also a constant firing temperature. This shows that the fuel split affects the stability of the combustion dynamics and can be observed by application of the precursor, whereas no obvious change could be observed on basis of the acoustic amplitude. The observed resolution for the stability margin confirms it is viable to operate the gas turbines at the boundary of stable operation under all conditions during a load reduction, by performing adequate online monitoring of the combustion dynamics.

Monitoring of Stable Combustion

After setting the threshold for combustion dynamics, the precursor was tested on data of turndown test TD12, to validate the functioning of the strategy. TD12 differs from TD11 by a relatively small change in fuel split. The result is shown in Fig. 7, in which the precursor is shown below the operating conditions and the spectrogram of the pressure fluctuations in the combustor cans. The precursor starts well above the threshold. Synchronized with the load reduction steps, the precursor approaches the threshold, which warns for the combustion instability. When the first warning is given, no sign of instability is seen in the acoustic spectrum. When the precursor crosses the threshold again and more severely, it is associated with a short spike in the acoustic energy. When the warning is ignored and a further load reduction is undertaken to ascertain that an instability is pending, self-sustained limit cycle oscillations indeed develop.

For the calculation of the precursor, configuration settings are required to optimize the decay rate identification. These settings correspond to the definition of the band-pass filter that isolates the mode of interest and the degree of averaging that is applied in the identification process. The averaging in the identification (i.e. smoothing) of the precursor is a trade-off between the accuracy of the stability margin identification and its response time to a change in stability. Since the precursor is based on previously measured data, a small time lag is inevitable. A sufficiently high threshold for the precursor can intercept both a low identification accuracy and an identification time lag. The precursor settings used in Fig. 7 result in a relatively smooth line, that is able to adapt promptly to the changing stability as a result of the load reduction. The warning for combustion instability comes before an increase in acoustic energy is even observed, providing additional time to take stabilizing measures, such as employing a small increase of the gas turbine load.

Copyright © 2018 by ASME

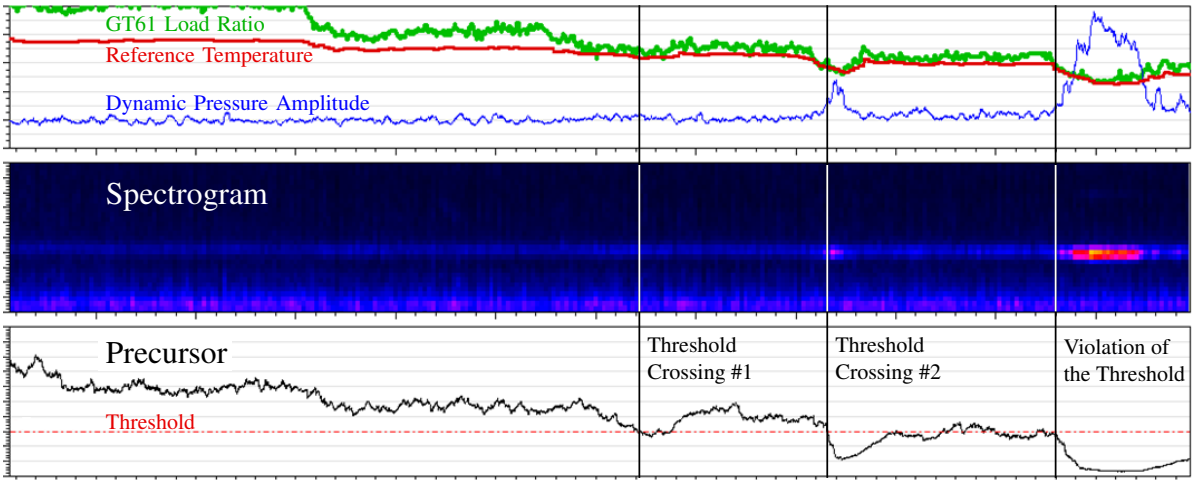

FIGURE 7. VALIDATION OF THE SET THRESHOLD ON THE PRECURSOR VALUE ON TURNDOWN TEST TD12. THE FIRST WARNING IS GIVEN BEFORE ANY INCREASE OF AMPLITUDE CAN BE OBSERVED. CONTINUING FURTHER WITH THE LOAD REDUCTION CAUSES A SPIKE IN THE AMPLITUDE AND EVENTUALLY A SHORT PERIOD OF LIMIT CYCLE OSCILLATIONS WITH INCREASED AMPLITUDE

IMPLEMENTATION AND COMMISSIONING

For long-term online monitoring of combustion dynamics, an IfTA ArgusOMDS system is used by SWM, which synchronously records the high-temperature pressure transducer signals around the circumference and the gas turbine parameters. The calculation of the precursor is performed on the digital signal processor (DSP) directly for every newly available chunk of measured data, to ensure quick identification of the stability margin.

The Mark V control system is adapted so that the transfer to a non-premixed combustion mode at preset combustion chamber reference temperature is shifted to a lower value, allowing the exploitation of the extended part-load range. Additional boundaries for part-load operation are determined by CO-measurements in the exhaust gas and the precursor for the relevant combustion dynamic instability. In the background, the amplitude of combustion dynamics is monitored, to forestall harmful amplitudes at other frequencies and in case the precursor malfunctions. Figure 8 shows data from the commissioning of the monitoring-based turndown extension of GT62, test case TD2C. Starting around the conventional turndown limit, the load is reduced below 40%. As a response, the precursor value significantly drops and the CO-emissions increase. Note that a time delay is involved in the determination of the emissions in the down-stream exhaust gases. Further lowering of the load is performed with caution, as the precursor approaches the threshold and simultaneously, the CO-emissions approach the regulation limit. That both limiting factors restrict the part-load simultaneously means that the fuel split is optimal for the turndown limit.

When one of the limits is crossed, the load can be automatically increased slightly, to ensure continued operation. By using the precursor as guide in this commissioning test, it is possible to approach the limit of combustion stability, without crossing the point of linear instability. Therefore the amplitude can rise in a controlled way, without the typical jump accompanied by an instability. During this commissioning run, a turndown ratio of 36% was achieved on GT62, on the edge of allowed emissions, acoustic amplitudes and thermoacoustic stability.

Note that the achieved load reduction is lower in comparison to turndown test TD21, where 42% was the minimal load ratio reached. This can be explained by a scheduled maintenance performed on the gas turbines between the turndown tests and the commissioning of the turndown extension. It is a direct example of the influence that assembly tolerances, fouling and/or aging of gas turbines can have on their operability range, which illuminates the benefit of real-time monitoring over setting preset operation limits.

CONCLUSION

At load ratios significantly below the conventional operating limit, a low frequency humming emerges in the combustion chambers of the two GE Frame 9E gas turbines. This is caused by combustion dynamics, propagating from can to can through

Copyright © 2018 by ASME

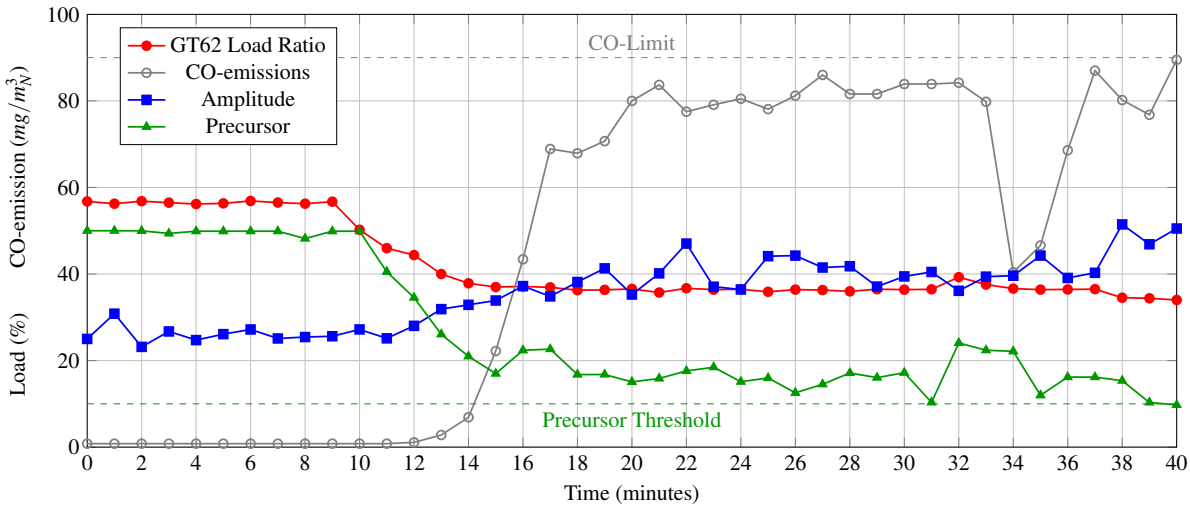

FIGURE 8. DATA FROM THE COMMISSIONING OF THE MONITORING BASED TURNDOWN EXTENSION (TD2C), WITH LOW TEMPORAL RESOLUTION. AMPLITUDE AND PRECURSOR ARE NORMALIZED, TO START AT 25 AND 50 RESPECTIVELY. A LOAD RATIO OF 36% IS ACHIEVED ON GT62, FULFILLING THE EMISSION RESTRICTIONS AND WITHOUT HIGH AMPLITUDE COMBUSTION DYNAMICS. THE PRECURSOR AND THE CO-EMISSIONS REACH THE BOUNDING LIMITS AT APPROXIMATELY THE SAME LOAD. THE ACOUSTIC ENERGY INCREASES, BUT INSTABILITY COULD BE AVOIDED BY RESPECTING THE PRECURSOR THRESHOLD

the cross-firing tubes. Either CO-emissions or these thermoacoustic oscillations mark the turndown limit under low-NO_x premixed operation, depending on the fuel split among other things. The time from warning to instability can be controlled by the height of the precursor threshold and the load reduction rate of the gas turbine. In this deployment on an industrial gas turbine, the IfTA PreCursor adequately responds to a stability reduction of combustion dynamics by the identification of the linear decay rate. The precursor responds approximately linear to a decrease in firing temperature, caused by a load reduction. The effect of a change in fuel split is also registered clearly. It has been demonstrated that it is possible to safely extend the turndown ratio of General Electric Frame 9E gas turbines, by careful online monitoring of emissions and the stability margin of the combustion dynamic mode that manifests under these conditions. Depending on the specific machine state and atmospheric conditions, a turndown ratio below 40% can be reached, compared to the conventional turndown limit at about 50%. This 20% reduction of the part-load limit results in significant fuel savings in case of must-run situations without explicit electricity demand. This is particularly profitable in a market where gas turbines are increasingly fired for power reserves, because the marketable load range is increased at the same time. This increased flexibility enables this power plant to better meet the requirements to generate district heat and electricity for the local grid.

REFERENCES

[1] Nag, P., Little, D., Teehan, D., Wetzl, K., and Elwood, D., 2008. "Low load operational flexibility for Siemens G-class gas turbines". In Power-Gen International 2008, Orlando, Florida.

[2] Romoser, C. E., Harper, J., Wilson, M. B., Simons, D. W., Citeno, J. V., and Lal, M., 2016. "E-class late fuel staging technology delivers flixibility leap". In Proceedings of ASME Turbo Expo 2016: Turbomachinery Technical Conference and Exposition GT2016.

[3] Sarkar, S., Chakravarthy, S. R., Ramanan, V., and Ray, A., 2016. "Dynamic data-driven prediction of instability in a swirl-stabilized combustor". *International Journal of Spray and Combustion Dynamics,* ***8(4)***.

[4] Gotoda, H., Shinoda, Y., Kobayashi, M., Okuno, Y., and Tachibana, S., 2014. "Detection and control of combustion instability based on the concept of dynamical system theory". *Physical Review,* ***89***, p. 022910.

[5] Nair, V., and Sujith, R., 2014. "Multifractality in combustion noise and predicting an impending combustion instability". *Journal of Fluid Mechanics,* ***747***, pp. 635–655.

Copyright © 2018 by ASME

[6] Lieuwen, T., 2005. "Online combustor stability margin assessment using dynamic pressure data". *Transactions of the ASME,* ***127***, pp. 478–482.
[7] Rouwenhorst, D., Hermann, J., and Polifke, W., 2017. "Online monitoring of thermoacoustic eigenmodes in annular combustion systems based on a state-space model". *Journal of Engineering for Gas Turbines and Power,* ***139***(2), p. 021502.
[8] Davis, L.B., B. S., 2000. Dry low NOx combustion systems for GE heavy-duty gas turbines. Tech. rep., GE Power Systems.
[9] Johnson, D., Miller, R., and Ashley, T., 1996. GER-3658D: SPEEDTRONIC Mark V gas turbine control system. Tech. rep., General Electric.
[10] 13. BImSchV, 2013. Dreizehnte Verordnung zur Durchführung des Bundes-Immissionsschutzgesetzes (Verordnung über Großfeuerungs-, Gasturbinen- und Verbrennungsmotoranlagen - 13. BImSchV).

Copyright © 2018 by ASME

Check for updates

International journal of spray and combustion dynamics

Original Research Article

International Journal of Spray and Combustion Dynamics
2018, Vol. 10(4) 351–361
© The Author(s) 2018
Article reuse guidelines:
sagepub.com/journals-permissions
DOI: 10.1177/1756827718799043
journals.sagepub.com/home/scd
SAGE

In situ identification strategy of thermoacoustic stability in annular combustors

Driek Rouwenhorst[1], Jakob Hermann[1] and Wolfgang Polifke[2]

Abstract

In annular combustion systems, thermoacoustic eigenmodes can manifest as standing waves, traveling waves or some form in between. Which dynamic solution appears in a combustor depends on details, regarding the flow field and (unintentional) breaking of the cylindrical symmetry of the annular combustion system. When these details are unknown, the specific behavior cannot be predicted from the characteristics of a single burner. Due to the (nearly) degenerate nature of the acoustic solution, annular eigenmodes come in pairs with practically the same eigenfrequency. In order to identify the thermoacoustic modes, conventional analysis of a spectral peak from a measurement does not suffice, because the peak is a superposition of the two eigenmodes. A method has been proposed to identify the two eigenmodes of given azimuthal mode order from multiple simultaneous measurements around the circumference of the combustion system. Using output-only identification on the acoustic signals, it is possible to estimate the individual mode shapes, frequencies and growth rates of the co-existing eigenmode pair. In this work, the strategy is applied to experimental data from an annular combustor. A split in the growth rate pair is observed during stable operation, depending on the equivalence ratio and flame-to-flame distance. It shows that in situ identification of annular thermoacoustics can reveal subtle dynamic effects, which is useful for testing and online monitoring of annular combustors. The moment when instability occurs can be foreseen under prevailing conditions, with simultaneous identification of the azimuthal mode structure.

Keywords

Annular combustor, azimuthal modes, combustion dynamics, monitoring, stability analysis

Date received: 27 October 2017; accepted: 16 August 2018

1. Introduction

In combustion systems with an annular combustion chamber, the low frequency azimuthal modes are a major concern regarding thermoacoustic stability. These modes, in which the flames of individual burners couple with acoustic waves traveling around the combustion chamber circumference, can reach such high amplitudes that a limited operability window must be accepted or structural damage might occur.

Compared to axial thermoacoustic modes, azimuthal modes are more complex. Due to the cylindrical symmetry of the geometry, acoustic solutions consist of pairs with the same wavelength. These degenerate pairs cannot be isolated in frequency domain because their eigenfrequencies are identical. Existing methods to identify modal damping are not suited for the (nearly) degenerate thermoacoustic mode pairs found in annular combustors.

Another complication is that the flames are excited by transverse acoustics leading to several sources of heat release fluctuations. Following the review paper of O'Connor et al.[1] concerning transverse flame excitation, heat release fluctuations are predominantly generated by axial fluctuations, caused by 'injector coupling'.

[1]IfTA GmbH, Gröbenzell, Germany
[2]Professur für Thermofluiddynamik, Technical University of Munich, Garching, Germany

Corresponding author:
Driek Rouwenhorst, IfTA Ingenieurbuero fuer Thermoakustik GmbH
Industriestrasse 33, Groebenzell 82194, Germany.
Email: driek.rouwenhorst@ifta.com

Creative Commons Non Commercial CC BY-NC: This article is distributed under the terms of the Creative Commons Attribution-NonCommercial 4.0 License (http://www.creativecommons.org/licenses/by-nc/4.0/) which permits non-commercial use, reproduction and distribution of the work without further permission provided the original work is attributed as specified on the SAGE and Open Access pages (https://us.sagepub.com/en-us/nam/open-access-at-sage).

Nevertheless, transverse fluctuations with respect to the flame do influence the heat release directly, for example investigated by Saurabh and Paschereit.[2] These minor contributions to the heat release response can be decisive on the modal behaviour in both the stable and limit cycle regime. With a model including a nonlinear dependency on azimuthal particle velocity, Ghirardo and Juniper[3] were able to obtain standing thermoacoustic limit cycle solutions. A classical stability analysis approach in which axial flame transfer functions (FTFs) are joined to an annular acoustic network is not able to account for a direct transverse flame response.

Several publications on the dynamic behaviour of azimuthal modes in limit cycle have been published, including Worth and Dawson,[4] Noiray and Schuermans[5] and Prieur et al.[6] to name a few. However, limited attention is paid for the fixed-point stable regime. Knowledge about stable operation can be important for optimization and online monitoring of annular combustors in their actual operational state. Rouwenhorst et al.[7] published a strategy to identify the azimuthal eigenmode pairs and obtain their decay rates from real-time measurements. The identification strategy was demonstrated on surrogate data only. The aim of this work is to apply the output-only identification on experimental data from an annular combustor, as a validation of the proposed strategy for practical time series.

The modal amplitudes are a nonlinear or even a discontinuous function of the modal stability, resulting in the step-like amplitude characteristic observed in Figure 2. When the effective damping becomes negative, the amplitude instantaneously rises to dangerous levels in limit cycle. An increase in amplitude before instability is often hard to recognise and a certain amplitude level is not monotonically related to the stability margin. Monitoring of the damping can predict a sudden increase of the amplitude, as it signifies the stability margin. Moreover, the resolution in the stable regime is higher, in comparison to the amplitude of thermoacoustic oscillations.

Several methods are available for the identification of the damping rate of thermoacoustic modes. Noiray[8] proposes to estimate damping or growth rate by the dynamics of the amplitude envelope. In the work of Mejia et al.,[9] four methods are tested on data from a laminar slot burner. However, none of these methods are suited for azimuthal eigenmodes. In general, the methods assume a single mode with no other modes with a nearby eigenfrequency, for example, the fitting of the probability density function. Otherwise, it is assumed the specific eigenmode of interest can be excited, such that the damped oscillating impulse response can be fitted. Azimuthal modes come in eigenvalue pairs with (nearly) equal eigenfrequencies and decay rates. Moreover, in industrial annular gas turbines, excitation is usually not feasible and it is unknown what azimuthal mode structure will develop. Therefore, the dedicated output-only identification method introduced in Rouwenhorst et al.[7] is proposed for the in situ identification of azimuthal thermoacoustic modes.

2. Methodology

Simultaneously measured acoustic signals recorded around the annular combustion chamber circumference are used to identify the dynamics of azimuthal thermoacoustic modes. The parameters of a low-order model are fitted to the data, such that the key dynamics is captured well. Modal behaviour, growth rates and frequencies can be determined from the model parameters. The objective is to identify the system in the low-amplitude stable regime, which justifies a linear description of the dynamics.

2.1. Model

The slow dynamics of the characteristic waves around the annulus is treated as a pair of coupled harmonic oscillators. The two wave amplitudes F and G are the anticlockwise (ACW) and clockwise (CW) acoustic waves, respectively, with angular resonance frequency ω_a. In combination with corresponding complex harmonic basis functions, they describe the acoustics in the combustion chamber of fixed mode order m.

$$p(t,\theta) = \Re(Fe^{i\omega_a t - im\theta} + Ge^{i\omega_a t + im\theta}) \tag{1}$$

It is assumed that the growth rate and frequency modifications that are caused by thermoacoustic feedback are very small compared to the acoustic resonance frequency. This allows linearization around the acoustic solution, decoupling the slow dynamics (amplitude modulations) and the fast dynamics (acoustic oscillations). A system of ordinary differential equations (ODEs) can describe the coupling between the two slowly varying harmonic oscillator amplitudes, including thermoacoustic feedback.

$$\begin{aligned} \frac{dF}{dt} &= a_{FF}F + a_{FG}G \\ \frac{dG}{dt} &= a_{GF}F + a_{GG}G \end{aligned} \tag{2}$$

Equation (2) governs the azimuthal dynamics of acoustic amplitude similar to the equations used by Noiray et al.,[10] limited to the general linearized form. It describes the rate of change of the amplitudes,

resulting from their own presence, as well as the presence of the wave travelling in the opposite direction. The coefficient a_{FF} comprises the linear heat release response H_F

$$\dot{Q}_F(\theta)e^{-im\theta} = H_F(\theta, \omega_a)Fe^{-im\theta} \tag{3}$$

Through a normalized Rayleigh integral that relates the acoustic growth to the product of the heat release and acoustic pressure distribution in equation (4), the thermoacoustic feedback coefficient a_{FF} (from F to $\dot{F}$) is complete

$$R_{FF} = \frac{1}{\dot{Q}_F}\frac{dF}{dt} \propto \frac{1}{\dot{Q}_F}\int \dot{Q}_F^* e^{im\theta} F e^{-im\theta} \mathrm{d}\theta \tag{4}$$

The * denotes the complex conjugate. Note that the heat release response is evaluated at the acoustic resonance frequency ω_{a}. By definition of R_{FF}, the feedback coefficient is given by $a_{FF} = H_F R_{FF}$, which can be verified by combining equations (1) to (3). Including a (real-positive) natural acoustic damping coefficient α_{F}, we have

$$a_{FF} = H_F R_{FF} - \alpha_F \tag{5}$$

Equal definitions for the coefficient a_{FG} read

$$\dot{Q}_G(\theta, \omega_a)e^{im\theta} = H_G(\theta, \omega_a)Ge^{im\theta} \tag{6}$$

$$R_{FG} = \frac{1}{\dot{Q}_G}\frac{dF}{dt} \propto \frac{1}{\dot{Q}_G}\int \dot{Q}_G^* e^{-im\theta} F e^{-im\theta} \mathrm{d}\theta \tag{7}$$

$$a_{FG} = H_G R_{FG} \tag{8}$$

Fundamentally, the cross-coefficient a_{FG} is zero, as the Rayleigh integral vanishes because the acoustic wave and the heat release fluctuations travel in opposite direction, i.e. $\int e^{-2im\theta}\,\mathrm{d}\theta = 0$. However, when H_G is not constant, but has an azimuthal dependency in the form of $H + C_{2m}e^{2m\theta}$, then thermoacoustic coupling between F and G is established, as first identified by Noiray et al.[10]

The two coefficients for the evolution of G are defined in an identical manner.

The dynamic system in equation (2) is subjected to stochastic noise from the turbulent combustion and is measured at several positions around the circumference. In matrix notation, a state-space representation is obtained.

$$\dot{\mathbf{x}} = \mathbf{M}\mathbf{x} + \mathbf{w}_{\mathbf{x}} \tag{9}$$

$$\mathbf{y} = \mathbf{C}\mathbf{x} + \mathbf{w}_{\mathbf{y}} \tag{10}$$

The vector $\mathbf{x} = [F, G]^T$ contains the complex pair of oscillator amplitudes. The complex 2×2 system matrix $\mathbf{M}$ characterizes the system dynamics with the four coefficients a_{XX}, forced by the stochastic process $\mathbf{w}_{\mathbf{x}}$ which originates from the turbulent combustion. The output vector $\mathbf{y}$ contains the N analytic pressure sensor output signals around the combustor circumference, possibly containing measurement noise $\mathbf{w}_{\mathbf{y}}$. The $N \times 2$ output matrix $\mathbf{C}$ contains information about the angular sensor positions and the monitored mode order. A nomenclature is attached at the end of this paper.

The system matrix $\mathbf{M}$ describes the evolution of the thermoacoustics. Amplitudes remain constant for pure acoustics (undamped and without thermal source term), in which case the system matrix is a null matrix. Damping rates of the two oscillators are real negative values on the diagonal. The anti-diagonal of the matrix establishes linear coupling of the oscillators. The two eigenvalues λ of $\mathbf{M}$ yield the thermoacoustic damping rates and frequency deviations from the acoustic resonance frequency ω_a.

$$\alpha_t = -\Re(\lambda) \tag{11}$$

$$\omega_t = \omega_a + \Im(\lambda) \tag{12}$$

The corresponding eigenvectors provide the mode structures, i.e. whether the observed modes are predominantly standing or traveling waves.

Since the heat release $H_{F/G}$ responds to the waves with their effective thermoacoustic frequency ω_t, rather than the pure acoustic resonance frequency ω_a, the presented model is a linearization of a transcendent eigenvalue problem. In practice, the nonlinear behaviour related to a non-constant FTF can lead to a discontinuous solution for continuous parameter changes, as demonstrated in Parmentier et al.[11] A relatively smooth FTF with moderate gain prevents the latter.

In equations (5) and (8), only thermoacoustic feedback and acoustic damping were considered. However, other phenomena could also contribute or influence the matrix coefficients, such as fluid dynamic coupling with the acoustics and an azimuthal flow that convects the acoustic field. In Rouwenhorst et al.,[12] more modelling details can be found. In this work, the system matrix $\mathbf{M}$ is considered as a black box to be identified, ignoring the underlying physical processes.

2.2. System identification

The thermoacoustics as modelled in equation (9) can be identified in several ways, which was shown in Rouwenhorst et al.[7] Such in situ identification yields the coupled thermoacoustic dynamics under the prevailing conditions. The pair of eigenvalues of the system matrix $\mathbf{M}$ yield the eigenfrequency deviations

and damping rates (i.e. stability margin) corresponding to the monitored azimuthal mode order.

In this work, two methods are applied to analyse the experimental data, based on subspace identification and least squares fitting, respectively. Main motivation to apply two methods is cross-validation, because no expected values or analytical predictions for the thermoacoustic system are available.

2.2.1. Preprocessing of the data. In both methods, a bandwidth of the Fourier spectrum is selected, isolating the spectral peak of interest, which is the first azimuthal mode order in this work. Only the positive frequencies in the bandwidth are transferred back to time domain, such that an analytic, filtered signal is obtained. The rectangular filter corresponds to a sinc filter in time domain. This filtering is required to keep oscillating dynamics that is not related to the azimuthal mode pair in question (such as other acoustic modes or blade passing frequencies), out of the analysis. Such dynamics, which is not accounted for in the low-order model description, is a source of structured noise for the identification method. Such noise affects the outcome of the identification significantly more than the (relatively white) noise floor of the measurement, including the quantization error of the pressure data digitization.

Discrete pre-processed data points are available to identify the state-space representation, requiring a discrete formulation of equations (9) and (10) as presented in equations (13) and (14).

$$\mathbf{x}(i+k) = \mathbf{A}\mathbf{x}(i) + \mathbf{v}_{\mathbf{x}}(i) \tag{13}$$

$$\mathbf{y}(i) = \mathbf{C}\mathbf{x}(i) + \mathbf{v}_{\mathbf{y}}(i) \tag{14}$$

In the discrete state-space representation, k is the sample offset between two system states replacing the time derivative in the continuous description. Matrix $\mathbf{A}$ is the discrete version of system matrix $\mathbf{M}$ and the noise vectors $\mathbf{v}$ replace their continuous model parameters $\mathbf{w}$. The eigensolution of the continuous matrix $\mathbf{M}$ is uniquely related to the eigensolution of $\mathbf{A}$.

2.2.2. Stochastic subspace identification. A stochastic subspace identification (SSI) algorithm has been applied following Tanaka and Katayama,[13] in which the entire structure of the discrete state-space representation in equations (13) and (14) is identified. An algorithm, including a weighted singular value decomposition of a matrix with time-delayed data sets, estimates the dominant dynamics for the chosen degrees of freedom. As the mathematics goes beyond the scope of this work, we refer the interested reader to the book of Katayama on this subject.[14]

It is important to note that the mode shape cannot be prescribed in this method, such that it is not possible to enforce a harmonic basis around circumference and exploit knowledge concerning the relation between sensor positions and azimuthal mode order.

Per sensor, three delayed time series were considered with mutual delay intervals of approximately two thermoacoustic cycles. Physically, this means that the dynamics is identified on basis of the evolution of all observed states, during a period of about four cycles each.

2.2.3. Least squares fitting. In the least squares fitting method, we first fit the characteristic waves F and G on basis of the pre-processed sensor outputs, applying the pseudoinverse on equation (14). Subsequently, the discrete system matrix is fitted to the temporal development of a set of these states, by inverting equation (13). Since the state vector is rank two, the two sets of equations in the state space representation can be inverted analytically.

This straightforward fitting strategy is referred to as LSQ. We choose the basis of ACW and CW traveling waves (F and G) to span the eigenspace of acoustic solutions, as used in the model description. For given mode order and at least three measurement locations, the wave amplitudes can now be fitted by taking the Moore–Penrose pseudoinverse of the overdetermined problem in equation (14).

$$\mathbf{x} = (\mathbf{C}^T\mathbf{C})^{-1}\mathbf{C}^T\mathbf{y} \tag{15}$$

When the system states $\mathbf{x}$ are obtained for several consecutive time instances, $\mathbf{A}$ is estimated by inverting equation (13). The concatenation of a set of state vectors $\mathbf{x}$ is denoted by $\mathbf{X}$, yielding the following expression for the pseudoinverse of equation (13).

$$\mathbf{A} = \mathbf{X}_{i+k}\mathbf{X}_i^T(\mathbf{X}_i\mathbf{X}_i^T)^{-1} \tag{16}$$

By using a recursive algorithm to update the estimate of matrix A, the amount of states taken per fit has no influence on the resulting estimate. This allows the real-time tracking of the system's state. Nevertheless, the estimate must be based on data from the past, to average out the forcing noise and measurement noise. Moreover, it must be noted that this two-step identification approach does not yield a bias-free estimate in the presence of measurement noise $\mathbf{v}_{\mathbf{y}}$.

Similarly to SSI, this method identifies the state-space based on a time delay Δt, which is equally set to the span of about four thermoacoustic cycles. A parameter study on the influence of this time delay parameter has shown that it should be picked carefully; after long time delays, the correlation between the two states

vanishes and too short time delays also result in poor results. The latter is thought to be related to the sinc filter used to isolate the frequency peak and/or the temporal correlation of the combustion noise.

3. Experimental data

Data from a laboratory scale annular combustor, kindly provided by Dawson and Worth,[15] have been used to validate the identification strategy on experimental data. The combustor rig, shown in Figure 1 was designed to investigate the azimuthal instabilities, including the effect of burner spacing. Fuel lines transport the perfectly premixed ethylene/air mixture towards the combustion chamber, where swirlers anchor the flames with co-rotating swirl, which is often used in industrial applications. The atmospheric rig is prone to instabilities of the first azimuthal mode order, producing high amplitude limit cycle oscillations with a frequency of around 1700 Hz. The burner spacing was varied by changing the number of fuel lines and swirl burners between the plenum and the annular enclosure, i.e. by replacing the middle section of the combustor in Figure 1.

For equal flame conditions, the Reynolds number at the swirl burners was kept constant in all cases. As a result, the total heat release increases with the number of burners and increasing equivalence ratio, therewith resulting in an increased speed of sound and natural frequencies.

A more extensive description of the experimental setup and measurement methods can be found in the excellent publications of Worth and Dawson.[4,15]

3.1. Measurements

Dynamic pressure was measured in three fuel lines, with 120° intervals equally distributed around the combustor circumference. The fuel lines were equipped with two pressure transducers, of which we used the ones closer to the combustion chamber for this work.

Three different burner separation distances were tried, adding up to a respective total of 12, 15 and 18 equally spaced burners around the combustor annulus, to investigate the effect of flame separation distance. For these three cases, a discrete set of 17 equivalence ratios was tested ranging between $\phi = 0.6$ and $\phi = 1$ with steps of 0.025. Measurements were performed under steady operation with a sampling rate of 30 kHz for a period of 4.36 seconds.

The combined root mean square of the three pressure transducers for the three burner separation cases is shown in Figure 2. For every burner spacing, the acoustic amplitude is low for equivalence ratios $\phi \leq 0.8$ and high for equivalence ratios $\phi \geq 0.85$, marking the transition from stable operation to limit cycle operation. The amplitude of the acoustics roughly increases an order of magnitude, corresponding to a factor 100 for the acoustic energy.

With the increasing equivalence ratio, the flame response will change. In first instance, the phase and gain are likely to be altered by the different fuel mixture. In addition, the temperature increase in the combustion chamber should be addressed, which can significantly change the burner impedance, depending on the acoustic characteristics of the plenum and fuel lines.

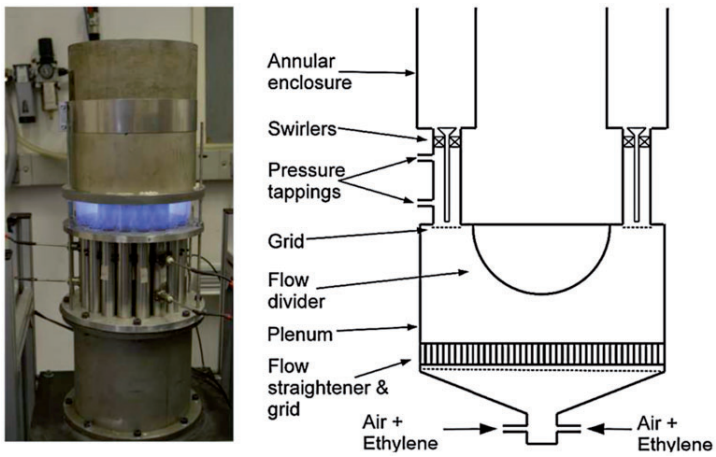

Figure 1. Photo and schematic of the laboratory-scale annular test rig, reproduced from Worth and Dawson[15] with permission.

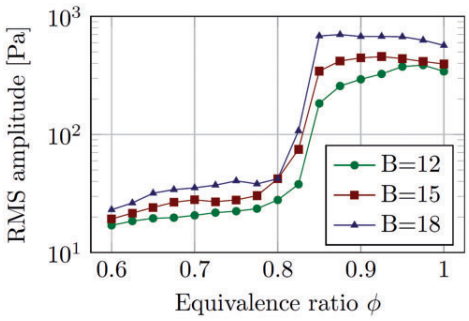

Figure 2. Root mean square of the acoustic amplitude as a function of equivalence ratio and burner spacing, previously published in Worth and Dawson.[4]

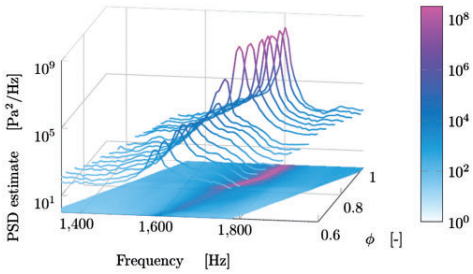

Figure 3. Power spectral density (PSD) as a function of equivalence ratio in the analysed bandwidth for the case with 18 burners.

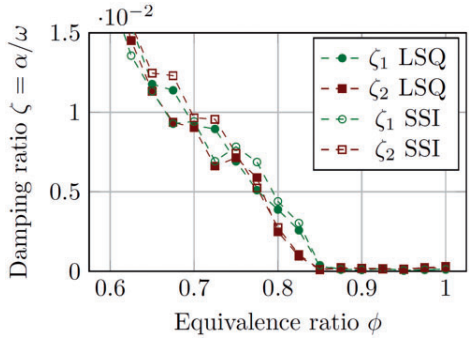

Figure 4. Pair of identified damping ratios as a function of equivalence ratio, for the first azimuthal mode order for the case with 12 burners.

4. Identification results

In this work, the aim is to identify the stability of the system as a whole, rather than discriminating between the phenomena that lead to the instability. The two identification methods are briefly described in Section 2. Methodology is applied to the data to obtain the global characteristics of the system, such as the damping rates and dynamic structure, which are contained in the eigensolution.

A bandwidth $\Delta f = 470$ Hz is used for identification, separating the first azimuthal mode from other spectral content, which moves with the resonance frequency for increasing the equivalence ratio. A waterfall plot with the power spectral density in this bandwidth is shown in Figure 3 for the case of 18 burners. The resonance frequency is located between 1550 and 1800 Hz under all operating conditions. A good isolation of the peaks is required such that other spectral content does not influence the identification process.

Since the operating conditions are kept constant per data set, the entire time series are analysed at once in this work. It must be noted that the same results are obtained using a recursive updating algorithm, generating intermediate identification results after every, for example, 1024th time stamp. Because the entire time series were required to obtain satisfactory stochastic convergence for some cases, intermediate results are not shown and uncertainties could not be evaluated.

A sample delay interval of $k = 1$ is used, such that the time delay is kept small and the correlation between two subsequent states is still clear.

4.1. Damping ratio

The growth rate that is recovered by the real part of the eigenvalue of the system matrix is rewritten to a damping ratio of a harmonic oscillator. To this end, the negated growth rate is divided by the identified frequency (in radians), which is given by the imaginary part of the eigenvalue.

$$\zeta_i = \alpha_i/\omega_t = -\Re(\lambda_i)/\omega_t \tag{17}$$

Figures 4 to 6 show the identified damping ratios for the case with 12, 15 and 18 installed burners, respectively. The results show that the system has a pair of damping ratios at low equivalence ratios, that vanishes between $\phi = 0.8$ and $\phi = 0.85$. The damping ratio does not become negative because the system quickly saturates to a limit cycle, rather than showing continuous exponential growth.

The pair of damping ratios is for many operating conditions clearly distinct, indicating split eigenvalues and a dynamic system that is not (exactly) degenerate. Especially for the case with 18 burners, the stability margins show an interesting behaviour with pronounced splitting of the growth rate.

Even though the effect of eigenvalue splitting is very small in comparison to the resonance frequency,

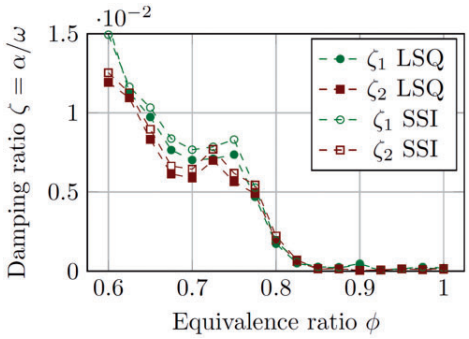

Figure 5. Pair of identified damping ratios as a function of equivalence ratio, for the first azimuthal mode order for the case with 15 burners.

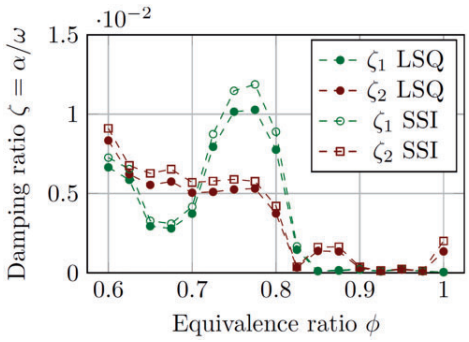

Figure 6. Pair of identified damping ratios as a function of equivalence ratio, for the first azimuthal mode order for the case with 18 burners.

it cannot be neglected with respect to the stability margin. This is directly related to the damping ratio, which is typically strongly underdamped ($\zeta \ll 1$) for thermoacoustic eigenmodes.

The near-degenerate pair of fixed-point stable eigenmodes always coexists, being excited by the combustion noise. This stands in contrast to limit cycle oscillations, in which an attractor often has a unique location in the phase space, see for example Noiray et al.[10] Therefore, in limit cycle operation, only one solution is observed (possibly depending on initial conditions), unless the stochastic forcing is quite large with respect to the limit cycle amplitude or the limit cycle itself has a small stability margin. The identification results during limit cycle operation are included in the figures ($\phi \geq 0.85$) and are related to the stability of the limit cycle oscillations. The interpretation and validity of the results for limit cycle oscillations are rather involved and fall outside the scope of this work.

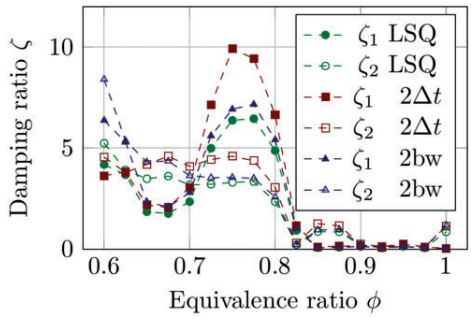

Figure 7. Influence of identification parameters on the identified damping ratios. Longer time delay and wider analysis bandwidth.

The two methods return remarkably similar results for the identified damping ratios, giving confidence in the implementation of the methods. However, when changing the bandwidth of the identification, or the involved time delays, quite large deviations might occur, especially for the higher damping ratios, that are naturally less pronounced in the data. In Figure 7, the influence of model parameters is visualized for the LSQ method, showing cases with a doubled analysis bandwidth and a doubled time delay. Deviations for the SSI method show a similar trend in the deviations resulting from parameter settings. These deviations can be explained by foreign dynamics in the bandwidth and a loss of correlation between time stamps, respectively. This means that in industrial applications, where the parameters are not tailored for specific operating conditions, the quantitative damping ratio cannot be determined with high accuracy with these methods; nevertheless, a clear qualitative behaviour is revealed.

4.2. Eigenvectors

At all distinct operation points, two eigenvalues are obtained by solving the eigenvalue problem of the identified system matrix. The eigenvalues become the subscripts 1 or 2, based on the similarity of the mode structure at adjacent equivalence ratios. So the damping and frequency are ordered, based on the highest resemblance between the eigenvectors, which is given by the maximum of their inner products. This way the connected lines in the plots in Figures 4 to 9 are established, yielding relatively continuous descriptions for the damping ratios and eigenfrequencies as a function of the equivalence ratio.

In Table 1, some eigenvector pairs for the case of 12 and 18 burners are presented in the form of the spin ratio SR and the phase difference Ang between F and G.

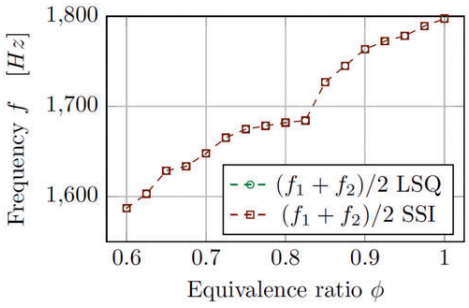

Figure 8. Mean of the identified thermoacoustic eigenfrequency pair as a function of equivalence ratio for 18 burners.

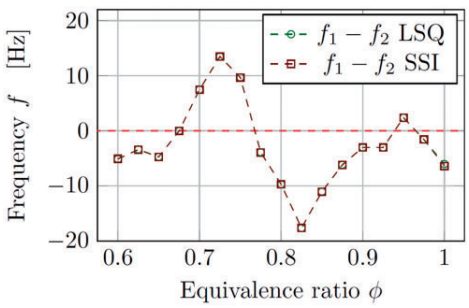

Figure 9. Difference in eigenfrequency of the mode pair as a function of equivalence ratio for 18 burners.

The spin ratio, introduced by Bourgouin et al.,[16] is defined as follows

$$SR = \frac{|F| - |G|}{|F| + |G|} \tag{18}$$

The amplitudes $|F|$ and $|G|$ correspond to the eigenvector contributions of the two waves traveling around the circumference in opposite direction. When they have a similar magnitude ($SR \approx 0$), the mode is a standing wave. In that case, the phase difference between the waves (Ang) is of interest, as it determines the angular standing wave orientation. Spin ratios of 1 and -1 refer to pure ACW and CW waves, respectively.

The mode structures (i.e. eigenvectors) are not very coherent, which is attributed to the near-degenerate state of the system and the relatively short measurement duration. Nevertheless, a weak tendency is observed from undefined or predominantly standing wave solutions ($SR < 0.5$) for the case with 12 burners, to predominantly traveling waves ($SR > 0.5$) in the case of 18 burners. Data of more stable operation points are not shown, because the eigenvectors are even less coherent from point to point.

Table 1. Identified eigenvectors for equivalence ratios shortly before instability, for the distant (12) and close (18) burner separation using LSQ.

Case	ϕ	SR_1	Ang_1	SR_2	Ang_2
12	0.75	0.29	0.49	−0.54	2.02
	0.775	0.01	0.27	−0.78	1.38
	0.8	0.10	−0.29	−0.10	1.83
	0.825	−0.42	−0.35	0.09	1.94
18	0.75	0.81	−1.03	−0.62	−0.33
	0.775	0.78	−1.58	−0.39	−1.77
	0.8	0.82	−0.14	−0.61	−1.88
	0.825	0.70	1.69	−0.47	−1.63

Note: One eigenvector is represented by the spin ratio (SR) and the angle (Ang) between $|F|$ and $|G|$.

4.3. Eigenfrequencies

In Figure 8, the average of the identified eigen-frequencies (with ω_a added) is shown for the case of 18 burners. With the increasing equivalence ratio, the eigenfrequency rises significantly. This can be expected to play an important role in the stability of the thermoacoustic system.

The splitting of the eigenvalues that caused the distinct damping ratios also causes splitting in the eigenfrequencies, as shown in Figure 9. To the knowledge of the authors, this is the first time a split in azimuthal eigenfrequencies has been discerned from experimental data. The maximum relative deviation $\Delta f/f \approx 0.01$ is of the same order of magnitude as the maximum split in damping ratio.

Based on the eigenvalues splitting at $\phi = 0.825$ in the case of 18 burners, it can be substantiated that fitting of the probability density function would yield an erroneous damping estimation. The frequency split of 18 Hz at very low damping yields a significant thicker peak in the power spectral density. A detailed inspection of the corresponding line of the waterfall plot in Figure 3 (The line near the middle with intermediate amplitude), appears to be composed by two superimposed modal peaks. With higher damping and lower frequency, mode one forms a shoulder on the left side of the peak of mode two. It would yield a significant overestimation of the decay rate, when the peak is designated to a single eigenmode.

The frequency estimates of the two identification methods show a nearly perfect coincidence, such that the SSI-method obscures the marks of the LSQ-method.

4.4. Flame-to-flame distance

The amount of burners has a pronounced effect on the stability, in a non-trivial manner. In the case with the closest flame spacing (18 burners), the damping of one of the eigensolutions varies non-monotonically as a function of the equivalence ratio. On basis of the results, the behaviour cannot be explained in detail, but we will hypothesize a reason for the qualitative behaviour observed.

In the case of 12 burners, the flames barely interact directly. The swirlers cause individual vortices with limited influence of the global flow field. Due to unavoidable minor imperfections in the experimental setup, the cylindrical symmetry is broken, splitting the eigenmodes in two (predominantly) standing wave solutions.

For close burner spacing (18 burners), the flames are merging. This happens in a directional manner, because the swirlers are co-rotating. To get an insight into the complex heat release pattern in this case, please refer to the publication of Worth and Dawson[15] on this topic. One can imagine this can cause an increased flame response to azimuthal particle velocity. Additionally, a global mean flow field develops around the circumference because the vortices on top of the swirlers start to merge, which can lead to eigenfrequency splitting of the acoustic subsystem. These effects can promote traveling wave solutions for the (fixed point stable) azimuthal thermoacoustics.

The case with 15 burners seems to behave in an intermediate state between the system with individual burners and the system with flame–flame interaction.

5. Monitoring strategy

The results show that the proposed identification method can be applied to annular combustors that are prone to azimuthal instabilities. The advantage of the method is that the stability of the mode pair can be identified without prior knowledge about the mode structure. Splitting of the eigenvalues is even detected on a rotationally symmetric laboratory rig in this work. In practice, this can serve as a stability margin that can enhance flexible operation of industrial machines by constant monitoring of potentially hazardous azimuthal eigenmodes.

In particular, the LSQ method is very suited for online determination of the damping, because of the low computational cost of linear regression. For the eigenvalues of the 2×2 system matrix, just a quadratic formula needs to be solved. An updated stability margin is obtained in a fraction of a second after the data were measured, which allows for monitoring, protection and control purposes. The chuck-wise FFT calculation of the raw data is the most computationally expensive step of this method and is usually routinely carried out already. The SSI method is also feasible to perform in real-time, but does require significantly more DSP processing power.

Such in situ stability determination is beneficial compared to a stability map, in that it reflects the current state of the machine and operation conditions. Effects due to azimuthal velocity and flame-flame interaction are hard to predict, without performing measurements on a full annular setup. Such details are not easily included in a low-order stability analysis, but its effect on the stability can directly be identified, using the in situ state-space representation of the dynamics.

6. Discussion

A very accurate estimation of the decay rate does not necessarily mean it makes an impeccable stability margin. As the case with 18 burners shows, there is no guarantee that the damping decreases monotonically decreases with the control variables at hand. This behaviour needs to be assessed for the specific azimuthal mode for the gas turbine in question, such that a suitable control strategy can be implemented based on the identified damping rate.

In addition, it must be noted that the stability margin (damping ratio) is not necessarily continuous, for continuously changing system parameters, in case that the FTFs change considerably as a function of frequency. In that case, the system matrix depends on its own eigensolution, i.e. the eigensolution is of transcendent nature. Furthermore, triggering can occur due to a nonlinear response of the heat release to the finite acoustic amplitudes. For these reasons, instability might occur before the identified damping reaches zero, which addresses the need for a certain safety margin in practical applications.

7. Conclusions

In previous work,[7] it was shown that azimuthal thermoacoustic dynamics found in annular combustors are effectively described using a complex two-dimensional state-space representation (representing a four-dimensional system). In addition, it was shown that a quantitatively accurate identification of the dynamics can be carried out for surrogate data which is generated on basis of this model description. Assertion that the identification strategy also works successfully on experimental data had not yet been delivered, which is now provided in this work.

The output-only identification strategy has been performed on experimental data of a laboratory scale annular combustor. Qualitatively, the results are promising; consistent damping ratios and modal frequencies are obtained for the rather short experimental data

sets and the pair of damping ratios decrease towards zero before instability occurs and high amplitude limit cycle oscillations are found. The eigenvalue pairs are mostly very similar, yet some structured deviations from a degenerate system are found, which was expected for an experimental setup.

Two different identification methods have been used to obtain the system characteristics of the thermoacoustic dynamics. The results of the two methods are very similar, which gives confidence in the obtained results. However, unlike the artificially generated data, the results depend significantly on model settings, such as analysis bandwidth and the delay parameter. As the actual damping ratios are unknown for these data, it cannot be validated whether the presented damping ratios are quantitatively accurate.

The case with close burner spacing (18 burners) shows predominantly traveling wave solutions, with pronounced splitting of the eigenvalues. Although the physics cannot be explained on basis of the results, the effect it has on both the stability and eigenfrequency splitting is captured in detail. We hypothesize that the flame response to azimuthal acoustic excitation and the mean flow field in the annulus contribute to the eigenvalue splitting.

It is observed that eigenvalue splitting can become relevant for vanishing system stability, even though the magnitude is negligible with respect to the acoustic resonance frequency. This observation stresses the necessity to decompose the signals on a two-dimensional basis, allowing for the typical azimuthal solutions as a mix of traveling and standing waves. In less controlled environments of industrial applications, eigenvalue splitting is expected to be more pronounced.

In the first place, the identification can serve as a stability margin measure to monitor annular combustion systems during operation. When the stability margin falls below a predefined threshold, a signal would be sent to the control system to freeze the current operating conditions, or even to retreat to operating conditions that were further away from the instability.

When the dependency on model parameters is understood better and a validation strategy is developed, identification results can be compared in a quantitative way. In gas turbine testing, the methods can enable quantitative comparison of the thermoacoustic behaviour, when changes or upgrades are made to the machine.

Acknowledgements

The presented work is part of the Marie Curie Initial Training Network Thermo-acoustic and aero-acoustic nonlinearities in green combustors with orifice structures (TANGO). The authors gratefully acknowledge the openhearted sharing of experimental data by Nicholas Worth and James Dawson.

Declaration of Conflicting Interests

The author(s) declared no potential conflicts of interest with respect to the research, authorship, and/or publication of this article.

Funding

The author(s) disclosed receipt of the following financial support for the research, authorship, and/or publication of this article: We gratefully acknowledge the financial support from the European Commission under call FP7-PEOPLEITN-2012.

References

1. O'Connor J, Acharya V and Lieuwen T. Transverse combustion instabilities: acoustic, fluid mechanic, and flame processes. *Prog Energy Combust Sci* 2015; 49: 1–49.
2. Saurabh A and Paschereit CO. Combustion instabilities in a swirl flow combustor with transverse extensions. In: *ASME turbo expo 2013: turbine technical conference and exposition, Vols. 1B: combustion, fuels and emissions*, San Antonio, Texas, USA, 3–7 June 2013, p. V01BT04A057. San Antonio: ASME.
3. Ghirardo G and Juniper MP. Azimuthal instabilities in annular combustors: standing and spinning modes. *Proc R Soc A* 2013; 469: 20130232.
4. Worth NA and Dawson JR. Self-excited circumferential instabilities in a model annular gas turbine combustor: global flame dynamics. *Proc Combust Inst* 2013; 34: 3127–3134.
5. Noiray N and Schuermans B. On the dynamic nature of azimuthal thermoacoustic modes in annular gas turbine combustion chamber. *Proc R Soc A* 2013; 469: 20120535.
6. Prieur K, Durox D, Schuller T, et al. A hysteresis phenomenon leading to spinning or standing azimuthal instabilities in an annular combustor. *Combust Flame* 2016; 175: 283–291.
7. Rouwenhorst D, Hermann J and Polifke W. Online monitoring of thermoacoustic eigenmodes in annular combustion systems based on a state-space model. *J Eng Gas Turbines Power* 2016; 139: 021502.
8. Noiray N. Linear growth rate estimation from dynamics and statistics of acoustic signal envelope in turbulent combustors. *J Eng Gas Turbines Power* 2016; 139: 041503.
9. Mejia D, Miguel-Brebion M and Selle L. On the experimental determination of growth and damping rates for. *Combust Flame* 2016; 169: 287–296.
10. Noiray N, Bothien M and Schuermans B. Investigation of azimuthal staging concepts in annular gas turbines. *Combust Theory Modell* 2011; 15: 585–606.
11. Parmentier J-F, Salas P, Wolf P, et al. A simple analytical model to study and control azimuthal instabilities in annular combustion chambers. *Combust Flame* 2012; 159: 2374–2387.
12. Rouwenhorst D, Hermann J and Polifke W. Bifurcation study of azimuthal bulk flow in annular combustion systems with cylindrical symmetry breaking. *Int J Spray Combust Dyn* 2017; 9: 438–451.

13. Tanaka H and Katayama T. Stochastic subspace identification via "LQ decomposition". In: *42nd IEEE conference on decision and control*, Maui, Hawaii, USA, 9–12 December 2003, Vol. 4, pp.3467–72. Maui: IEEE.
14. Katayama T. *Subspace methods for system identification*. London: Springer-Verlag London Limited, 2005.
15. Worth NA and Dawson JR. Modal dynamics of self-excited azimuthal instabilities in an annular combustion chamber. *Combust Flame* 2013; 160: 2476–2489.
16. Bourgouin J, Durox D, Moeck JP, et al. Self-sustained instabilities in an annular combustor coupled by azimuthal and longitudinal acoustic modes. In: *ASME turbo expo 2013*: *turbine technical conference and exposition. Volume 1B*: *combustion, fuels and emissions*, San Antonio, Texas, USA, 3–7 June 2013, p. V01BT04A007. San Antonio: ASME.

Appendix

Notation

a	coefficient of matrix M
A	discrete system matrix
Ang	angle between waves F and G
C	output matrix
f	frequency
F	ACW acoustic wave
G	CW acoustic wave
H	Heat release response
m	mode order
M	system matrix
R	Rayleigh integral
SR	Spin ratio
v	discrete noise vector
w	noise vector
x	state vector
X	matrix of concatenated state vectors
y	output vector
α	decay rate
ζ	damping ratio
λ	eigenvalue
ϕ	equivalence ratio
ω_a	acoustic resonance frequency
ω_t	thermoacoustic eigenfrequency
$\Im(.)$	imaginary part
$\Re(.)$	real part